The Influence of Microtubules and Microtubule-Based Structures on Osteoclast and CD4+ T Cell Function

Michael Mark Sutton

Submitted in partial fulfillment of the
requirements for the degree of
Doctor of Philosophy
under the Executive Committee
of the Graduate School of Arts and Sciences

COLUMBIA UNIVERSITY

2022

Abstract

The Influence of Microtubules and Microtubule-Based

Structures on Osteoclast and CD4+ T Cell Function

Michael Mark Sutton

The burden of osteoporosis and low bone mass is unrelenting, affecting over 50% of the U.S. population over the age of 50. In a similar reach but different clinical realm, nearly 40% of all men and women will be diagnosed with cancer at some point during their lifetimes. The impact of both of these diseases is compounded by the limited knowledge of cellular mechanisms and the insufficiency of effective treatment options. At the microscopic level of the cell cytoskeleton, increasing evidence has led researchers to further explore microtubules (MTs) and MT-based structures, such as primary cilia, as potential keys to unlocking improved treatment options. However, the way in which microtubules regulate the processes giving rise to these diseases remains a critical gap in knowledge. The works outlined here aimed to elucidate mechanisms that may be used to combat diseases attacking the skeletal and immune systems.

In order to characterize the influence of primary cilia with respect to osteoclast differentiation, we implemented a series of treatments to an immortalized macrophage cell line: cilia lengthening (using Fenoldopam) and mechanical stimulation (using oscillatory fluid flow). The results were analyzed by a combination of immunocytochemistry and quantitative PCR. Our first result showed definitively that while osteoclasts do not possess primary cilia, their macrophage precursors do. We also discovered that these macrophage primary cilia are dynamic and can be modulated; cells whose cilia had been lengthened showed a significant decrease in osteoclast formation, indicating that macrophage cilia resorption may be a necessary step for

osteoclast differentiation to occur. Combined with findings from previous studies, there is increasing evidence that the primary cilium, as a therapeutic target for bone diseases, may offer a dual beneficial approach to both promote bone formation and downregulate osteoclast activity.

We then explored the possibility of directional MT translocation during T-cell activation being linked to Rho GTPases, which regulate actin polymerization. WASp and WAVE2, known to have functional roles in T-cell activation, were identified as primary candidates. In order to investigate this relationship, we implemented a stepwise micropatterning procedure by which PDMS was used to transfer local areas of activation (presenting fluorescently-tagged antibodies against CD3 and CD28) which, upon T-cell receptor (TCR) triggering, could mimic immune synapse (IS) formation. We showed that, although there was no correlation between the spatial organization of MTs and WASp, MTs and WAVE2 location were highly correlated, providing strong evidence for a link between these two systems. In addition, MT disruption via nocodazole resulted in a significant decrease in T-cell activation and mechanosensing capabilities. Given the role of WAVE2 in promoting cell spreading and adhesion during IS formation, this result provides additional evidence that this cytoskeletal filament is in fact connected to proteins involved in actin nucleation and elongation.

We anticipate the work in Aim 1 to help reveal a previously unexplored therapeutic target for osteoporosis, a disease that currently has no clinical manifestations prior to a fracture event. Further investigation has the potential to contribute to diagnosis and prevention techniques, as well as new treatments. Similarly, given the emergence of adoptive T-cell immunotherapy for immune-related disorders, the findings of Aim 2 will advance our understanding of both the biological and mechanical influence of the cytoskeleton and motivate microtubules as one component of a more comprehensive armamentarium of treatment approaches.

Table of Contents

I. List of Graphs

Figure 1.15. Force in T-cell recognition. T cells scan APCs where they are able to sensitively discriminate activation cues from a large pool of non-activation cues by the TCR binding to MHC presenting self or non-self ligands. The 2D agonist pMHC/TCR interaction is further mediated by co-receptor binding, checkpoint inhibition, and force through a catch-bond mechanism. Once sufficiently triggered, the TCR complexes accumulate together, sliding along the membrane in lipid rafts where they form microclusters and eventually the immunological synapse to localize internal signaling and release of effector molecules (*Harrison et al., 2019*).

Figure 2.1. Mechanism of SOP. With aging, the ability of BMSCs to differentiate into osteoblasts decreases and that of adipocytes increases. A decrease in peroxisome proliferator-activated receptor-γ coactivator 1 increases bone loss and fat accumulation during bone aging. Aging leads to the increase in reactive oxygen species (ROS), the accumulation of oxygen free radicals, the destruction of bone cells, and the inhibition of bone formation. With the growth of age, estrogen synthesis in vivo is reduced, CFTR chloride channel is lost, OPG is decreased, and overexpression of RANKL leads to osteoporosis. ClC-3 chloride channel in osteoblasts regulates the bone formation function of osteoblasts by regulating estrogen A receptor. In addition, the decrease in immune cells during aging leads to the decrease of OPG production and the increase in secretion of pro-inflammatory factors, which accelerates bone loss, affects bone metabolism and leads to osteoporosis. MiRNA networks can regulate bone formation through Wnt signaling pathway and bone resorption through RANKL/RANK pathway. In aging, autophagy level decreases and homeostasis of miRNA networks is broken. Finally, aging can down-regulate the expression and activity of 1α-hydroxylase in human bone marrow mesenchymal stem cells and inhibit the osteogenic differentiation of human bone marrow mesenchymal stem cells (*Fang et al., 2022*).

Figure 2.2. Measures of pain and disability after anti-osteoporosis treatment. A total of 132 patients diagnosed with acute osteoporotic spinal fractures (OSFs) were enrolled and allocated into three groups: Group I ($n = 39$, no anti-osteoporosis medication), Group II ($n = 66$, bisphosphonate), and Group III ($n = 27$, parathyroid hormone (PTH). Radiological parameters including magnetic resonance (MR) classification, occurrence of intravertebral cleft (IVC), and clinical outcomes such as (a) Oswestry disability index (ODI) and (b) numerical rating scale (NRS) were assessed (*Min et al., 2019*).

Figure 2.3. Paracrine signals from MLO-Y4 cells increase osteogenic signaling in MC3T3-E1 osteoblastic cells in a flow-duration dependent manner. (A) Model of paracrine signaling from osteocytes to osteoblasts with the primary cilium indicated as a potential load-induced fluid-flow mechanosensor. (B) MLO-Y4 osteocytes were placed on a rocking platform and subjected to oscillatory fluid flow of increasing durations, or left static as a control. Conditioned media was then collected and used to culture MC3T3 osteoblasts. (C) Conditioned media from 2, 6, and 12 hours of fluid flow was placed on static osteoblasts for 24 hours, at which point osteoblast OPN mRNA expression was assessed. $n \geq 4$ for each group (*Spasic et al., 2022*).

Figure 2.4. Presence of primary cilia in PBMCs and BMMCs. (A) Confocal Image of primary cilia in NIH3T3 fibroblasts (positive control) using antibodies against acetylated alpha-tubulin (labeling primary cilia; red), gamma-tubulin (labeling basal bodies; green), and DAPI (labeling nuclei; blue). Top panel, magnification 63×; scale bar, 5μm. Normal human PBMCs and BMMCs possess primary cilia (middle and bottom, respectively). Mononuclear cells were isolated from peripheral blood or bone marrow and immunolabeled for gamma-tubulin (green), acetylated alpha-tubulin (red), and DAPI (blue). Acetylated alpha-tubulin is enriched in cilia axoneme and gamma-tubulin is enriched in basal bodies. The spatial arrangement of the staining of these proteins was used to identify primary cilia in PBMCs and BMMCs. (B) 3D surface projection image of PBMCs created by combining all Z-stacks. The image shows the presence of primary cilia on the surface of cells (red) (*Singh et al., 2016*).

Figure 2.5. Differentiation of RAW 264.7 cells into osteoclasts. (A) Timeline of cell passaging and differentiation process. (B) Representative phase-contrast micrographs demonstrating the distinct phases of osteoclast differentiation. The first image of Panel B shows RAW 264.7 cells on Day 0; the second image is captured from Day 4, after RAW 264.7 cells have been incubated with M-CSF to differentiate into macrophages; the third image is captured from Day 10, with one mature osteoclast outlined in green. Scalebar = 100 μm.

Figure 2.6. Mathematical model of a rocking system. (A) The side view of a culture dish of length L and width b that contains culture medium of depth of h_0 rocks up and down sinusoidally in the vertical plane (xz) along the pivotal point O. The critical flip angle (θ_0) is defined when the fluid free surface contacts the outer edge P of the dish bottom. Depending the maximal flip angle θ_{max}, there are two cases considered. (B) If $\theta_{max} \leq \theta_0$, the entire dish bottom is covered by the medium and a finite fluid depth z_e occurs at the outer edge of the dish; (C) If $\theta_{max} > \theta_0$, some peripheral region of the dish bottom including points O and P may be exposed to air during the rocking. The fluid free surface makes a contact with the dish bottom at the location of x_e. For both cases and at an arbitrary location x, the fluid height h_f at the vertical cross-section (dashed line) and the fluid volume V_f located on the right side of the cross-section can be estimated from purely geometric considerations, assuming a horizontal free fluid surface (*Zhou et al., 2010*).

Figure 2.7. Sample rocker photo and schematic. A platform rocker used to subject cells to fluid flow–induced shear stress (left) and a schematic representation of gravitational movement of fluid in a well plate during different time points of one cycle (t) (right) (*Osman et al., 2014*).

Figure 2.8. RAW 264.7 cells can be stained for primary cilia using multiple antibodies. Maximum projection of confocal image z-stack at 40X. Scalebar = 10 μm.

Figure 2.9. RAW 264.7 cells display primary cilia and centrosome overlay. Maximum projection of confocal image z-stack at 100X. Scalebar = 10 μm.

Figure 2.10. Macrophages possess primary cilia, but mature osteoclasts do not. Maximum projection of confocal image z-stack. (A) Primary cilia were found on macrophages. Blue = DAPI (nuclei), green = acetylated alpha-tubulin (primary cilia), red = γ-tubulin (centrosomes). Arrows highlight examples of centrosome/primary cilium overlay. (B) Primary cilia were mostly absent from differentiated osteoclasts, shown via distinct multi-nuclear and cortical actin staining. Blue = DAPI (nuclei), green = phalloidin (actin), red = acetylated alpha-tubulin (primary cilia). Scalebar = 10 μm. C) Macrophages were found to have a primary cilia incidence of 46.8% (n = 5), while differentiated osteoclasts were found to have a cilia incidence of just 3.3% (n = 12).

Figure 2.11. Fenoldopam effectively increases macrophage-primary cilia incidence and length. Macrophages were treated with fenoldopam mesylate or DMSO vehicle control. Fenoldopam-treated cells showed a significant increase in both (A) cilia incidence (from 42.9% to 53.5%; n = 11, 10) and (B) cilia length (from 1.75 μm to 2.26 μm; n = 23, 21) compared to control samples.

Figure 2.12. Macrophage primary cilium lengthening inhibits osteoclastogenesis. mRNA quantification showed that macrophages treated with fenoldopam prior to osteoclast differentiation treatment resulted in (A) an 18.2% decrease in expression of tartrate-resistant acid phosphatase (ACP5) and (B) a 20.3% decrease in expression of cathepsin K (CTSK), both measures of osteoclast differentiation and function, when compared to the DMSO vehicle control (n = 4). (C) Samples treated with fenoldopam also formed osteoclasts at a lesser rate, indicated by a 13% drop in osteoclast surface area coverage (n = 24, 23).

Figure 2.13. Mechanical stimulation of macrophage primary cilia did not result in a significant change in osteoclastogenesis. Macrophages were subjected to oscillatory fluid flow prior to being incubated with M-CSF and RANKL to induce osteoclast differentiation. Mechanically-stimulated cells did not demonstrate a significant change in osteoclastogenesis when compared to the static control samples (n = 15, 7).

Figure 2.14. Linkage of the centrosome–cilium cycle to the cell cycle. Primary cilia assemble specifically when cells exit the cell cycle and become quiescent or differentiate. Cells are also competent to form cilia in G1. Phases of the cell cycle are indicated, and blue and yellow arrows indicate cilium assembly and disassembly, respectively. Only the mother centriole (light blue) can initiate ciliogenesis. The daughter centrioles are shown in dark blue. During the process of ciliogenesis, an axoneme is assembled. This microtubular structure (indicated with parallel green rods) is disassembled as cells progress towards S phase, concomitant with remodelling of the distal end of the basal body (aqua ring). During S phase, centrosomes commence duplication, at which point cilia have largely disassembled. After mitosis, centrosomes are again competent to assemble primary cilia, either in G0 or in early G1 phase (*Sánchez & Dynlacht, 2016*).

Figure 2.15. Osteoclasts recycle via osteomorphs during RANKL- stimulated bone resorption (*McDonald et al., 2021*).

Figure 2.16. Effect of Cd exposure on the migration ability of osteoclast precursor cells. In the presence of M-CSF and RANKL, RAW264.7 cells were induced for 48 h, then treated with different concentrations of Cd (0, 10 nM, 2 μM, and 5 μM) for 24 h. Cells in the upper layer of the membrane were removed, and the cells in the lower layer were stained with DAPI and counted (Scale bar = 20 μm). Data are shown as the mean ± SD (n = 3). *p < .05 indicates a significant difference compared with the control group; **p < .01 indicates a very significant difference compared with the control group (*He et al., 2022*).

Figure 2.17. The role of AC3- and CaMK-dependent cAMP modulation in osteoclast differentiation. AC3 induction by RANKL results in the accumulation of intracellular cAMP, which culminates in the PKA-mediated phosphorylation and subsequent inactivation of NFATc1. On the other hand, CaMK activities evoked by RANKL curtail intracellular cAMP elevation, limiting the inhibition of osteoclastogenesis by the AC3-cAMP-PKA pathway. Ultimately, the AC3 and CaMK pathways constitute a delicate signaling network for the regulation of osteoclast differentiation (*Yoon et al., 2011*).

Figure 3.1. IL-2 secretion correlates primarily with CD28 geometry. (A) Additional geometries of anti-CD3 and anti-CD28 ligands. (B) Six-hour IL-2 secretion on these patterns. Data from each pattern are different from all other conditions (Kruskal–Wallis analysis, α = 0.05) (*Shen et al., 2008*).

Figure 3.2. Schematic of force augmentation by CD28 signaling. Inhibitors are indicated in red (*Bashour et al., 2014*).

Figure 3.3. Loss of F-actin dynamics reduces cellular force generation. Fluorescence images of EGFP-actin expressing Jurkat T-cells on an elastic substrate 1 min before (left) and 9 min after (right) application of (a) 1 μM latrunculin-A, (c) 100 μM CK666, (e) 1 μM jasplakinolide, and (g) 0.1% DMSO. Color maps of traction stresses of the same cells before (left) and after (right) addition of (b) 1 μM latrunculin-A, (d) 100 μM CK666, (f) 1 μM jasplakinolide, and (h) 0.1% DMSO. (i) Total traction force as a function of time for a representative cell in each of the conditions described. The dashed line represents the time point at which the drug was added. (j) Comparison of the after-to-before ratios of traction stresses for application of Lat-A (N = 20 cells), CK666 (N = 17 cells), and Jasp (N = 10 cells) with control (DMSO carrier, N = 20 cells) (*Hui et al., 2015*).

Figure 3.4. Dynamic Remodeling of the Actin Cytoskeleton during TCR-Induced Spreading. (A) Jurkat cells expressing EGFP-actin were plated on coverslips coated with the indicated antibodies. EGFP-actin was imaged at the coverslip every 30 s using the CCD-equipped microscope. The images presented here were acquired 5 min after the initial contact with the coverslip. (B) Jurkat cells expressing EGFP-actin were labeled with DiI, plated on coverslips coated with the TCR-specific antibody UCHT1, and imaged every 7.5 s using the CCD-equipped microscope. Time was measured from the initial contact with the coverslip. EGFP-actin is shown in green. The membrane stain DiI appears yellow orange (see Experimental Procedures) and is not relevant to this discussion. White arrows mark large, sheet-like lamellipodia. (C) EGFP-actin-expressing Jurkat cells were plated on coverslips coated with UCHT1 for 5 min and fixed. Confocal images of EGFP-actin spanning 10 μm of height were collected at 0.5 μm intervals. The images presented were reconstructed as follows: (i) projection of the z-stack onto a horizontal plane; (ii–iii) vertical slices corresponding the arrows in (i); (ii) cross-section through the actin-rich border; (iii) cross-section through the cell body (*Bunnell et al., 2001*).

Figure 3.5. Minus-end microtubule transport motors are sufficient for transport of lytic granules to the secretory site during target cell killing. a, En face view of the organization of the CTL immunological synapse. b, c, Single x–y confocal section (b) and en face (y–z) reconstruction (c) of a human CTL, expressing actin–GFP (green) and with CD63-labelled granules (red), conjugated to a target cell. d, Organization of microtubules (thin black lines) with lytic granules (red), relative to the immunological synapse (thick black line) and centrioles (blue). e–h, Projected serial confocal sections through human CTLs, expressing GFP–RILP (green), shown alone (e, g) or conjugated to targets (f, h), and labelled with markers of the centrosome (g-tubulin is red in e, f, but blue in g, h) and granule markers (cathepsin D, blue in e, f; perforin, red in g, h). i, Fluorescence-activated cell sorting (FACS) profile showing GFP expression (FL1-H) of mock-infected (filled histogram) human CTLs and four CTL clones expressing GFP–RILP (unfilled histograms). j, Killing assay using mock-infected CTLs (diamonds), GFP-(squares) or GFP–RILP-(triangles, circles, crosses) expressing CTL clones. Error bars show standard deviation from the mean. Scale bars for b, c and e–h, 10 mm (*Stinchcombe et al., 2006*).

Figure 3.6. MT influx suppresses local actin retrograde flow. (A and B) Cell contact and four regions of different polar angles in which the numbers of MTs entering each region were counted as a function of time. (C) Actin flow speed against MT influx in different polar angles. The pdfs of MT growth speed (D), actin flow speed (E), and the actin flow–MT influx relation for T cells spreading in the presence of vehicle and inhibitors (F) are shown. Data were taken at between 9 and 10 min of activation (*Hui & Upadhyaya, 2017*).

Figure 3.7. Schematic of wafer design used for microcontact printing.

Figure 3.8. Schematic of stamping procedure onto glass coverslips (*J. H. Lee et al., 2015; Weibel et al., 2007*).

Figure 3.9. MTOC alignment of murine CD4+ cells to local areas of activation. Micropattern (red) made from 2-10 μm wafer and transferred to glass coverslips via PDMS molds were incubated in both anti-CD3 and anti-CD28. The left panel image was captured at 40x; scalebar = 20 μm. The right panel image was captured at 100x; scalebar = 10 μm. Microtubules (green) can be visualized both inside the cell and on the cell periphery.

Figure 3.10. Images of spatial proximity of WAVE2 with respect to peripheral microtubules. The pattern used is comprised of segregated activating antibodies; the large red dots (2 μm in diameter, 10 μm spaces between each dot) are incubated with anti-CD3, and the small red dots (1 μm in diameter, 5 μm spaces between each dot) are incubated in anti-CD28. The left panel image shows microtubules (green), while the right panel image shows WAVE2 (blue). The yellow arrows of this panel indicate regions of cells where high intensity of both proteins appears evident. Scalebar = 10 μm.

Figure 3.11. Scatter plot and correlation showing quantitative relationship between microtubules and WAVE2 concentration. The graph shows the correlation of pixel intensity values of just one individual cell along its exterior with respect to microtubules and WAVE2 (334 segments). Correlation values of 15 samples (other plots not shown) are listed in the table on the right (correlation values above 0.8, indicating a strong relationship, appear in dark green text); average Pearson's correlation was 0.8771±0.0665.

Figure 3.12. Images of spatial organization of WASp. Using both colocalized (first two panels) and segregated (third panel) patterns, we see that the highest intensity locations of WASp staining are inconsistent and rarely present on the cell periphery. Scalebar = 10 μm.

Figure 3.13. Organization of WAVE2 is unchanged despite microtubule inhibition. The left panel image shows microtubules (green), while the right panel image shows WAVE2 (blue). The organization of the intracellular microtubules are clearly disrupted (MTOC and filaments emitting from center are not visible); however, the relative areas of high and low intensity from WAVE2 staining are the same. Scalebar = 10 μm.

Figure 3.14. IL-2 secretion assay (4 hours) using microtubule inhibitors. A) Percentage of cells secreting IL-2 by inhibitor group under varying substrate stiffness values. B) Mean fluorescence per group, showing total amount out of IL-2 secreted under different conditions as an indicator of comparative activation levels.

Figure 3.15. T cell interaction with micropatterned, costimulatory arrays. A) CD4+ cells were presented with surfaces that capture the microscale organization of ligands associated with T cell costimulation. Colocalized patterns were created by mixing anti-CD3 and anti-CD28 antibodies (yellow) in a single step B), while segregated patterns were defined by sequential patterning of anti-CD3 (red) and anti-CD28 (green) on a single surface (C). (Inset) Fluorescence profile across a segregated site. ICAM-1 was coated onto the remainder of these surfaces but is omitted here for clarity. Scale bar = 10 μm (*Shen et al., 2008*).

Figure 3.16. IL-2 secretion results under varying substrate stiffness values. A) Results from using human cells, a mixture of CD4+ and CD8+ lymphocytes, a stiffness range from 0.1-2MPa, and PDMS (*O'Connor et al., 2012*). B) Results from using murine CD4+ lymphocytes, a peak stiffness of 200 kPa, and polyacrylamide (PA) gels (*Judokusumo et al., 2012*).

Figure 3.17. Short term IL-2 secretion modulated by substrate stiffness and ligand density. (A) IL-2 secretion of T cells characterized by flow cytometry. (B) IL-2 secretion of T cells activated for 4 h on hydrogels with standardized coating (n = 12 across 5 independent experiments), 0.1x coating (n = 3 across 2 independent experiments), and 10x coating. Data are mean ± s.d., n = 6 across 2 independent experiments. *p < 0.05, **p < 0.01, ***p < 0.001, ****p < 0.0001, 2-way ANOVA, Tukey multiple comparison test. (C) IL-2 secretion of CD4+ and CD8+ T cell subsets. Data are mean ± s.d., n = 12 across 5 independent experiments. *p < 0.05, **p < 0.01, ***p < 0.001, ****p < 0.0001, 2-way ANOVA, Tukey multiple comparison test.

Figure 3.18. Correlation between actin flow rates and tyrosine phosphorylation during T cell activation. Results from two types of experiments were combined to assess how actin flow rates affect TCR signaling. Jurkat T cells stably expressing GFP-actin were transduced with recombinant lentiviruses expressing shRNAs specific for vinculin or talin, or with an empty control vector. Actin flow rates within the lamellipodial region were determined by kymographic analysis. In parallel studies, cells were allowed to spread on stimulatory coverslips for 5 min, fixed, permeabilized, and labeled for phosphotyrosine. Average phosphotyrosine signal per cell was then plotted as a function of actin flow rates. In vector-transduced control cells, VCAM-1 engagement slows the actin flow rate and decreases phosphotyrosine signaling. Knocking down the clutch molecules talin or vinculin relieved the slowing effect of integrin engagement, suggesting that mechanical drag is at least partly responsible for the slowing of the actin network (*Roy & Burkhardt, 2018*).

Figure 3.19. Cytolytic mechanopotentiation by WASP-dependent synaptic protrusions. A schematic diagram of the cytolytic IS showing peripheral WAVE2-dependent protrusions and central WASP-dependent protrusions. Red arrows denote force exertion (*Tamzalit et al., 2019*).

Figure 3.20. Effects of microtubule-active drugs on microtubule dynamics. Shown are a control axon and axons during the first moments of exposure to microtubule-active drugs. In the control axon, the microtubules (MT) display dynamic instability at their plus ends. In taxol-treated axons, the microtubules are stabilized (no longer lose subunits) and no longer show dynamic instability at their plus ends. Hence, they continue to assemble. In axons treated with low concentrations of microtubule depolymerizing drugs, the microtubules become 'kinetically stabilized,' which means they lose and gain subunits at the same rate, resulting in no length change (*Baas & Ahmad, 2013*).

Figure 4.1. Schematic representation of critical steps in immunological synapse (IS) assembly and ciliogenesis. Both IS assembly and ciliogenesis are inducible processes that are initiated in response to external stimuli or triggering events. The encounter of an antigen presenting cell (APC) bearing a cognate peptide-loaded major histocompatibility complex (pMHC) initiates the formation of a stable IS in the T cell (a). At variance, ciliogenesis is activated in vitro by a variety of stressful conditions (e.g., serum and nutrient starvation, ultraviolet light radiation), which generally inhibit cell division (b). In the T cell the centrosome moves toward the synapse as a consequence of early T cell receptor (TCR) signaling events (a) and, at this location, sets the stage for polarized vesicular trafficking. Cilium assembly crucially depends on centrosome-to-basal-body conversion that consists in the polarization and subsequent docking of the mother centriole to the plasma membrane, where it nucleates the ciliary axoneme. At the IS newly polymerized actin filaments contribute to the initial clustering of TCRs in the central supramolecular activation clusters (cSMAC). Following polarization of the centrosome, actin retracts to the distal SMAC (dSMAC) to form a ring, which surrounds the peripheral SMAC (pSMAC) enriched in LFA-1 (a). A redistribution of actin in contractile bundles at the ventral side and a cortical network at the dorsal side helps to break cell symmetry and promotes centrosome migration during ciliogenesis (b). In both structures the docking phase of the centrosome is concomitant with a local clearance of cortical actin (*Cassioli & Baldari, 2019*).

Figure 4.2. IFT in primary cilia and at the immune synapse. (a) Transport of cargo to primary cilia and back to the cell body is ensured by multimeric IFT particles in concert with the BBSome. Molecular motors assist the movement of particles along the axonemal microtubules. (b) When a T cell encounters an antigen-specific APC, the TCR/CD3 complex clusters in the central area of the immune synapse. One of the principal mechanisms of TCR clustering at the immune synapse is through polarized delivery of receptor complexes localized in recycling endosomes. Assembly of a stable immune synapse requires the translocation of the centriole close to the membrane patch at the immune synapse. Following TCR engagement, IFT20 interacts with the TCR and assembles in a complex with IFT57 and IFT88. This IFT complex promotes polarized recycling of the TCR to the immune synapse (*Finetti et al., 2011*).

Figure 4.3. Regulation of osteoclast differentiation by osteoblasts through macrophage colony-stimulating factor, receptor activator of nuclear factor-κB ligand, and osteoprotegerin production. Osteoblasts express RANKL as a membrane-associated form in response to bone resorption-stimulating factors. Osteoclast precursors express c-Fms (M-CSF receptor) and RANK (RANKL receptor) and differentiate into osteoclasts in the presence of M-CSF and RANKL. Osteoblasts also produce osteoprotegerin (OPG), which inhibits osteoclastogenesis by blocking the RANKL-RANK interaction (*Yamashita et al., 2012*).

II. List of Tables

III. List of Abbreviations

ADPKD – Autosomal dominant polycystic kidney disease

APC – Antigen presenting cell

ARP 2/3 – Actin-related protein 2/3

ATP – Adenosine triphosphate

BBS – Bardet-Biedl syndrome

BCR – B-cell receptor

BMD – Bone mineral density

CAR-T – Chimeric antigen receptor T-cell

CD3 – Cluster of differentiation 3

CD4 – Cluster of differentiation 4

CD28 – Cluster of differentiation 28

CD80 – Cluster of differentiation 80

CD86 – Cluster of differentiation 86

Cdc42 – Cell Division Cycle 42

CTL – Cytotoxic lymphocyte

CTLA-4 – cytotoxic T lymphocyte associated molecule-4

CTSK – Cathepsin K

DC – Dendritic cell

DR5 – Dopamine receptor 5

FDA – Food and Drug Administration

GTP – Guanine triphosphate

IL-1 – Interleukin-1

IL-6 – Interleukin-6

IL-11 – Interleukin-11

IS – Immune synapse

M-CSF – Macrophage-colony stimulating factor

MHC I – Major histocompatibility complex I

MHC II – Major histocompatibility complex I

MT – Microtubule

MTOC – Microtubule organizing center (also called the centrosome)

NCI – National Cancer Institute

NPF – Nucleation promoting factor

NZ – Nocodazole

OCL – Osteoclast

OPG – Osteoprotegerin

PA – Polyacrylamide

PAMP – Pathogen-associated molecular pattern

PCR – Polymerase chain reaction

PD-1 – Programmed cell death protein-1

PD-L1 – Programmed death-ligand 1

PDMS – Polydimethylsiloxane

pMHC – Peptide major histocompatibility complex

PRR – Pattern recognition receptor

PTH – Parathyroid hormone

RANK – Receptor activator of nuclear factor-kappa B

RANKL – Receptor activator of nuclear factor-kappa B ligand

TCR – T-cell receptor

TRAP – Tartrate-resistant acid phosphatase

USD – United States dollars

WASp – Wiskott-Aldrich Syndrome protein

WAVE2 – WASp Family Verprolin-homologous Protein-2

IV. Acknowledgments

"We pretend that success is exclusively a matter of individual merit. But there's nothing in any of the histories we've looked at so far to suggest things are that simple…success [is] not just of [your] own making. It [is] a product of the world in which [you] grew up." - Malcolm Gladwell. In the case of a little Black kid from Aliquippa, PA, this rings poignantly true. My journey at Columbia University has been at times a long and trying one. But more importantly, it has been one filled with bright minds, lending hands, warm hugs, and joyful company.

I must first express my deepest gratitude to the staff of Columbia University. These individuals keep the higher education system functioning on a day-to-day basis and rarely receive even the simplest of thanks for their hard work. To start, I want to thank the ICM staff of Fairchild for taking care of my animals, without which my research could not have been conducted, with special thanks to Alberto and Shala. Thank you to our maintenance and facilities staff for keeping our spaces clean and properly functioning, especially Hakeem, who throughout the last few years regularly took time out of his morning to see how I was doing and tell me how proud he was of me. I am eternally grateful to the BME Office staff for all that they've done and continue to do, with a special shoutout to Michelle Cintron, Paulette Louissaint, and Karen Evans, not only for processing and managing our numerous supply orders, several of which we submitted late on Friday afternoons, but also for being a welcome break in monotonous days when I really needed a good laugh. And lastly, I want to recognize the GSA Office and PDL Team for their hard work and professionalism, with special thanks to Ellie Bastani, Alvaro Rojas-Caamano, Betty Matias Hsu, Jenny Mak, and Liz Strauss; there were weeks where I spent more time in Mudd 530 than I did in my own research lab, and they ensured that I always felt welcomed and supported.

My extracurricular involvement at Columbia University has been extensive and has given me the opportunity to meet some incredible people and make even greater friends. I owe a special thanks to my EGSC family for their hard work in making SEAS a better place and for being fantastic to work with, especially Megan Armstrong, Arvind Srinivasan, Hrishikesh Jadhav, Sai Mali Ananthanarayanan, Tingkai Liu, and Shreya Narasimhan. I also want to thank my CUIM family, led by Jeff Ryder, Brian Jines, and Lauren Dudziak.

Next, I want to thank the Columbia BME faculty, with special acknowledgment to Dr. Katie Reuther, Dr. Aaron Kyle, and Dr. Barclay Morrison, who have all served an invaluable role in my life at Columbia; I can't express enough how much I have appreciated their kindness, mentorship, and guidance. I also want to extend this thanks to my defense committee for lending their advice and expertise to help me craft my dissertation: Dr. Henry Hess, Dr. Helen Lu, Dr. Jasmine McDonald, and Dr. Stefaan Verbruggen. I have come to know some of the above individuals on a more personal level and simply want to add that they are genuinely incredible people. The passion they have for their fields and dedication to learning gives me a great deal of faith in the next generation of medical researchers. Lastly, I want to thank my advisors. Dr. Christopher R. Jacobs passed away before I finished the second year of my degree, but in our short time together, he instilled in me the drive and initiative to be a successful research scientist. His pioneering contributions laid the groundwork for the first half of my thesis, and I can't thank him enough for giving me the opportunity to prove myself. Dr. Lance C. Kam welcomed me into his laboratory with a degree of support and calm that I could have never imagined. He has always availed himself whenever I needed help on a matter, big or small, and allowed me the space and opportunity to adapt my acquired skill set while also learning an entirely new field at my own pace. Thanks for helping me the rest of the way.

Last, but certainly not least, I give the biggest thanks to my labmates. From the CMBL, I want to acknowledge Dr. Emily R. Moore, Dr. Milos Spasic, and Dr. Michael P. Duffy. When I met them during interview weekend back in 2016, they seemed friendly. But I never imagined how warm, engaging, and inspirational of an environment we would build. I owe many of my technical abilities as a researcher to them, as they truly took me under their wing and helped bring me up to speed in a foreign scientific world: troubleshooting protocols, editing written submissions, and helping me make professional connections at conferences. The way in which we seamlessly intertwined daily conversations of primary cilia with fantasy football and Instagram memes is truly magical. I'm happy to call these individuals both my colleagues and my friends, and I look forward to seeing the careers they forge for themselves. And from the MBL, I thank Dr. Parthiv Chaudhuri, Dr. Joanne Lee, Dr. Dennis Yuan, Dr. Chirag Sachar, Dr. Lingting Shi, Xin Wang, Paula Schultheiss, and Anna-Liisa Sepp. When I first joined our lab, any sense of anxiety or reservations I had vanished instantly. You all welcomed me with open arms, eager to lend to me not only your scientific knowledge but also your friendship. Between our heated debates around romance, my constantly supplying you with snacks (despite your pleas for me to stop), Wednesday morning pastries from Westside Market, and Friday hugs, I'm not sure what I will miss the most. Eh, who am I kidding; it's the hugs.

V. Dedication

That which is thicker than water resists the ebb and flow.
It does not rise with the tides, nor recede with the times.
It binds me to
the organ of Abundant Life,
the sidewalks of Marion Hill,
the smoke-filled lungs of J&L.
But also to
church pews reduced to rubble and ash,
festered scabs of dreams deferred,
the stolen immortal life,
forty percent discounts,
and middle passage guests bound by iron chains.

This is for you —
My devoted mothers and invisible fathers.
My Sun and my stars (the blood I chose).
Those whose names were lost paving the stony road I tread.
Those who pushed me from the valley to the summit,
planted beneath the snow ordering my steps.
The ones who made mistakes on my behalf.

The guilty, the ignorant, the unlucky.

— M.M. Sutton

Chapter 1: Background and Motivation

1.1 The Cell Cytoskeleton

The cytoskeleton of eukaryotic cells is comprised of an interconnected network of protein filaments, each of which performs distinct roles that contribute to the overall structure and function of cells (*UC Davis Biological Sciences, 2018*). This network as a whole helps cells maintain their shape and internal organization, while also providing mechanical support; however, the individual filaments themselves also play vital distinct roles (*Microtubules, Filaments | Nature Reviews*, n.d.).

All cytoskeletons consist of three major elements, each of which differs in both size and protein composition, as well as, by nature, cellular function. Microtubules (MTs) are the largest type of filament of the cytoskeleton, with a diameter of about 25 nm. These filaments are formed from two polypeptide globular subunits, called α and β tubulin; heterodimers of these subunits polymerize in a head-to-tail array to form a single linear protofilament, thirteen of which are arranged in parallel to produce a microtubule (*Microtubules: The Basics | Learn Science at Scitable, n.d.*). Consequently, MTs are polarized structures with two distinct ends: a fast-growing plus end and a slow-growing minus end. The ability of microtubules to rapidly assemble and disassemble is facilitated by the ability of tubulin dimers to polymerize and depolymerize within protofilaments as a function of GTP. In short, GTP binds to the β-tubulin monomer of tubulin dimers; the energy from this GTP is used to create the bond with the dimer already existing in the microtubule, so GTP-tubulin is added to the plus end of microtubules. This GTP is hydrolyzed to GDP during or shortly after polymerization, a process which weakens the binding affinity of tubulin for adjacent molecules, thereby favoring depolymerization at the minus end and resulting in the dynamic behavior of microtubules (see Figure 1.1) (*Cooper, 2000b*). In

mammalian cells, the minus ends of microtubules are anchored in (and grow out from) a structure called the microtubule organizing center (MTOC), or centrosome, which is usually located adjacent to the nucleus and comprised of two perpendicular centrioles (a daughter centriole and a mother centriole) linked together by interconnecting fibers (*Centrosome - Structure And Functions Of Centrosome, n.d.*). A third type of tubulin, γ-tubulin, is specifically localized to the centrosome, where it plays a critical role in initiating the aforementioned microtubule assembly. In terms of function, microtubules are known to perform a wide array of tasks. Physically, they provide the basic organization of the cytoplasm, including the positioning of intracellular organelles. They also help the cell to resist compression, transport vesicles, and pull replicated chromosomes to opposite ends of a dividing cell during metaphase. Lastly, microtubules comprise the primary structural elements of flagella and cilia, which are necessary for some forms of cell transport and environmental sensing.

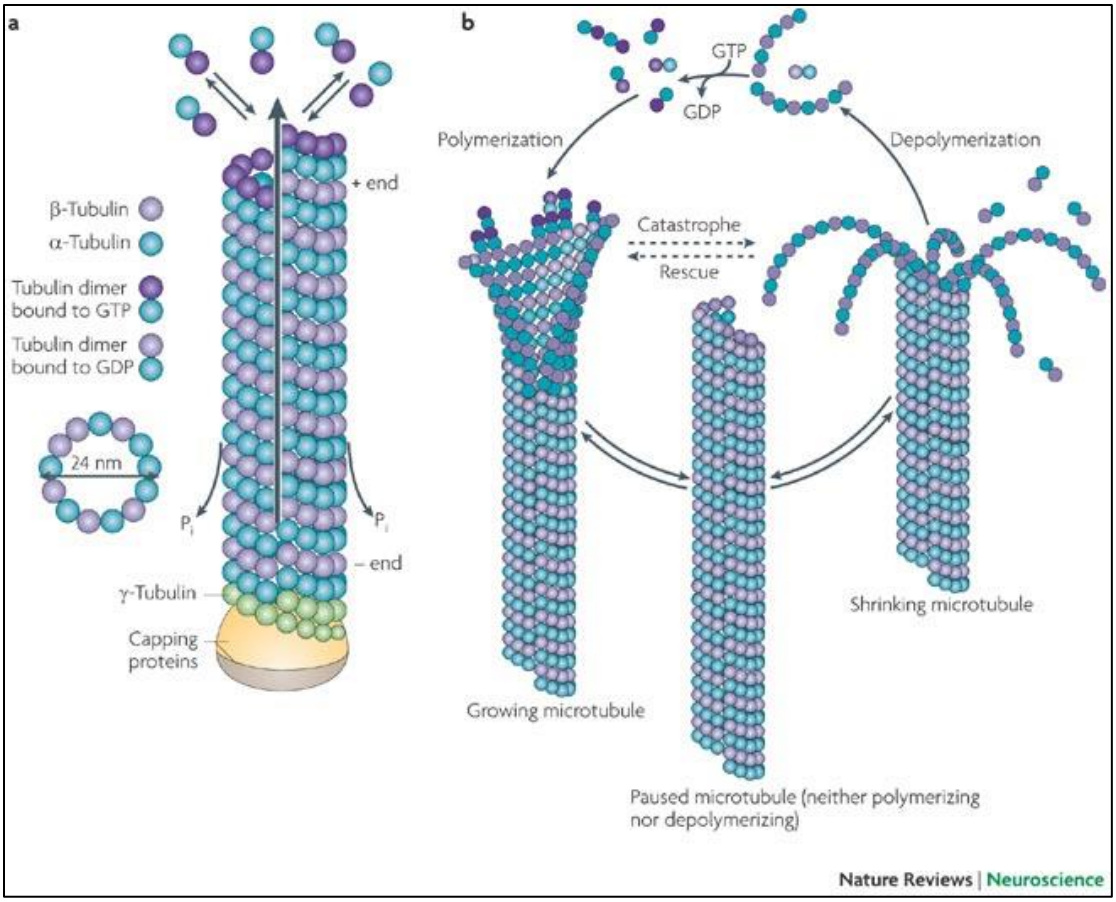

Figure 1.1. Microtubules are major components of the cytoskeleton. Microtubules are composed of alpha- and beta-tubulin subunits assembled into linear protofilaments. A single microtubule contains 10 to 15 protofilaments (13 in mammalian cells) that wind together to form a hollow cylinder. Microtubules are structures that can rapidly grow (via polymerization) or shrink (via depolymerization) in size, depending on how many tubulin molecules they contain (*Microtubules, Filaments | Nature Reviews, n.d.*).

Microfilaments (or, actin filaments, filamentous actin, or F-actin) are the most abundant proteins in most eukaryotic cells. They are the smallest type of filament of the cytoskeleton, with a diameter of about 6 nm. They are composed of G-actin subunits and possess a polarity similar to that of microtubules. Multiple models have sought to characterize the precise mechanism by which actin polymerization is facilitated, one of which is the convergent elongation model: cortical actin comprises a network of branched actin filaments, largely nucleated by the Arp2/3 complex, which is comprised of seven subunits; Arp2 and Arp3 act as monomers from which

new actin filaments elongate in a Y-branch orientation (70° angle) and recruit and hydrolyze ATP, while the other five subunits organize to form the structural core of the complex, providing an interface for binding to preexisting actin filaments and regulatory cofactors (*Goley & Welch, 2006*). In order for this complex to be activated and operate in an optimal capacity, it needs both ATP and any number of nucleation promoting factor (NPF) proteins, such as WASp and WAVE. These specific two proteins exist naturally in an auto-inhibited state and must be activated by either Cdc42 or Rac1, respectively, which induces a conformational change and frees the activating domain of the structure. Simultaneously, the NPF protein binds to G-actin, which strengthens the interaction between Arp 2/3 and the mother actin filament (*Rodnick-Smith et al., 2016*). Once bound, a new daughter filament begins to polymerize from this nucleation site (see Figure 1.2). Functionally, microfilaments are involved in a wide array of cellular processes, such as muscle contraction, cell motility, and cytokinesis.

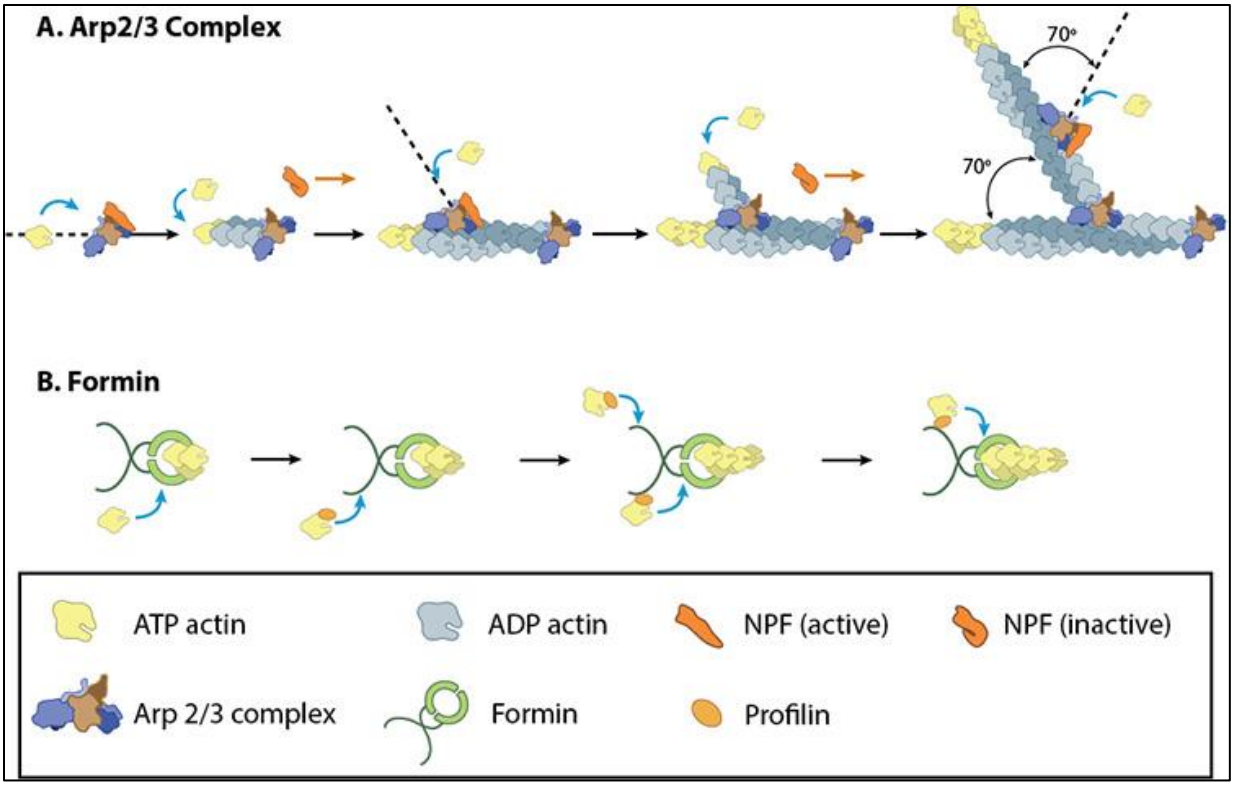

Figure 1.2. Models of actin nucleation. (A) NPFs (e.g., WASp; Scar) bring together the Arp2/3 complex and actin monomers to nucleate new actin filaments and to form new branches from the side of pre-existing filaments. Arp2/3 complex remains at the minus end of the filament. (B) Formin cooperates with profilin to nucleate new actin filaments. Formin remains at the plus end of the filament (*How Does Arp2/3-Mediate the Nucleation of Branched Filaments | MBInfo, n.d.*).

Intermediate filaments are the "medium" sized filaments of the cell cytoskeleton, with a diameter of about 10 nm. They are composed of a variety of proteins that are expressed in different types of cells. More than fifty different intermediate filament proteins have been identified and classified into six groups based on similarities between their amino acid sequences: acidic keratins, neutral/basic keratins, vimentin, neurofilament proteins, nuclear lamins, and nestin (*Cooper, 2000a*). In contrast to actin and microtubules, intermediate filaments are not directly involved in cell movements. Rather, they are thought to play primarily a structural role by providing mechanical strength to cells and tissues, specifically bearing tension,

maintaining the shape of the cell, and anchoring the nucleus and other organelles in place (see Figure 1.3).

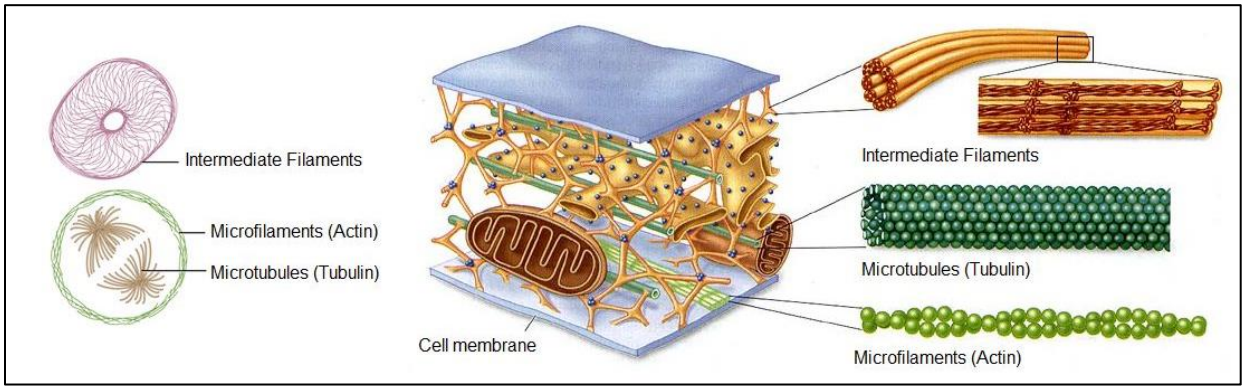

Figure 1.3. Schematic of cell cytoskeleton. Microfilaments thicken the cortex around the inner edge of a cell; like rubber bands, they resist tension. Microtubules are found in the interior of the cell where they maintain cell shape by resisting compressive forces. Intermediate filaments are found throughout the cell and hold organelles in place (*UC Davis Biological Sciences, 2018*).

1.2 Osteoporosis

Osteoporosis is a skeletal disease characterized by significant bone loss, deterioration of bone microarchitecture, and reduced bone strength, clinically diagnosed at the femoral neck or the lumbar spine (see Figure 1.4). This results in a matrix so brittle that even mild stresses, such as bending over or coughing, can lead to a fragility fracture, most commonly occurring in the hip, waist, or spine (*Osteoporosis - Symptoms and Causes - Mayo Clinic, n.d.*). Furthermore, low bone mass (defined using the metric of bone mineral density, or BMD) increases one's risk of developing osteoporosis in the future. There are over 1.5 million fractures annually reported, an incidence greater than the number of strokes, heart attacks, and breast cancer diagnoses combined. The devastation has an economic impact as well, with projected treatment costs accrues a total treatment cost expected to rise in excess of $25 billion USD by the year 2025 (*Blume & Curtis, 2011; Wright et al., 2014*).

There is no known singular cause for osteoporosis; however, a number of factors are thought to significantly affect the likelihood of such a diagnosis. Some risk factors — such as sex, age, and family history — are unchangeable, while such attributes as dietary factors and lifestyle choices can fluctuate. The overarching clinical recommendation is to practice good nutrition and regular exercise to prevent, or at least delay, the onset of osteoporosis (*Osteoporosis Causes & Symptoms | NIAMS, n.d.*).

In a similar vein, there is also no cure for osteoporosis. The most common way to treat osteoporosis and effectively prevent additional bone loss is to take either of two forms of prescription medications: antiresorptive (e.g., bisphosphonates) or anabolic. The mechanism of bisphosphonates is to bind to the surfaces of bones and promote the apoptosis of osteoclasts actively engaged in the degradation of mineral on the bone surface, allowing osteoblasts to comparatively work more effectively (*Drake et al., 2008*). In contrast, anabolic agents promote

bone formation via intermittent release of parathyroid hormone (*Dempster et al., 1993*). While treatment can prove effective for some patients, a wide range of short-term and long-term adverse side effects persist, such as an increased rate of mandibular necrosis, atypical fractures, esophageal cancer, and atrial fibrillation (*Black et al., 2010; Marx, 2003; Reyes et al., 2016*). Thus, there exists an unmet need to identify more efficacious therapeutics for osteoporosis.

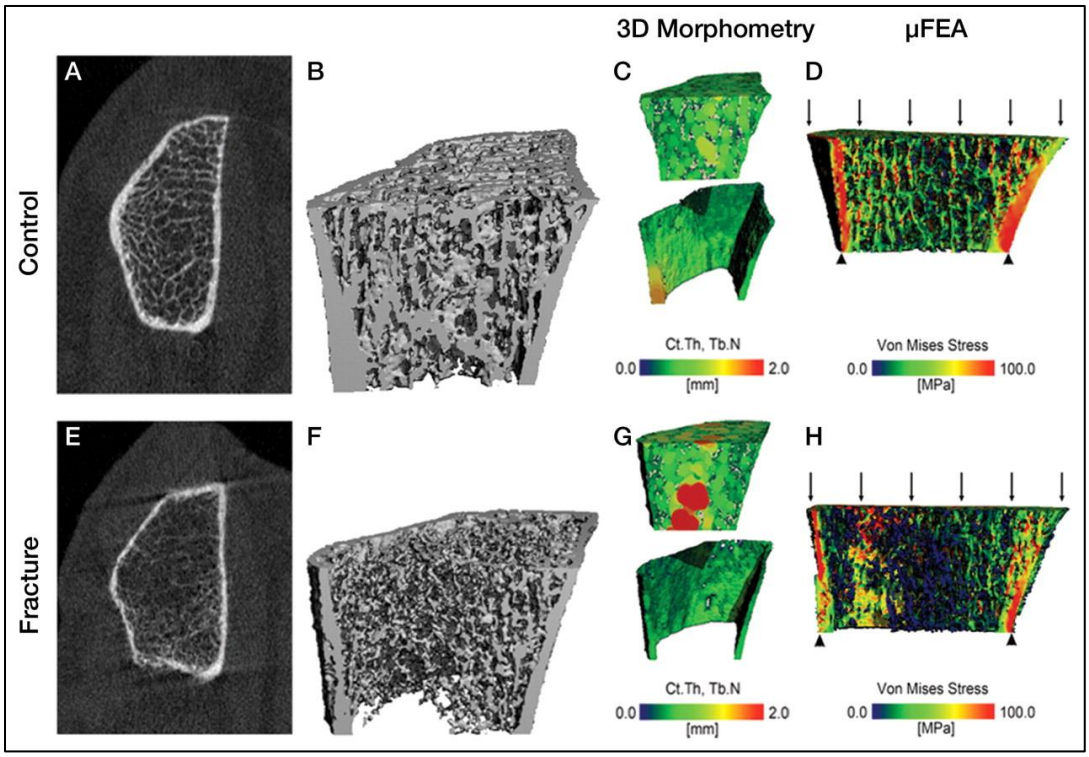

Figure 1.4. HR-pQ CT imaging studies of the distal radius in two postmenopausal women aged 63 and 68 years illustrate bone quality differences between a healthy control subject (top) and a patient with a history of hip and forearm fragility fractures (bottom). A, E, The 2D tomograms and B, F, 3D surface renderings illustrate dramatic differences in cortical and trabecular structure. C, G, These bone quality differences can be quantified by using 3D morphometry to determine cortical thickness (Ct.Th) and trabecular number (Tb.N, the inverse of the intertrabecular distances): The healthy individual exhibits a homogeneous trabecular structure and relatively thick cortex, while the fracture patient has a more heterogeneous distribution of trabeculae and thin cortex. D, H, Microfinite element analysis simulating a 1% compressive load illustrates the irregular distribution of stresses in the fracture subject compared with a more homogeneous distribution in the healthy control subject (*Link, 2012*).

As with any disease, there are epidemiological factors to consider in order to better understand clinical need. Osteoporosis affects individuals of all ages, sexes, and races, but the

relative risks and treatment profiles are vastly different. The U.S. population of individuals over the age of 50 is the most affected, with 2010 data estimating 10 million people in this demographic being diagnosed with osteoporosis and another 43 million diagnosed with low bone mass, encompassing nearly half of all American citizens in this age bracket (*Wright et al., 2014*). With respect to sex, women are four times as likely as men to develop osteoporosis, due in part to the fact that genetically, women start with lower bone density than their male peers while also losing bone mass more quickly as they age. This latter effect is mostly related to estrogen, a hormone primarily responsible for helping regulate a woman's reproductive cycle. However, estrogen also plays a role in keeping bones strong and healthy; while premenopausal women have more estrogen than men, they experience dramatic drops in estrogen production during menopause and are thus more likely to experience bone loss as they age (*Osteoporosis Risk Factors: Are You At Risk?*, *n.d.*; *Why Osteoporosis Is More Common in Women - Osteoporosis Center - EverydayHealth.Com*, *n.d.*). Nonetheless, there exists concern that osteoporosis in men has been severely under-screened and underdiagnosed. Additionally, men tend to have more osteoporosis-related complications than women, such as higher mortality rate after sustaining a hip fracture (*Alswat, 2017*). Lastly, osteoporosis prevalence also varies across race, with non-Hispanic White adults (1.9x), Hispanic adults (2.2x), and non-Hispanic Asian adults (2.7x) much more likely to develop osteoporosis than African-Americans (*"QuickStats: Percentage of Adults Aged ≥50 Years with Osteoporosis, by Race and Hispanic Origin — United States, 2017–2018," 2021*). However, these data make the disparities surrounding osteoporosis screening and treatment by race even more disturbing. One retrospective review found a significant imbalance in recommendation for osteoporosis screening between African-American and White women, with the latter group having screenings for BMD at more than 6x the rate of the former (*Curtis et*

al., 2008). A follow-up study by the same group showed that African Americans are significantly less likely than Caucasians to receive osteoporosis medication, with minority women less likely to receive hormone replacement therapy as well (*Curtis et al., 2009*).

1.3 Skeletal Biology and Bone Remodeling

The skeletal system is the central framework of the human body, consisting of bones as well as connective tissue, such as cartilage, tendons, and ligaments. If an organ is defined as "any part of the body having a special function," then the skeleton is the largest organ in the body, accounting for approximately 20% of our body weight. This biological system as a whole serves a number of vital physiological functions, classified by different groups. Bones of the appendicular skeleton facilitate movement, while bones of the axial skeleton protect internal organs. These bones can be further categorized by shape and function as short, long, flat, sesamoid, or irregular (*Overview of Skeleton | Learn Skeleton Anatomy*, *n.d.*; *Skeletal System*, *n.d.*).

Of particular interest, long bones have two primary parts: the diaphysis and the epiphysis. The diaphysis is the tubular shaft that runs between the proximal and distal ends of the bone. Its internal hollow region is called the medullary cavity, which is filled with yellow marrow, and the exterior walls are composed of compact bone. The wider section at each end of a long bone is called the epiphysis, which is filled with cancellous (spongy) bone and contains red marrow.

Bone cells actually compose only a small amount of total bone volume, but they are crucial to the function of the larger skeletal system. There are four unique types of cells found within bone tissue: osteoblasts, osteocytes, osteoclasts, and osteogenic cells (see Figure 1.5) (*Mohamed, 2008*). Osteoblasts are responsible for forming new bone by synthesizing and secreting the collagen matrix and calcium salts. As the surrounding matrix calcifies, the osteoblast becomes trapped within it; as a result, it changes in structure and becomes an osteocyte, the primary cell of mature bone. Osteocytes are located in a space called a lacuna and help maintain the mineral concentration of the matrix via the secretion of enzymes and regulation of bone remodeling. They can communicate with each other, as well as other skeletal cells, via

long cytoplasmic processes that extend through canaliculi, a series of channels within the bone matrix (*Bone Structure | Anatomy and Physiology I, n.d.*). Osteoclasts are large, multinucleated cells found on the bone surface and are responsible for bone resorption. These cells possess a built-in machinery by which crystalline hydroxyapatite and organic bone matrix are degraded. They are formed via the fusion of both monocytes and macrophages, two leukocytes, and are thus formed from the hematopoietic stem cell lineage, not the mesenchymal line like osteogenic cells (*Väänänen et al., 2000*).

One unique feature of osteoblasts, osteocytes, and osteoclasts is that they are incapable of mitosis. Osteogenic cells are undifferentiated with high mitotic activity and are in fact the only bone cells that divide. Immature osteogenic cells are found in the deep layers of the periosteum and the marrow. They differentiate and develop into osteoblasts, which is how the replenishing of these cells is initiated (*38.2B: Cell Types in Bones - Biology LibreTexts, n.d.*).

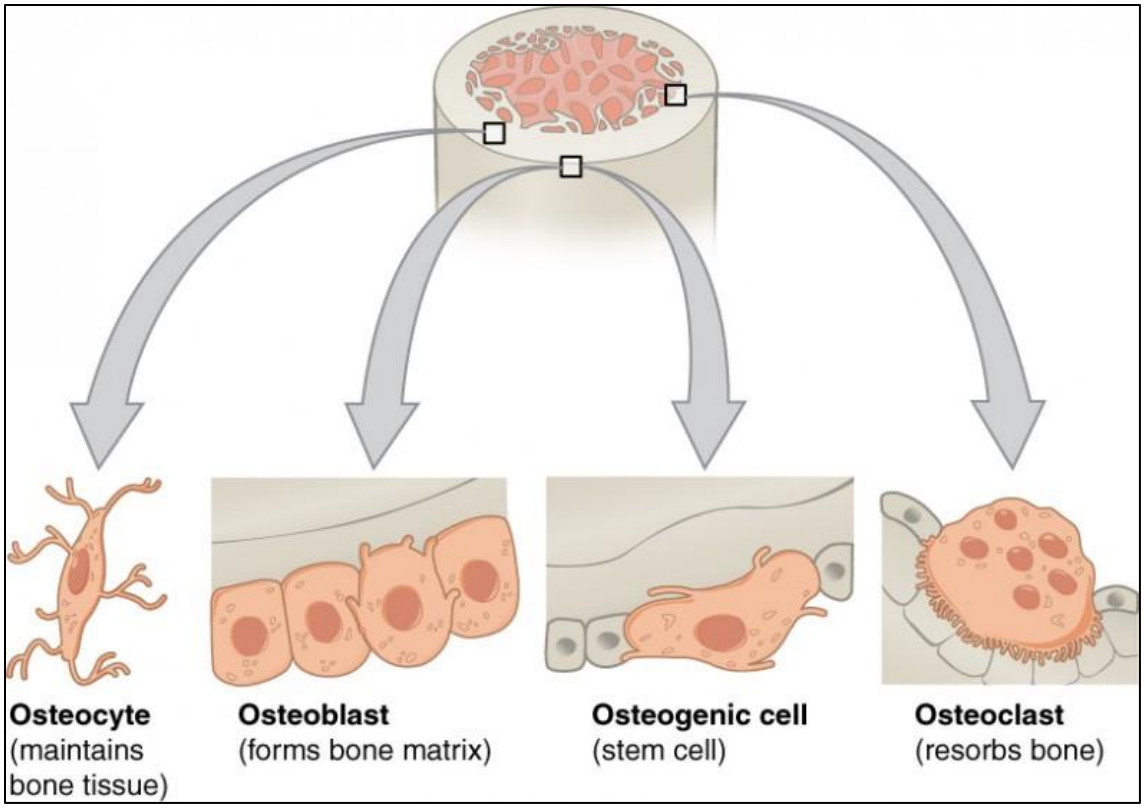

Figure 1.5. Bone Cells. Four types of cells are found within bone tissue. Osteogenic cells are undifferentiated and develop into osteoblasts. When osteoblasts get trapped within the calcified matrix, their structure and function changes, and they become osteocytes. Osteoclasts develop from monocytes and macrophages and differ in appearance from other bone cells (*Bone Structure | Anatomy and Physiology I, n.d.*).

The skeleton is a metabolically active organ that undergoes continuous remodeling throughout the lifespan of vertebrates. Bone remodeling is the process by which old mineralized bone is removed (by osteoclasts) and new bone matrix is formed (by osteoblasts, which then become mineralized themselves). This serves to adjust skeletal architecture and meet changing mechanical needs within the organism (*Hadjidakis & Androulakis, 2006*). On a broader physiological scale, bone remodeling also helps maintain plasma calcium homeostasis. When the body enters a state of hypocalcemia, chief cells of the endocrine system secrete parathyroid hormone (PTH) *in vivo (Kroll & Kroll, 2000*). PTH binds to receptors present on stromal and osteoblastic cells, which in turn generate and release a number of cytokines, including M-CSF,

RANKL, IL-6, and IL-11. RANKL, in particular, is a part of the larger OPG–RANKL–RANK pathway. Receptor activator of nuclear factor-kappa B (RANK) is present both on the surface of monocytes and macrophages (hematopoietic precursors of osteoclasts) and in fully formed osteoclasts. RANK ligand (RANKL) binds to RANK to stimulate precursor fusion and promote mature osteoclast differentiation and survival. These osteoclasts then resorb the bone matrix, effectively recirculating calcium back into the bloodstream. Osteoprotegerin (OPG) acts as a non-competitive inhibitor by binding to RANKL and thereby preventing its access to the receptor RANK, so this mechanism of osteoclastogenesis is effectively modulated by the balance between the RANKL/OPG ratio (see Figure 1.6) (*Nakchbandi et al., 2001; Silva & Bilezikian, 2015*). IL-1, IL-6, and IL-11, which are thought to play a role in several osteolytic bone disorders, also seem to be capable of inducing osteoclast differentiation, but in a manner completely independent of the OPG–RANKL–RANK pathway (*Harmer et al., 2018; Kudo et al., 2003*).

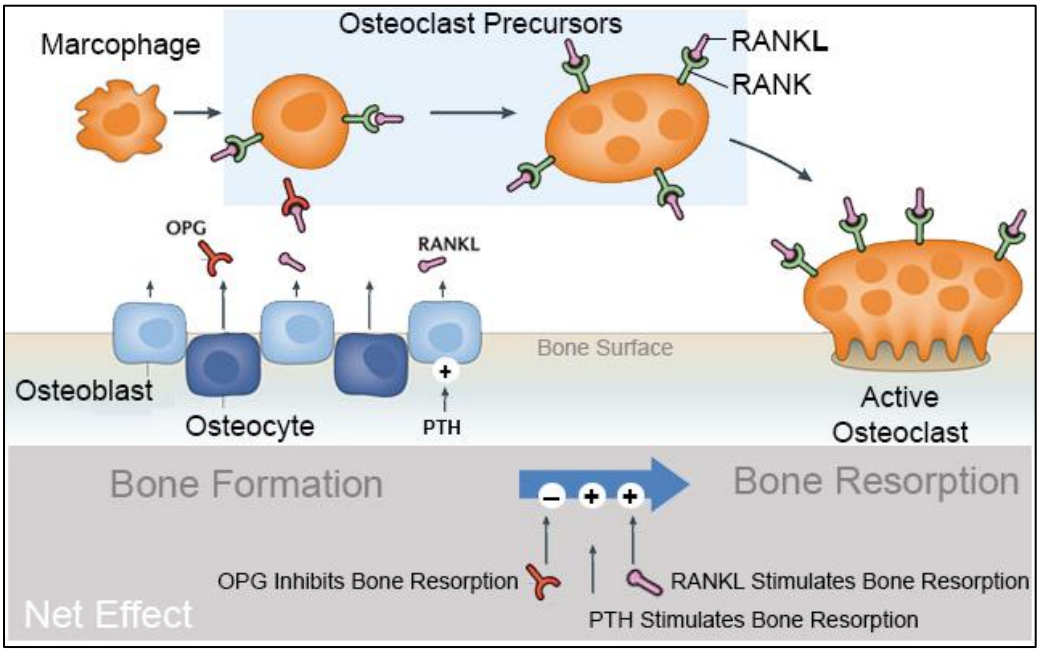

Figure 1.6. Schematic of osteoclastogenesis (*Bone Signaling & RANKL - Basic Science - Orthobullets, n.d.*)**.**

1.4 Primary Cilia and Mechanosensing

Cilia are microtubule-based, antenna-like organelles that extend from the surface of nearly every cell type of vertebrates. Most cell types assemble only one cilium (a primary cilium), whereas some cells build cilia bundles that consist of hundreds of cilia *(Fliegauf et al., 2007*). These primary cilia are distinct from those of multi-ciliated cells in both structure and function (see Figure 1.7). The primary cilium is a dynamic, immotile organelle that assembles and disassembles in a cell-cycle-dependent manner. Although primary cilia share some basic structural properties to their oft-studied counterparts, there are a number of distinct differences. Motile (secondary) cilia have structures based in a "9x2+2" microtubule arrangement (nine outer microtubule couplets surrounding two inner microtubule singlets), while that central inner pair of microtubules is absent from primary cilia (which are arranged as a "9x2+0") and explains the lack of motility capabilities. Primary cilia are also marked by heavy acetylation of axonemal tubulin. It is believed that these structural differences give way to primary cilia's functional differences as well. Motile cilia are mainly responsible for moving water and other contents across cell surfaces; one such example exists in the epithelial cells that line the human respiratory tract, where cilia constantly move mucus up from the lungs to the back of the throat (*Ainsworth, 2007*). Primary cilia were first observed in the mid-19th century but were long thought to be vestigial organelles without a clear function (*Beales & Jackson, 2012*). Since the 1990s, scientists have conducted more research on the primary cilium and implicated it as a contributor to vital physiological roles, such as chemical sensation, mechanical signal transduction, and control of cell growth. Today, it is broadly understood as a sensory cellular antenna capable of coordinating signaling pathways, supported by the prevalence of ciliopathies, such as autosomal dominant polycystic kidney disease (ADPKD) and Bardet-Biedl syndrome (BBS) (*Copelovitch & Kaplan, 2012; Satir & Christensen, 2008*).

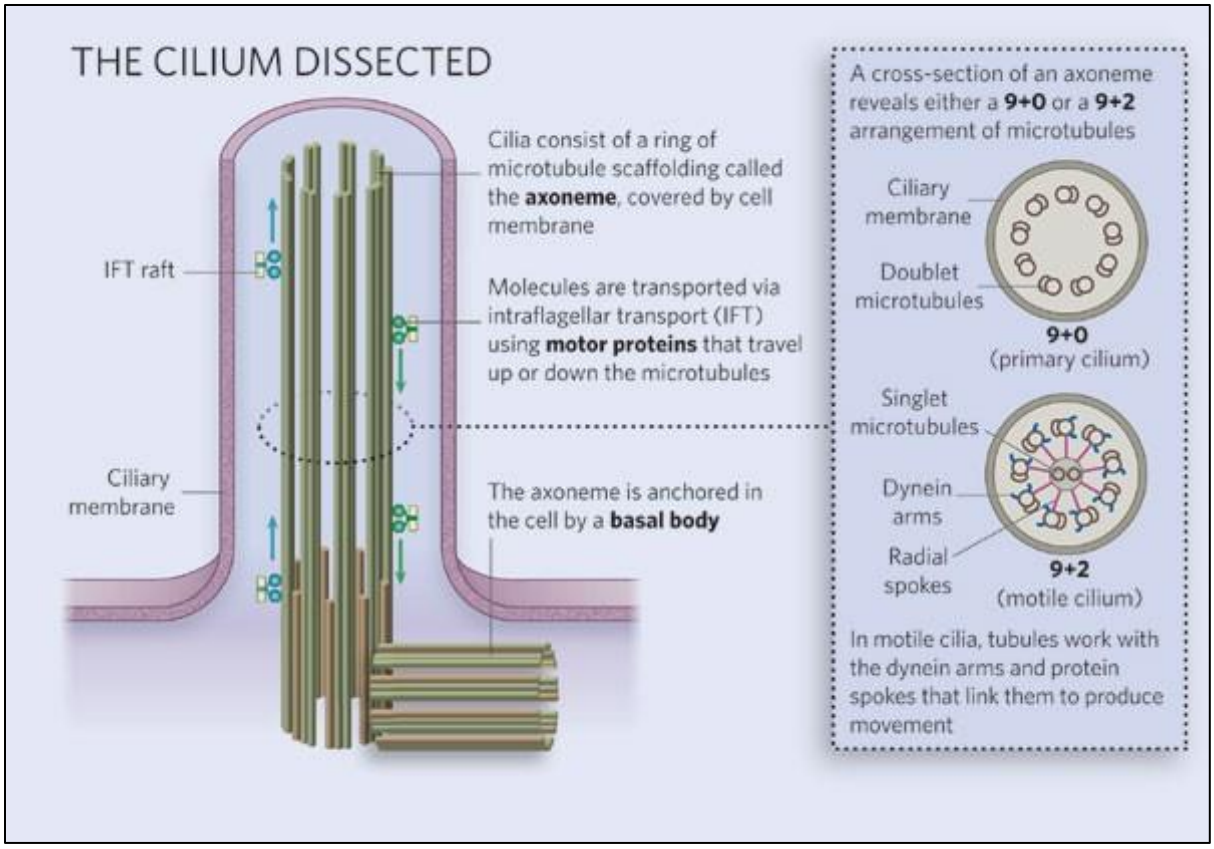

Figure 1.7. Diagram of primary ciliary structure. A cilium possesses a number of subcompartments: a basal body, axoneme, ciliary membrane, and intraflagellar transport proteins (*Ainsworth, 2007*).

Continued regulation and homeostasis of skeletal development requires mechanical stimulation. Physical loading induces adaptive changes in bone that strengthen the overall bone structure. This response is regulated by the ability of certain cells, primarily osteocytes, to perceive and translate mechanical energy into a cascade of biochemical changes — a process known as mechanotransduction *(Robling & Turner, 2009*). Similarly, a lack of regular bone loading causes the architecture to weaken. At the cellular level, disuse results in osteocyte apoptosis and imbalanced bone resorption, leading to severe osteoporosis (*Bergmann et al., 2011*). Osteocyte ablation in a mouse model was shown in a previous study to result in increased intracortical porosity and decreased sensitivity to unloading, suggesting that osteocytes play a major role in mechanotransduction in bone (*Tatsumi et al., 2007*). Some researchers have

described this transduction process in terms of stages: 1) mechanical loading induces a cellular-level physical signal that can be sensed by the osteocyte, 2) the physical signal is transduced into a biochemical signal, and 3) the biochemical signal is communicated to other cells in the system (*Burger et al., 1995*). For some time, the mechanism(s) by which mechanical loading leads to biochemical signals in these cells was not well understood. The primary cilium was eventually identified as a likely extracellular sensor of mechanical loading in bone, as this organelle had previously been implicated in the mechanosensing abilities of the kidney *(Praetorius & Spring, 2001, 2003*). Many follow-up studies expounded on the present-day understanding of primary cilia with respect to skeletal remodeling and maintenance. A 2007 study revealed that osteocytes respond to fluid flow with cilia-dependent increases in *Cox-2* gene expression and PGE_2 release. Flow-induced increases in the OPG/RANKL ratio were eliminated with cilia removal through pharmacological agents or siRNA knockdown of *Ift88*; however, these results were independent of intracellular Ca^{2+}, suggesting that the cilia mechanotransduction signaling pathway in bone differed from previously studied organs (*Malone et al., 2007*). A 2017 study demonstrated not only the ability of the osteocyte primary cilium to be potentiated (increases in incidence and length via fenoldopam and lithium), but also that such manipulations increased osteocyte mechanosensitivity, implicating cilium length as a potential therapeutic target for combating numerous conditions characterized by impaired cilia function, especially within the skeletal system (*Spasic & Jacobs, 2017*).

1.5 Osteoclast Impact and Significance

Because skeletal loading is a natural anabolic stimulus, targeting the cellular mechanosensing system of bone could potentially unlock new therapeutic approaches to treatment. Several studies have previously identified the osteocyte primary cilium as a promising pharmaceutical target to exploit the body's natural response to physical loading (*Malone et al., 2007*). A number of ciliopathies (e.g., Bardet-Biedl syndrome) exhibit skeletal patterning defects and even low bone mass (*Nguyen & Jacobs, 2013; Xiao & Quarles, 2010*). Despite very evident links between these ciliopathies and bone pathology, the role of primary cilia in bone remodeling processes and bone diseases remains understudied. Most notably, while many studies have focused on understanding primary cilia of osteoblasts and osteocytes, very little is known about the potential impact of targeting the primary cilium in relation to osteoclasts, the bone-resorbing cell that oft-prescribed bisphosphonates specifically target. Thus, the objective of Aim 1 of this research focuses on this gap in knowledge. Specifically, we dissected the origin of osteoclast formation, investigated the absence/presence of primary cilia with respect to osteoclasts and their precursors, and lastly characterized a functional role of primary cilia with respect to osteoclast formation and maturation.

1.6 Cancer

Under normal physiological conditions, most human cells grow and divide in a controlled process, and when they become old or damaged, they die so that new cells can take their place. Whenever this orderly process breaks down, abnormal cells are permitted to grow and proliferate. Such cells have the capacity to form benign or malignant tumors, the latter of which invade nearby tissues and often metastasize. Additionally, rather than forming solid tumors, some malignant cells instead flood the bloodstream, developing from cells of hematopoietic lineage (*What Is Cancer? - National Cancer Institute, n.d.*). Cancer is a disease which is characterized by the uncontrollable growth and spread of such malignant cells. These cells suppress, evade, and exploit the natural function of the immune system, ultimately destroying bodily tissue in the process.

Malignant transformation is the complex process by which cancerous cells develop from healthy cells (Figure 1.8). The first step in cancer development is initiation, whereby a mutation in a cell's DNA primes the cell to become cancerous. This may occur genetically, epigenetically, or as the result of a carcinogen (*What Does It Mean to Have a Genetic Predisposition to a Disease?: MedlinePlus Genetics, n.d.*). In a healthy, normally functioning cell, proto-oncogenes help facilitate cell growth, while tumor suppressor genes instruct cells on when to stop growing, when to repair damaged DNA, and when to die. Most cancer cells have mutations in both oncogenes and tumor suppressor genes, which lead to their uncontrolled behavior (*Cancer Cells: Types, Formation, and Characteristics, n.d.*). The second step of transformation, promotion, is facilitated by promoters, which are substances in the environment. Unlike carcinogens, promoters do not cause cancer by themselves; rather, they allow a cell that has already undergone initiation to progress to the point of becoming cancerous (*Development and Spread of Cancer - Cancer - Merck Manuals Consumer Version, n.d.*). It is worth noting that some

carcinogens are sufficiently potent to cause cancer without the need for promotion (e.g., ionizing radiation). It is in the promotion stage of development that hyperplasia and dysplasia are observed. The final step of cancer progression is spread, the type of which varies by type of cancer. Cancer cells can directly invade surrounding tissue or spread to more distant tissues and organs in a process known as metastasis. In carcinoma and lymphoma, cancer cells spread throughout the lymphatic system, while cancer spreading via the blood stream is typical of sarcoma and leukemia (*Cancer Overview | The University of Kansas Cancer Center, n.d.*).

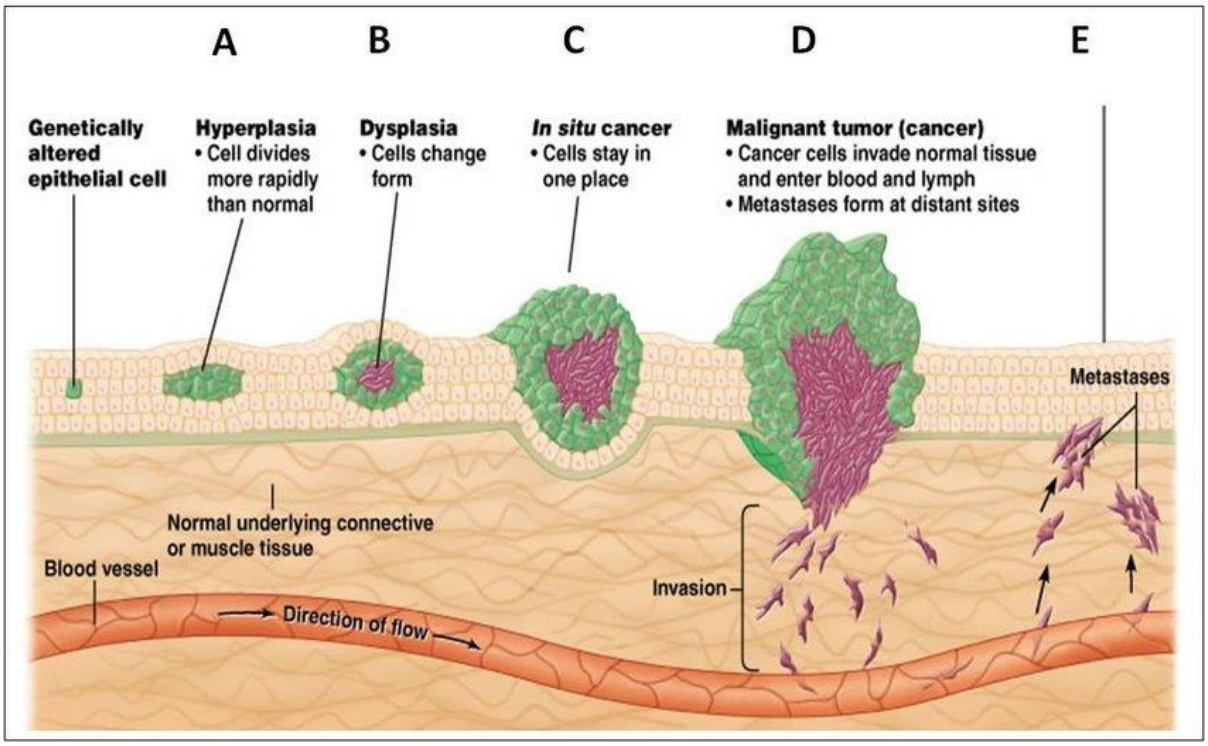

Figure 1.8. Stages of tumor development and mechanism of metastasis (*Kanwal et al., 2013*).

Part of the biological rationale for why cancer is such a debilitating illness is that cancer cells learn how to avoid being recognized and/or destroyed by the immune system's built-in mechanisms. The genetic mutations give cancer cells any number of biological advantages that enable their immune system-evading abilities. Some cancer cells downregulate their own MHC I expression, making it more difficult for lymphocytes to detect their presence, while others can

secrete immunosuppressive molecules to inhibit a full immune response. A more complex but involved process takes advantage of a naturally presenting receptor on cells of the immune system (*The Immune System and Cancer | EdCaN, n.d.*). PD-1 is an inhibitor of both adaptive and innate immune responses and is highly expressed on tumor-specific T cells. It functions in two opposing roles: reducing the regulation of ineffective or harmful immune responses and maintaining immune tolerance (which is beneficial) but also causing the amplification of malignant cells by interfering with the protective immune response. PD-L1 is expressed by cancer cells and acts as a pro-tumorigenic factor by binding to its PD-1 receptors and activating proliferative and survival signaling pathways for itself by dampening the T cell's response *(Han et al., 2020*). In a similar capacity, CD80 and CD86 of APCs bind to the CTLA-4 receptor of T cells, which keeps them in an inactive state.

Because cancer is caused by genetic alterations, the notions around the concept of efficacious prevention efforts are ever-evolving. However, it is widely accepted in the scientific community that one's chances of developing cancer are deeply impacted by the lifestyle choices they make. Maintaining a healthy diet and exercise, as well as avoiding carcinogens and exposure to radiation, are generally recommended to reduce cancer risk (*Cancer Prevention: 7 Tips to Reduce Your Risk - Mayo Clinic, n.d.*). When prevention measures are ignored or fail, the goal of treatment becomes to achieve a complete cure for a patient's cancer, allowing them to live a normal life span. If a cure is not feasible, treatments may be used instead to shrink tumor size or decelerate the cancer's spread to improve prognosis. After a diagnosis, any number of treatments (and sometimes a combination of multiple) may be prescribed. Some treatments are local (e.g., surgery or radiation therapy), which are used to treat a specific tumor or area of the body. Drug treatments (e.g., chemotherapy, immunotherapy, or targeted therapy) are often called

"systemic" treatments because they can affect the entire body (*Cancer Treatment Options | Houston Methodist, n.d.*; *Types of Cancer Treatment | American Cancer Society, n.d.*). A treatment plan may also include multiple treatments to serve varying purposes. The goal of primary treatment is to completely destroy all of the cancer cells in a patient's body, so local treatments are very commonly utilized. Adjuvant treatment aims to kill any cancer cells that may remain after primary treatment has been implemented in order to reduce the chance of recurrence. Palliative treatments are used to relieve side effects of treatment or symptoms caused by cancer itself, so they may be used concurrently with primary and adjuvant treatments (*Cancer Treatment - Mayo Clinic, n.d.*).

A recent increase in both prevalence and burden of cancer in the United States has heightened the urgency with which novel therapies are increasingly being studied and developed. In 2020, the National Cancer Institute (NCI) estimated more than 1.8 million new cases of cancer with over 600,000 cancer-related deaths, making it the second-leading cause of death in the country (*Cancer Statistics - National Cancer Institute, n.d.*). In 2018, estimated national expenditures for cancer care in the United States were $150 billion USD, and costs are likely to increase in future years as the population ages and more people develop cancer.

In the past few decades, the scientific community has witnessed remarkable progress in the understanding of cancer initiation and progression, which has led to refinement of prevention and treatment approaches. Although these advancements have improved the survival rates of cancer patients in general, a closer look at cancer statistics indicates that certain racial groups are affected disproportionately with regard to cancer incidence, age of onset, aggressiveness, and mortality (*Deshmukh et al., 2017*). While this is in-part due to socioeconomic and environmental factors (e.g., poverty, access to healthcare and/or insurance, health literacy, and differences in

behavior and culture), emerging data now suggest that biological factors at the genetic and epigenetic levels can also be crucial for understanding racial inequalities in cancer incidence and clinical outcomes (*Wallace et al., 2011*). Moreover, these health disparities exist with regards to cancer screening as well as treatment. For example, with regards to prostate cancer, Black men are 1.8 times more likely to be diagnosed and 2.2 times more likely to die from prostate cancer than White men (*Cancer Disparities — Cancer Stat Facts*, *n.d.*). In addition, recent data show that while breast cancer incidence is very similar in both Black and White women, Black women are 42% more likely to die from the disease, and twice as likely when adjusted for age (*Yedjou et al., 2019*). They are also significantly less likely to receive breast cancer surgery as part of their treatment plan, evidence that more needs to be done not only with respect to screening and diagnosing with respect to certain ethnic demographics, but also in the way that treatment is prescribed.

1.7 Emergence of Immunotherapy

Although traditional methods of cancer treatment (e.g., surgery, chemotherapy, radiotherapy) have been successful in destroying cancer cells in some circumstances, these therapies possess substantial limitations, primarily related to an inability to selectively target malignant cells and a tendency to cause severe damage to healthy tissues (*Pettitt et al., 2018*). These conventional methods are also associated with a slew of side effects, including but not limited to alopecia, nausea, and neutropenia. As a result, there exists an unmet need to develop enhanced therapies for cancer that are more target-specific and pose fewer side effects. In particular, one therapeutic approach, rather than directly targeting the tumor, seeks to instead calibrate an individual patient's immune system to more effectively respond to cancer cells which easily evade its natural protective measures and prove resistant to traditional treatments; this approach is broadly known as immunotherapy (*Treating Cancer with Immunotherapy | Types of Immunotherapy*, *n.d.*). Mechanistically, immunotherapies have the capacity to function in three different ways: program the immune system to attack specific cancer cells, boost the number and effect of immune cells, and provide the body with additional components to enhance the immune response (*What Is Immunotherapy - Cancer Research Institute (CRI)*, *n.d.*).

One promising immunotherapeutic approach in recent years with application in a number of cancers has been the use of checkpoint inhibitors. Within the immune system, the role of checkpoints is to prevent vigorous immune responses from destroying healthy cells in the body. They carry out this role by engaging with antigens of binding-cells, sending an "off" signal to the T cell itself. As a result, checkpoint inhibitors work by preventing these checkpoint proteins from binding, allowing the T cells to activate and kill cancer cells (*Immune Checkpoint Inhibitors - National Cancer Institute*, *n.d.*). Pharmacologically, the three most common checkpoints targeted in therapies are PD-1, PD-L1, and CTLA-4, with a number of drug treatments already FDA-

approved for application in many cancers (see Table 1.1). Inhibitors of these molecules effectively turn off the T-cell's safety mechanism and allow it to activate. However, this inhibition simultaneously unleashes the mechanism by which the body can attack itself. Thus, many checkpoint inhibitors result in immune-dysfunction side effects, such as pneumonitis or myocarditis (*Martins et al., 2019*).

Checkpoint Protein	Inhibitor	Manufacturer	Inhibitive Mechanism
PD-1	Pembrolizumab (Keytruda)	Merck	Competitive inhibition (binds to PD-1, blocking the active site from PD-L1 access)
	Nivolumab (Opdivo)	Bristol Myers Squibb	
	Cemiplimab (Libtayo)	Regeneron	
PD-L1	Atezolizumab (Tecentriq)	Genentech	Non-competitive inhibition (binds to PD-L1, preventing the ligand from binding to PD-1)
	Avelumab (Bavencio)	EMD Serono	
	Durvalumab (Imfinzi)	AstraZeneca	
CTLA-4	Ipilimumab (Yervoy)	Bristol Myers Squibb	Competitive inhibition (binds to PD-1, blocking the active site from PD-L1 access)

Table 1.1. Summary list of oft-prescribed checkpoint inhibitors (*Checkpoint Inhibitors | Types of Immunotherapy | Cancer Research UK, n.d.*)**.**

One of the primary modalities within cancer immunotherapy, with hopes of creating clinically feasible treatments, has been adoptive T cell therapy. Under this approach, patient T cells are isolated, modified, expanded, and transfused back into the patient with the goal of increased recognition, targeting capacity, and programmed death of tumor cells *(Perica et al., 2015*). A group from the NCI was the first to demonstrate that this therapy was actually effective in curing forms of advanced cancer (*Topalian et al., 1987*). The concept branched off some years later as scientists were able to engineer T cells with the first chimeric molecule, which consists

of a portion of an antibody fused to a T cell receptor. Further evolution and design of these receptors eventually led to clinical trials against multiple blood and solid tumor types, with the Food and Drug Administration (FDA) approving the first CAR T cell therapy in 2017 (*FDA Approval Brings First Gene Therapy to the United States | FDA, n.d.*). Chimeric antigen receptor (CAR) T-cell therapy extracts T-cells from a patient's blood and mixes them with a special virus that improves the T-cells' recognition and binding affinity for tumor cells. Then, these genetically modified T cells are reinserted into the patient (see Figure 1.9). There are currently six CAR T-cell therapies that have been approved by the FDA (see Table 1.2).

FDA-Approved CAR T-Cell Therapies

Generic Name	Brand Name	Target Antigen	Targeted Disease	Patient Population
Tisagenlecleucel	Kymriah	CD19	B-cell acute lymphoblastic leukemia (ALL)	Children and young adults with refractory or relapsed B-cell ALL
			B-cell non-Hodgkin lymphoma (NHL)	Adults with relapsed or refractory B-cell NHL
Axicabtagene ciloleucel	Yescarta	CD19	B-cell non-Hodgkin lymphoma (NHL)	Adults with relapsed or refractory B-cell NHL
			Follicular lymphoma	Adults with relapsed or refractory follicular lymphoma
Brexucabtagene autoleucel	Tecartus	CD19	Mantle cell lymphoma (MCL)	Adults with relapsed or refractory MCL
			B-cell acute lymphoblastic leukemia (ALL)	Adults with refractory or relapsed B-cell ALL
Lisocabtagene maraleucel	Breyanzi	CD19	B-cell non-Hodgkin lymphoma (NHL)	Adults with relapsed or refractory B-cell NHL
Idecabtagene vicleucel	Abecma	BCMA	Multiple myeloma	Adults with relapsed or refractory multiple myeloma
Ciltacabtagene autoleucel	Carvykti	BCMA	Multiple myeloma	Adults with relapsed or refractory multiple myeloma

Table 1.2. Summary list of FDA-approved CAR T-cell therapies (*CAR T Cells: Engineering Immune Cells to Treat Cancer - National Cancer Institute, n.d.*)**.**

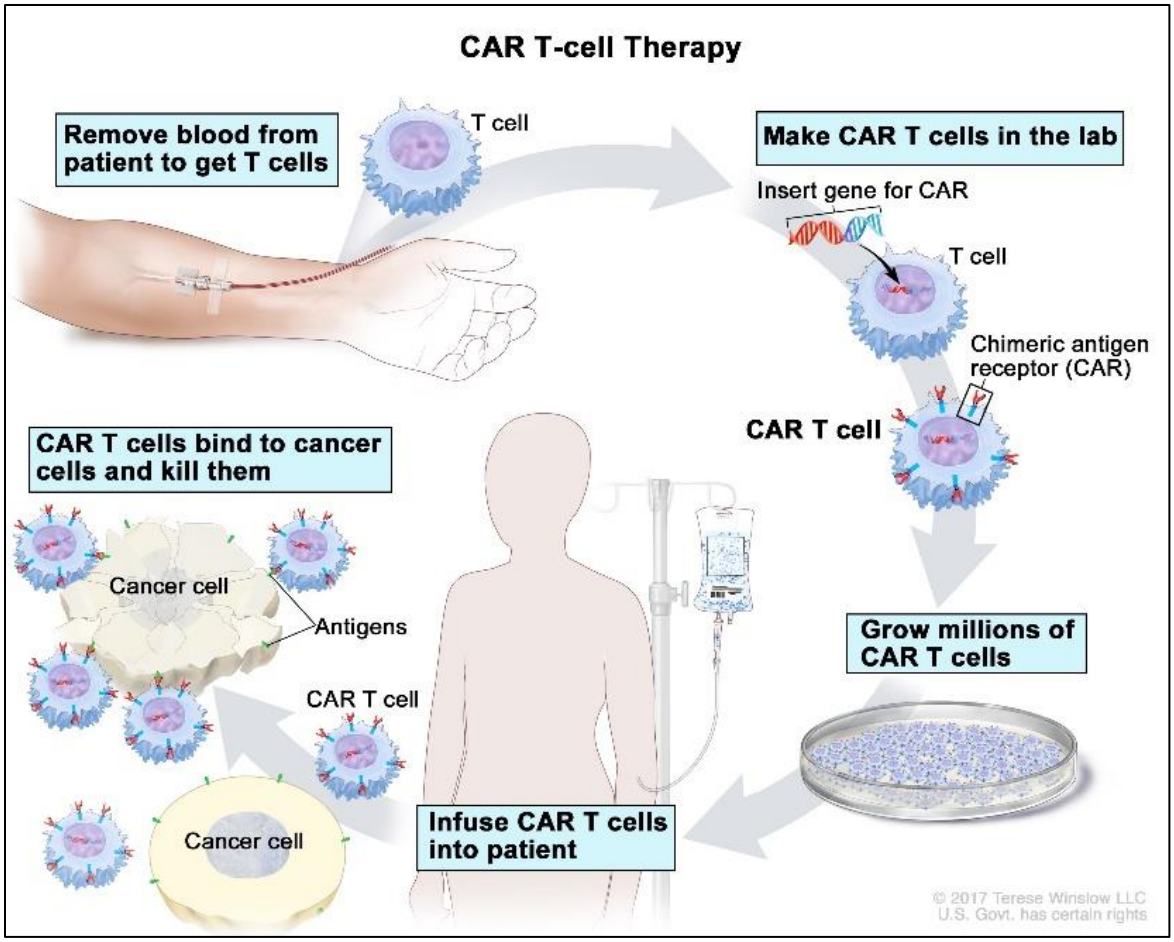

Figure 1.9. CAR T-cell therapy. Blood from a vein in the patient's arm flows through a tube to an apheresis machine (not shown), which removes the white blood cells, including the T cells, and sends the rest of the blood back to the patient. Then, the gene for a special receptor called a chimeric antigen receptor (CAR) is inserted into the T cells in the laboratory. Millions of the CAR T cells are grown in the laboratory and then given to the patient by infusion. The CAR T cells are able to bind to an antigen on the cancer cells and kill them (*Definition of CAR T-Cell Therapy - NCI Dictionary of Cancer Terms - National Cancer Institute, n.d.*).

Despite its overwhelming potential, CAR-T therapy also faces significant limitations. Treatment can induce a range of side effects, such as eliciting neurological toxicity, off-target effects, and anaphylaxis (*Bonifant et al., 2016*). Furthermore, T-cell manufacturing is a significant hurdle in and of itself, as T-cell therapies require production of a therapeutically relevant number of cells which must be frozen, transferred, thawed, and repeated to send the engineered product back to clinical facilities (*Dwarshuis et al., 2017; X. Wang & Rivière, 2016*).

Thus, failure to produce an adequate number of T cells is an issue that needs to be addressed. One reason for the lack of success is a low initial quantity and quality of T cells isolated from patients, which is a function of high donor variability and relative impact of disease. Many research efforts have focused on improving the process of T cell production, which, from a biological and cell physiology standpoint, starts with an understanding and regulation of immunity and T-cell activation.

1.8 Innate vs. Adaptive Immunity

The immune system is comprised of a complex network of organs, cells, and proteins that defend the body against pathogens. It is equipped with a two-part defense mechanism to fight off invaders once they've entered the body: the innate response and the adaptive response, which work both sequentially and in tandem.

The innate immune response essentially acts as the first line of defense, beginning within mere hours of foreign invasion. It is comprised of three types of obstacles that are designed to keep foreign particles out of the body or limit internal spread if such particles penetrate the body: 1) physical barriers (e.g., skin, hair, GI tract), 2) macro defense mechanisms (e.g., mucous, saliva, sweat), and 3) general immune responses (e.g., inflammation and non-specific cellular responses). This lack of specificity is a hallmark of the innate immune response: anything in the body appearing as "non-self" (indicated by the presence of antigens and chemical properties) becomes a target (*Alberts et al., 2002*).

The cells primarily responsible for mediating the innate immune response are phagocytes, a broad term describing leukocytes that carry out phagocytosis (e.g., macrophages, neutrophils, dendritic cells, etc.) In order to distinguish self from non-self, the innate immune system utilizes microbial structures called pathogen-associated molecular patterns (PAMPs), which are common characteristics of many pathogens but absent in the host species. To facilitate recognition, each of these phagocytes has pattern recognition receptors (PRRs) on their cell surface responsible for identifying foreign surface proteins of invaders. The phagocyte then engulfs the pathogen within a vesicle, forming a phagosome. There also exist within phagocytes lysozyme-containing vesicles, which merge and dump their hydrolytic contents into the phagosome to digest the pathogen. The phagocyte then isolates a small portion of pathogen-peptide, fuses it to a major histocompatibility complex type 2 (MHC II), and presents this new complex, pMHC, as an

antigen on the surface of its cell membrane; for this reason, phagocytes are also referred to as antigen-presenting cells (APCs) (see Figure 1.10) (*Mantegazza et al., 2013*).

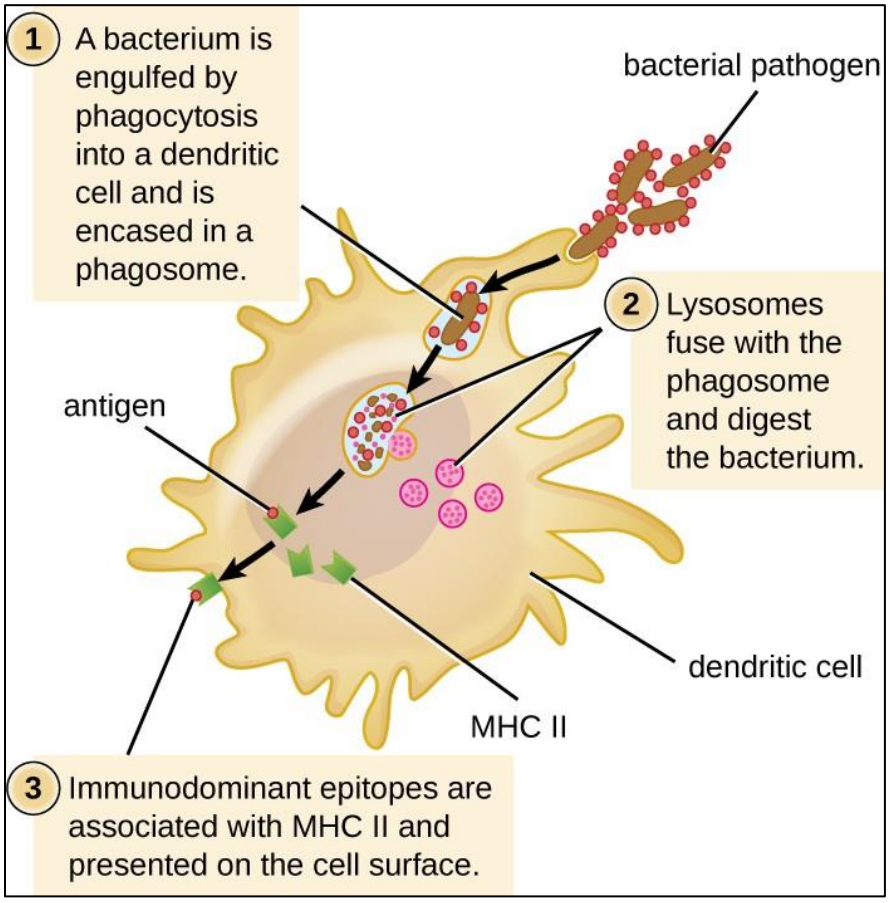

Figure 1.10. A dendritic cell phagocytoses a bacterial cell and brings it into a phagosome. Lysosomes fuse with the phagosome to create a phagolysosome, where antimicrobial chemicals and enzymes degrade the bacterial cell. Proteases process bacterial antigens, and the most antigenic epitopes are selected and presented on the cell's surface in conjunction with MHC II molecules. T cells recognize the presented antigens and are thus activated (*Parker et al., 2016*).

The adaptive immune response, which is much slower but much more targeted and specific than the innate response, is carried out by lymphocytes and has two components itself: the humoral response and the cell-mediated response. The humoral response involves B cells and is directly useful for pathogens that have not yet infiltrated any cells. As these bacteria or viruses are freely floating, a B cell whose B-cell receptor (BCR) presents a paratope specific to that pathogen will bind, engulf, and present a pathogen-peptide (similar to phagocytes). That B cell

then produces and secretes copies of antibodies with its BCR that bind to more pathogenic cells, while also differentiating and dividing into many effector cells that will do the same. These effector (or, plasma) cells can produce two thousand antibodies per second, triggering the initiation of an antibody-making factory that puts the immune system on high alert. The primary function of these antibodies is that they bind to the antigens of the pathogen copies, making them more noticeable and more likely to be consumed by phagocytes. It also presents a structural hindrance that makes cell-infiltration more difficult.

The cell-mediated response is essentially designed to pick up where the innate system leaves off. CD4+ (helper) T cells have receptors designed with the same specificity as B cells: during maturation in the thymus, the fragment of DNA that codes for the variable portion of the TCR undergoes intentional shuffling, a genetic feature that creates thousands of unique T cells. One of these T cells has a TCR that will bind to the pMHC of an antigen-presenting cell that has recently phagocytized a given pathogen. This naïve T cell binds to the APC and initiates activation, whereby it differentiates into both effector and memory cells and begins proliferating. Meanwhile, CD8+ (cytotoxic) T cells, with their own unique TCRs, are responsible for destroying cells that have already been infected.

1.9 T-Cell Activation, the Immune Synapse, and the Cytoskeleton

During the first, cell-mediated response, each helper T cell (T_h) possesses a T-cell receptor with a unique epitope that only binds to a specific peptide-MHC II complex. Within minutes of T-cell receptor recognition of pMHC ligands, an area begins to form at the portion of the T-cell membrane that is in direct and stable contact with the APC: this region is called the immunological synapse (IS) (Figure 1.11) (*K. Murphy, 2012*).

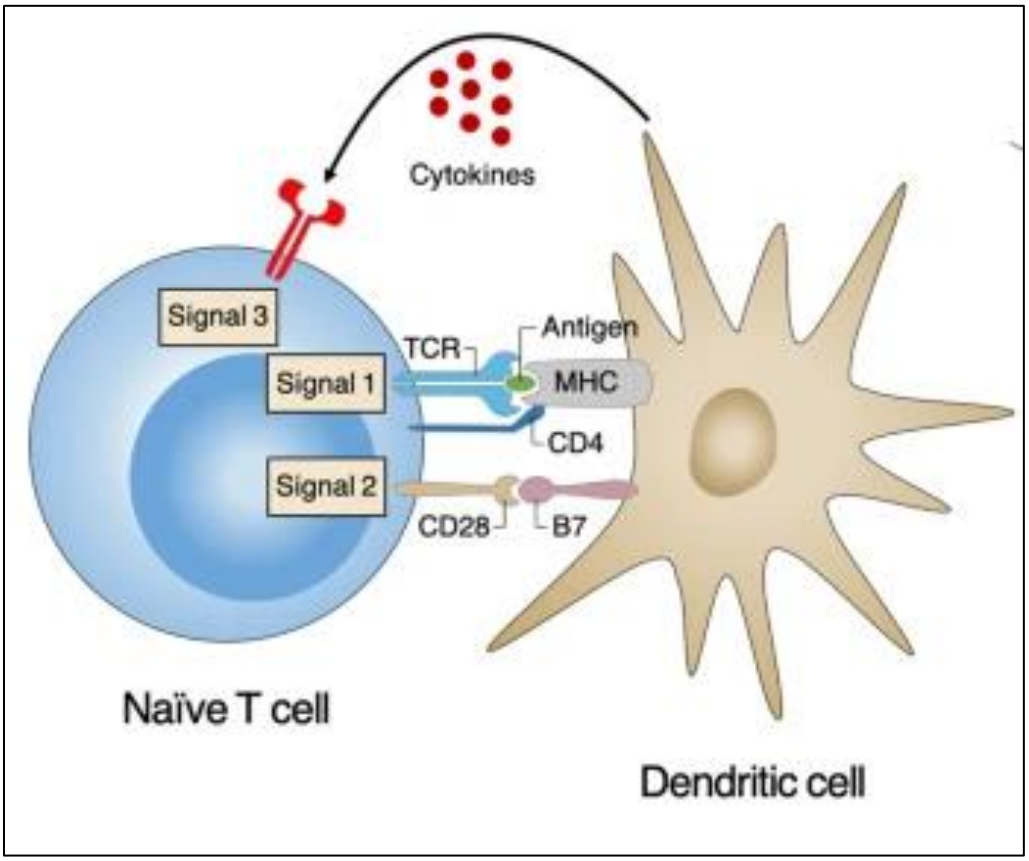

Figure 1.11. Antigen-specific T-cell activation requires three distinct signals. Signal 1 is antigen-specific signaling mediated by TCR engagement of pathogenic peptides presented by MHC molecules. Signal 2 is costimulatory signaling, which is mainly mediated by the interaction of CD28 with one of the B7 molecules (CD80 and CD86). Signal 3 is polarizing signaling mediated by various cytokine milieus produced by dendritic cells (*H. G. Lee et al., 2020*).

One early feature and regulatory mechanism of T-cell activation after synapse formation is the induction of cytoskeletal reorganization. A burst of actin polymerization is triggered upon TCR stimulation, leading to an enhancement of the cell-APC contact area as the T cell spreads over the surface of the APC (*Hui et al., 2012*). This results from a signaling cascade by which Rho GTPases contribute to actin assembly (see Figure 1.12). WAVE and WASp both normally exist in an auto-inhibited state, where the A domain is bound to the B domain, and the GBD domain is bound to the V domain; while inactive, Arp2/3 complexes cannot interact with WAVE/WASp. In order to initiate actin polymerization, Rac1 must bind to the GBD domain of WAVE, displacing the VCA domain to which Arp2 and Arp3 bind (this is done by Cdc42 for WASp). This induces very necessary conformational changes in each of the seven subunits of the Arp2/3 complex, which itself is also normally inactive and unable to interact with actin filaments. As this process is initiating, a G-actin monomer also binds to a different WAVE/WASp molecule at its VCA site and binds to Arp2/3, strengthening the binding affinity to the mother actin filament. The newly nucleated daughter filament continues to grow by polymerization (see Figure 1.13).

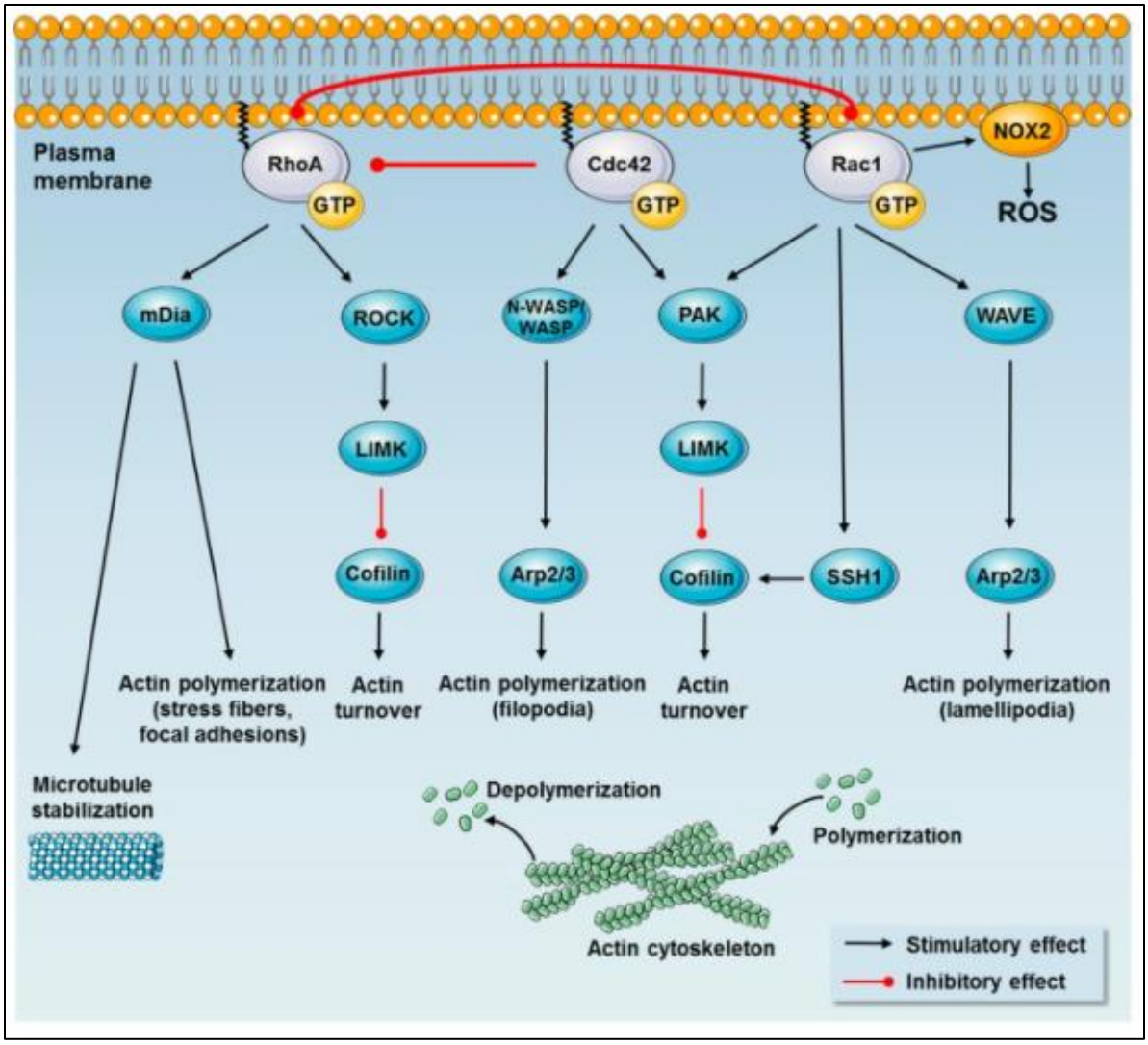

Figure 1.12. Downstream effector proteins of the major Rho GTPases, Rac1, Cdc42, and RhoA. Downstream effector proteins of Rac1 and Cdc42 include the Wiskott–Aldrich syndrome family of proteins (Wiskott-Aldrich Syndrome protein (WASP), neural-WASP (N-WASP), WASP family verprolin homologous protein 1 or 2 (WAVE1/2)) and p21-activated kinases (PAKs). WASP, N-WASP, and WAVE promote actin polymerization via activation of the Arp2/3 complex. PAKs activate LIM domain kinases (LIMKs) promoting phosphorylation and inactivation of the actin severing protein cofilin. Rac1-dependent activation of slingshot1 (SSH1) promotes cofilin dephosphorylation and actin depolymerization (actin turnover). Downstream effector proteins of Rac1 also include the NADPH oxidase complex (NOX2) to produce reactive oxygen species (ROS) at the cellular membrane. Downstream effector proteins of RhoA include Rho-associated protein kinase (ROCK) and the formin family of proteins (mDia). Among other downstream effector proteins, ROCK regulates the actin turnover via the LIMK–Cofilin pathway (*Møller et al., 2019*).

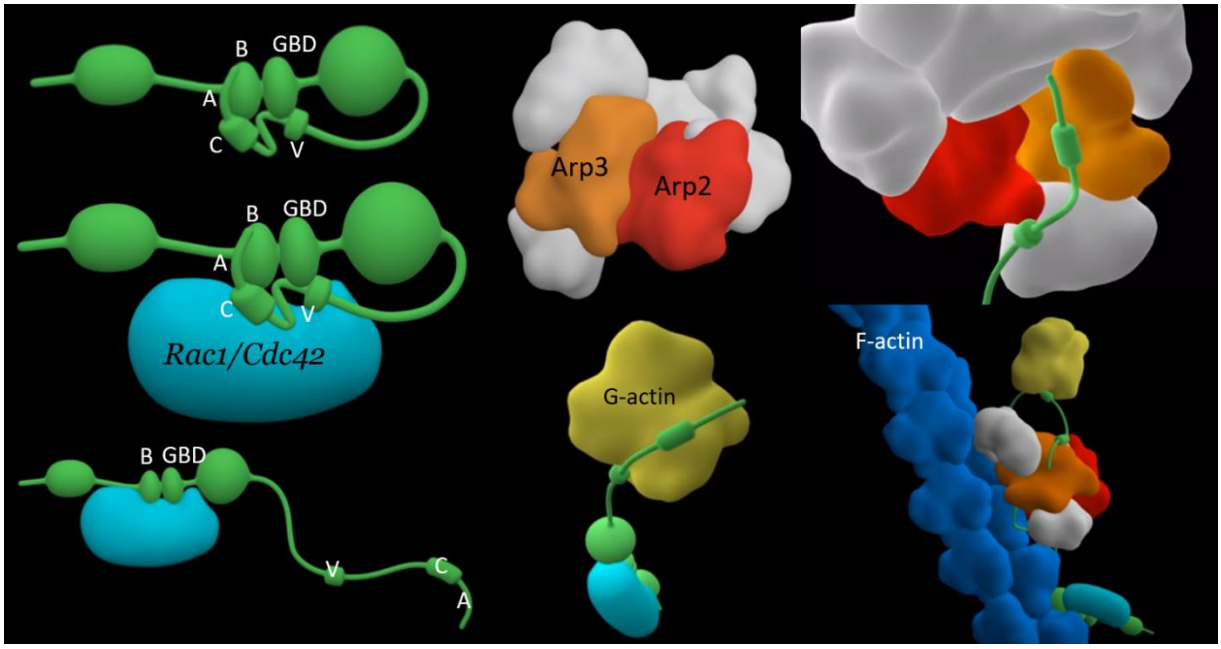

Figure 1.13. Steps of WAVE/WASp aiding in the polymerization of actin filaments. Molecules of WAVE or WASp (green) are bound by an activator molecule, allowing them to interact with Arp2/3 complexes as well as G-actin subunits. The binding results in conformational changes that enhance binding affinities and allow actin polymerization to initiate (annotated from *Mechanobiology Institute of Singapore, 2013*).

Accompanying IS formation, T cells also undergo a rapid polarization of the microtubule cytoskeleton (1–2 min after initial contact), which facilitates directional secretion of cytokines and cytolytic factors toward the APC (*Yi et al., 2013*). This follows a reorientation of the MTOC to the TCR/APC junction. This polarization helps facilitate targeted cytokine secretion (see Figure 1.14).

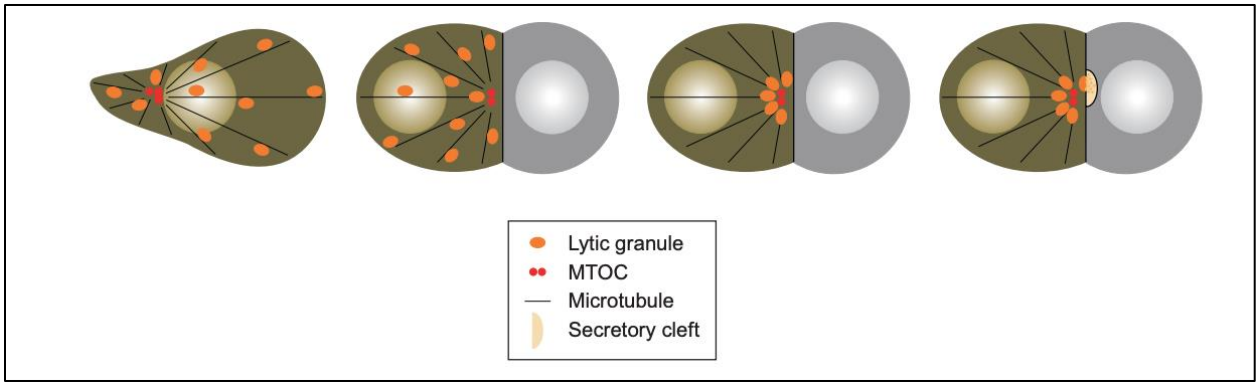

Figure 1.14. Polarization in a cytotoxic T lymphocyte (CTL) on conjugation to a target (*Stinchcombe & Griffiths, 2007*).

There has been increasing evidence that mechanical forces can critically regulate the entire process of T-cell activation: migration to infection sites, cell deformation, interaction with target APCs, surveillance of antigens, reorientation of organelles, and release of cytokines or cytotoxins (see Figure 1.15) (*Harrison et al., 2019*). Combined with the observation of cytoskeletal dynamics upon TCR triggering and the cytoskeleton's role in force generation across many cells types, it became of interest to determine whether or not the cytoskeleton contributed to T-cell mechanosensing.

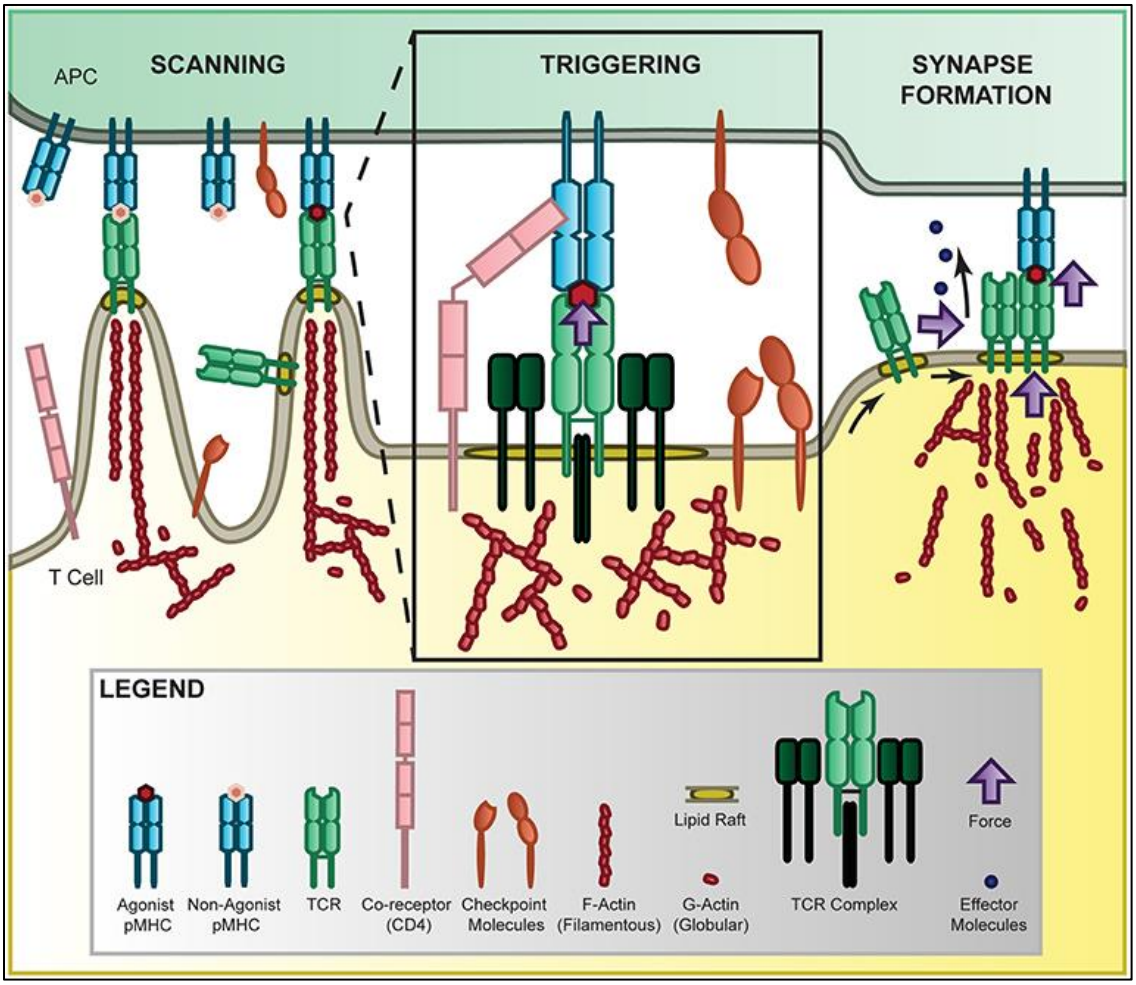

Figure 1.15. Force in T-cell recognition. T cells scan APCs where they are able to sensitively discriminate activation cues from a large pool of non-activation cues by the TCR binding to MHC presenting self or non-self ligands. The 2D agonist pMHC/TCR interaction is further mediated by co-receptor binding, checkpoint inhibition, and force through a catch-bond mechanism. Once sufficiently triggered, the TCR complexes accumulate together, sliding along the membrane in lipid rafts where they form microclusters and eventually the immunological synapse to localize internal signaling and release of effector molecules (*Harrison et al., 2019*).

One extension of this idea was the observation that actin plays a role in cytotoxic killing and in fact helps the T cell apply forces to the APC in doing so. Specifically, perforin release was found to occur at the base of actin-rich protrusions that extend from central and intermediate locations within the immunological synapse. These protrusions, which depend on the cytoskeletal regulators WASp and WAVE2, as well as the Arp2/3 actin nucleation complex,

were required for synaptic force exertion and efficient killing (*Tamzalit et al., 2019*). These proteins also mediated physical deformation of the target cell surface during cytotoxic lymphocyte (CTL)-target cell interactions, revealing the mechanical basis of cellular cytotoxicity. From a functional standpoint, these proteins possess fundamental contributions to the T-cell activation process as a whole: WASp is linked to IS stability and the formation of protrusive structures during antigen scanning upon TCR recognition, while WAVE2 promotes cell spreading and adhesion during IS formation.

1.10 T-Cell Impact and Significance

In the pursuit of more effective immunotherapy treatments, understanding the regulatory mechanics of T cells is increasingly proven to be a promising approach. From a cytoskeletal standpoint, while the importance of actin's role in the mechanics of T-cell activation is increasingly clear, there is still very little understood about how its polarization is regulated. The immunological synapse, where cytoskeletal reorganization is observed, is a site at which microtubules and actin could potentially interact to regulate signaling, which would motivate MTs as playing an indirect role in actin dynamics. However, there does not exist much literature investigating the regulation of MT translocation and how it might mediate actin flow. If a regulatory relationship exists, it is likely at the protein-level of filament organization. Thus, the objective of Aim 2 is to identify the proteins associated with microtubule translocation during T-cell activation as a function of actin flow modulation and determine under what circumstances this process can be manipulated.

Chapter 2: Elucidating the role of the primary cilium in osteoclastogenesis

2.1 Abstract

The primary cilium is a solitary, antenna-like sensory organelle with many important roles in bone development, maintenance, and function. The osteocyte, a fully differentiated bone cell embedded in the mineral matrix, has been widely accepted as a critical bone mechanosensing cell, with primary cilia of osteocytes, as well as of other cells of the mesenchymal cell lineage, playing a vital role in the regulation of bone formation and resorption. This has made the primary cilium a promising pharmaceutical target to maintain bone health. While the role of the primary cilium in the osteogenic cell lineage has been increasingly characterized, little is known about the potential impact of targeting the primary cilium in relation to osteoclasts, a hematopoietic cell responsible for bone resorption. Thus, the objective of this study was to determine the presence or absence of osteoclast primary cilia and investigate whether or not the primary cilium of macrophages, osteoclast precursors, serves a functional role in osteoclast formation. Using immunocytochemistry, we showed the presence of primary cilia on macrophages and the absence of this organelle on osteoclasts. Furthermore, we increased macrophage primary cilia incidence and length using fenoldopam mesylate and found that cells undergoing such treatment showed a significant decrease in genetic expression of ACP5 (tartrate-resistant acid phosphatase) and CTSK (cathepsin K), markers of osteoclast differentiation and activity, as well as decreased osteoclast formation, measured via surface area quantification. This work is the first to show that macrophage primary cilia resorption may be a necessary step for osteoclast differentiation. It was also found that osteoclastic gene expression by macrophages was not affected by fluid-flow mechanical stimulation, suggesting that the role of the primary cilium in osteoclastogenesis is not a mechanosensory one. Combined with

findings from previous studies, there is increasing evidence that the primary cilium, as a therapeutic target for bone diseases, may in fact offer a dual beneficial approach to both promote bone formation and downregulate osteoclast activity. This would have great significance as osteoporosis and low bone mass, diseases affecting over half the population over 50, have inadequate long-term treatment options for what is a multi-decade disease that can result in debilitating fragility fractures.

2.2 Introduction

Bone is maintained by the careful orchestration and balance of bone formation by osteoblasts and resorption by osteoclasts. In aging, the healthy balance of formation and resorption to maintain skeletal integrity is impeded by reduced osteoblast differentiation and proliferation, and increased maturation of osteoclasts (see Figure 2.1) (*Fang et al., 2022*). Imbalanced metabolic activity is a hallmark of osteoporosis, a skeletal disease characterized by significant bone loss, deterioration of bone microarchitecture, and reduced bone strength (*Osteoporosis - Symptoms and Causes - Mayo Clinic, n.d.*), which affects more than half of the U.S. population over 50 years old (*U.S. Office of the Surgeon General, 2004; Blume & Curtis, 2011; Wright et al., 2014*). Fragility fractures, most frequently occurring in the hip, waist, or spine, are common complications of osteoporosis that result in a significant loss of quality of life and a great economic burden. There are over 1.5 million fractures in the U.S. annually, an incidence greater than the number of strokes, heart attacks, and breast cancer diagnoses combined.

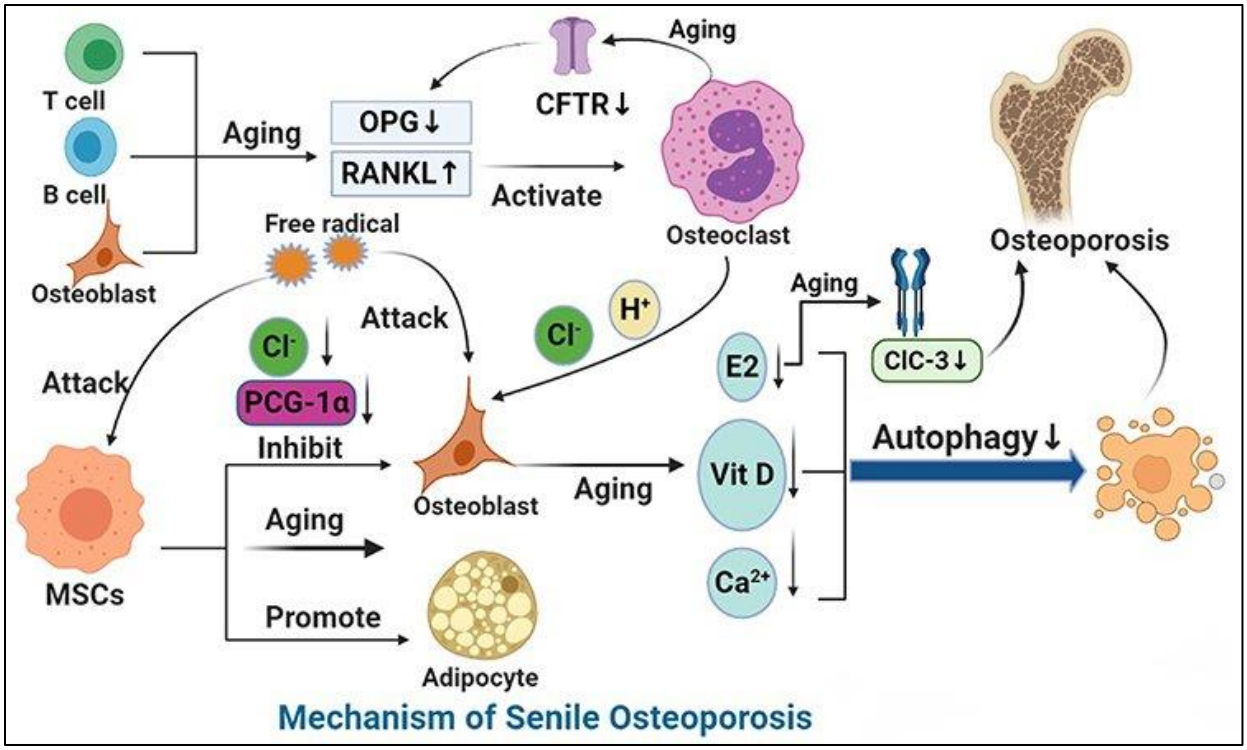

Figure 2.1. Mechanism of SOP. With aging, the ability of BMSCs to differentiate into osteoblasts decreases and that of adipocytes increases. A decrease in peroxisome proliferator-activated receptor-γ coactivator 1 increases bone loss and fat accumulation during bone aging. Aging leads to the increase in reactive oxygen species (ROS), the accumulation of oxygen free radicals, the destruction of bone cells, and the inhibition of bone formation. With the growth of age, estrogen synthesis in vivo is reduced, CFTR chloride channel is lost, OPG is decreased, and overexpression of RANKL leads to osteoporosis. ClC-3 chloride channel in osteoblasts regulates the bone formation function of osteoblasts by regulating estrogen A receptor. In addition, the decrease in immune cells during aging leads to the decrease of OPG production and the increase in secretion of pro-inflammatory factors, which accelerates bone loss, affects bone metabolism and leads to osteoporosis. MiRNA networks can regulate bone formation through Wnt signaling pathway and bone resorption through RANKL/RANK pathway. In aging, autophagy level decreases and homeostasis of miRNA networks is broken. Finally, aging can down-regulate the expression and activity of 1α-hydroxylase in human bone marrow mesenchymal stem cells and inhibit the osteogenic differentiation of human bone marrow mesenchymal stem cells (*Fang et al., 2022*).

There are two main categories of therapeutics to treat low bone mass – anabolics (e.g., Parathyroid hormone analog, anti-sclerostin antibody) that promote new bone formation, and antiresorptive agents (e.g., bisphosphonates, RANKL inhibitors) that inhibit osteoclast activity (*Tu et al., 2018*). One recent retrospective analysis sought to compare the effects of both

treatment options and found that the use of anabolic agents (compared to bisphosphonates or no medication at all) significantly enhanced fracture healing, reduced progressive collapse, and presented better clinical outcomes (see Figure 2.2) (*Min et al., 2019*). Anabolic agents show promise but are only either approved for a certain subset of patients or for a limited duration of use, which is inadequate for a multi-decade disease. Bisphosphonates, the most common agent used to prevent bone loss, bind to the surfaces of bones and promote the apoptosis of osteoclasts. While such treatment can prove effective for some patients, a wide range of short-term and long-term adverse side effects persist, such as an increased rate of mandibular necrosis, atypical fractures, esophageal cancer, and atrial fibrillation (*Black et al., 2010; Marx, 2003; Reyes et al., 2016*). Thus, there is a great need to identify more efficacious therapeutics for osteoporosis.

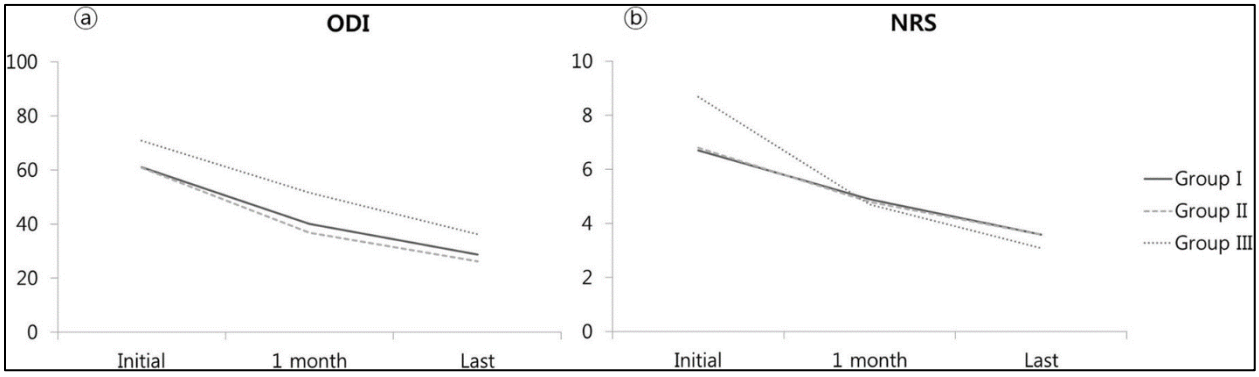

Figure 2.2. Measures of pain and disability after anti-osteoporosis treatment. A total of 132 patients diagnosed with acute osteoporotic spinal fractures (OSFs) were enrolled and allocated into three groups: Group I (n = 39, no anti-osteoporosis medication), Group II (n = 66, bisphosphonate), and Group III (n = 27, parathyroid hormone (PTH). Radiological parameters including magnetic resonance (MR) classification, occurrence of intravertebral cleft (IVC), and clinical outcomes such as (a) Oswestry disability index (ODI) and (b) numerical rating scale (NRS) were assessed (*Min et al., 2019*).

Bone has an innate ability to respond to mechanical loading; taking advantage of this mechanotransduction system could lead to the identification of new targeting strategies. Several modes of cell mechanosensing have been proposed, including by the primary cilium, a dynamic, immotile organelle that assembles and disassembles in a cell-cycle-dependent manner. Primary cilia have been shown to form a mechano-/chemical-signaling nexus capable of coordinating signaling pathways, and their function has been tightly linked to ciliary structure. Not only are shortened or absent primary cilia characteristic of diseases such as autosomal dominant polycystic kidney disease (ADPKD) and Bardet-Biedl syndrome (BBS) *(Copelovitch & Kaplan, 2012; Satir & Christensen, 2008*), but a number of aforementioned ciliopathies also exhibit skeletal patterning defects and even low bone mass *(Nguyen & Jacobs, 2013; Xiao & Quarles, 2010*). Several studies have previously identified the osteocyte primary cilium as a promising pharmaceutical target to exploit the body's natural response to physical loading *(Malone et al., 2007*). Our group and others have shown in vitro that fenoldopam, a dopamine D1-like receptor agonist that increases primary cilia length (*Kathem et al., 2014; Upadhyay et al., 2014*), heightens the mechanoresponse of osteocyte-like cells (*Spasic & Jacobs, 2017*) and promotes the differentiation of osteoblast precursors (*Corrigan et al., 2019*). Recently, we have shown that fenoldopam treatment increases osteogenic paracrine signaling of mechanical-stimulated osteocytes and load-induced bone formation in mice (see Figure 2.3) (*Spasic et al., 2022*), but little is known about the role of the primary cilium in osteoclast biology.

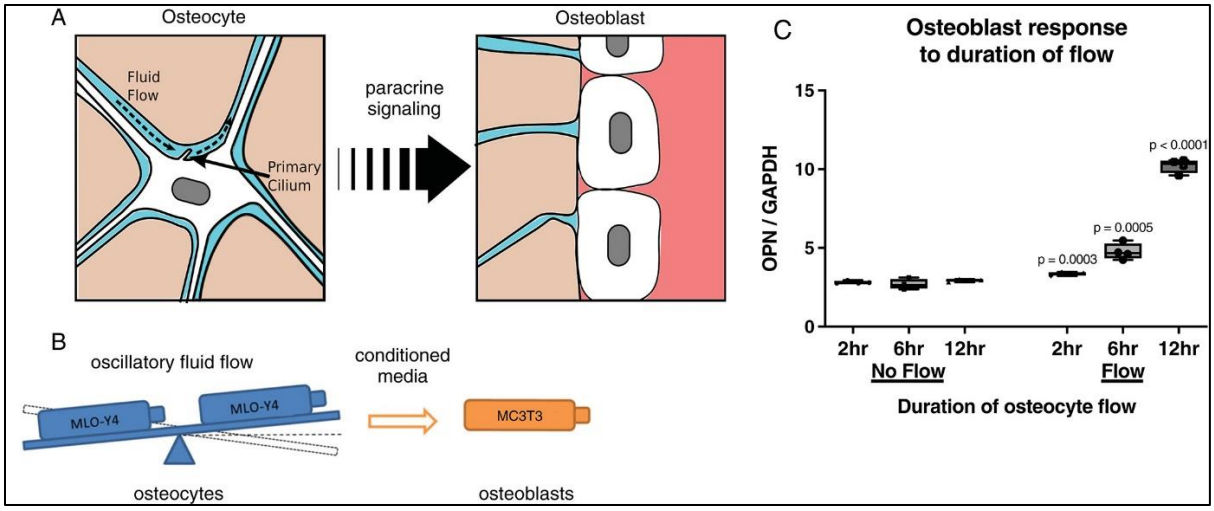

Figure 2.3. Paracrine signals from MLO-Y4 cells increase osteogenic signaling in MC3T3-E1 osteoblastic cells in a flow-duration dependent manner. (A) Model of paracrine signaling from osteocytes to osteoblasts with the primary cilium indicated as a potential load-induced fluid-flow mechanosensor. (B) MLO-Y4 osteocytes were placed on a rocking platform and subjected to oscillatory fluid flow of increasing durations, or left static as a control. Conditioned media was then collected and used to culture MC3T3 osteoblasts. (C) Conditioned media from 2, 6, and 12 hours of fluid flow was placed on static osteoblasts for 24 hours, at which point osteoblast OPN mRNA expression was assessed. $n \geq 4$ for each group (*Spasic et al., 2022*).

Osteoclasts are large, multinucleated cells found on the bone surface and possess the built-in machinery to degrade and digest the mineral and organic phases of the bone matrix. They are derived via the fusion of macrophages, which form a multinucleated cell with a characteristic actin ring in the cell cortex (*Väänänen et al., 2000*). Hematopoietic mononuclear cells are reported to have a primary cilium (see Figure 2.4) (*Singh et al., 2016*), but it is not known what happens as an osteoclast forms or what effect increasing primary cilia length has on osteoclast maturation. The objective of this study is to investigate whether the primary cilium is maintained in osteoclast formation, if lengthening the primary cilium with fenoldopam alters osteoclast formation, and if mechanical stimulation of the primary cilium with fluid flow impacts osteoclast maturation. With increasing evidence that the primary cilium may be a potential therapeutic target to treat bone metabolic disease, it is critical to understand its role in not only the

osteogenic mesenchymal lineage (*Delaine-Smith et al., 2014; Tummala et al., 2010*) but also in the bone-resorbing hematopoietic lineage cells.

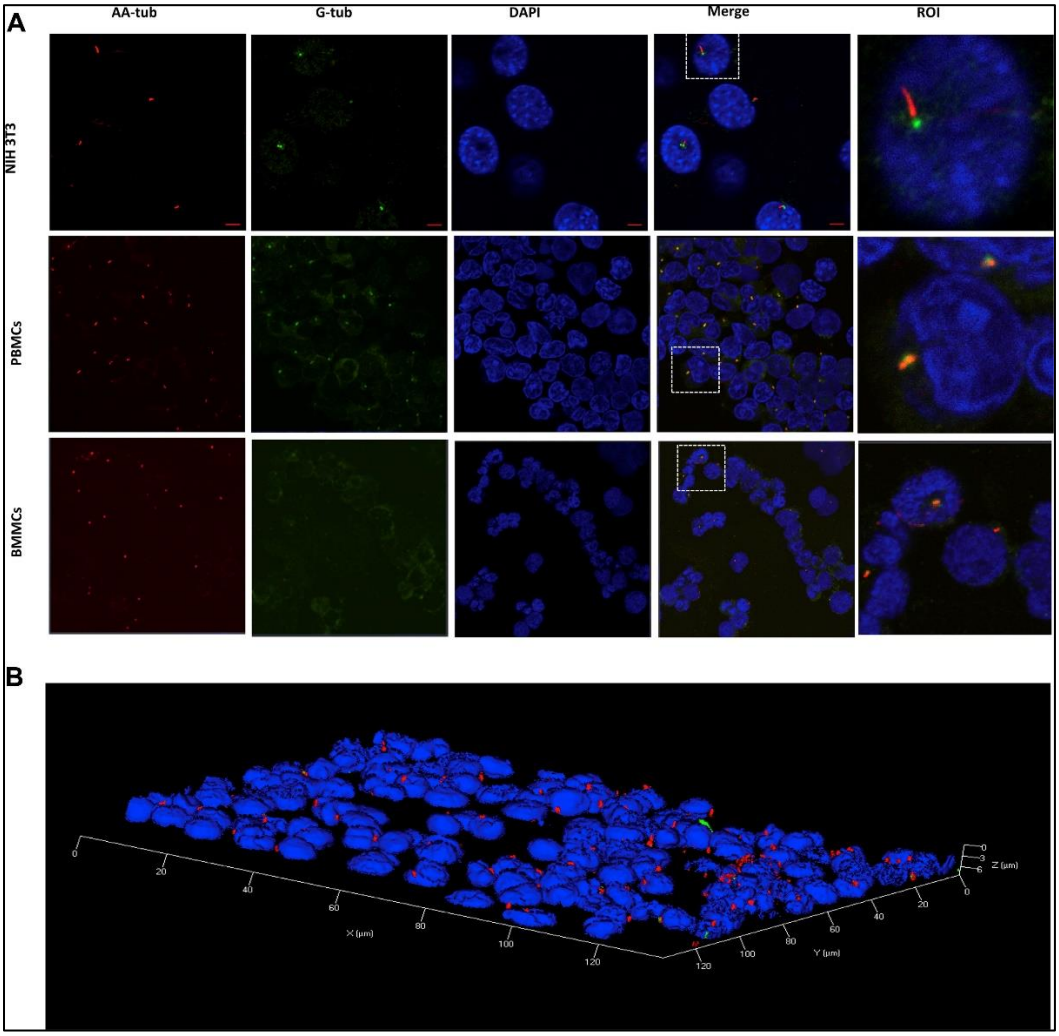

Figure 2.4. Presence of primary cilia in PBMCs and BMMCs. (A) Confocal Image of primary cilia in NIH3T3 fibroblasts (positive control) using antibodies against acetylated alpha-tubulin (labeling primary cilia; red), gamma-tubulin (labeling basal bodies; green), and DAPI (labeling nuclei; blue). Top panel, magnification 63×; scale bar, 5µm. Normal human PBMCs and BMMCs possess primary cilia (middle and bottom, respectively). Mononuclear cells were isolated from peripheral blood or bone marrow and immunolabeled for gamma-tubulin (green), acetylated alpha-tubulin (red), and DAPI (blue). Acetylated alpha-tubulin is enriched in cilia axoneme and gamma-tubulin is enriched in basal bodies. The spatial arrangement of the staining of these proteins was used to identify primary cilia in PBMCs and BMMCs. (B) 3D surface projection image of PBMCs created by combining all Z-stacks. The image shows the presence of primary cilia on the surface of cells (red) (*Singh et al., 2016*).

2.3 Materials and Methods

Cell Culturing

RAW 264.7 cells (adherent, immortalized cell line of monocyte/macrophage mixture) (ATCC) were seeded onto Petri dishes (Corning) at 1,000 cells per cm2 in DMEM (Gibco) supplemented with 10% fetal bovine serum and 1% penicillin/streptomycin for standard passaging and maintenance of the cell line. To differentiate this heterogeneous group into a population of mostly macrophages, which are cellular precursors to osteoclasts, macrophage colony-stimulating factor (M-CSF) (Shenandoah Biotechnology) was added at a concentration of 50 ng/mL for 72 hours. To differentiate these macrophages further into osteoclasts via cell fusion, these cells were incubated for an additional 4-8 days in the same medium as used for culturing the RAW 264.7 cells, but including 30 ng/mL of M-CSF and 100 ng/mL of receptor activator of nuclear factor-kappa B ligand (RANKL) (Shenandoah Biotechnology). Cells were washed with phosphate buffered saline (Gibco) with fresh media applied every 72 hours. A timeline of culturing and changes in cell morphology is shown in Figure 2.5.

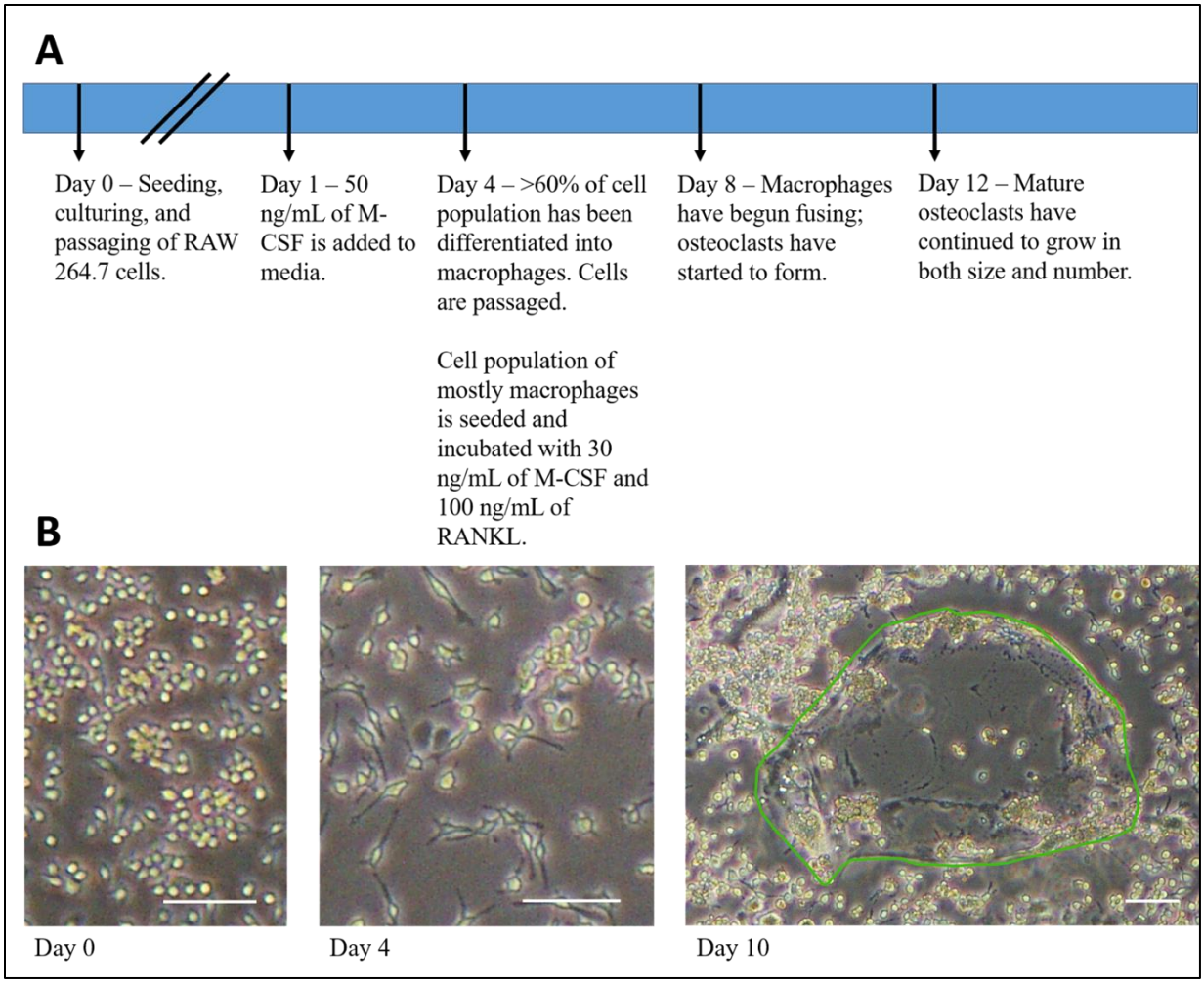

Figure 2.5. Differentiation of RAW 264.7 cells into osteoclasts. (A) Timeline of cell passaging and differentiation process. (B) Representative phase-contrast micrographs demonstrating the distinct phases of osteoclast differentiation. The first image of Panel B shows RAW 264.7 cells on Day 0; the second image is captured from Day 4, after RAW 264.7 cells have been incubated with M-CSF to differentiate into macrophages; the third image is captured from Day 10, with one mature osteoclast outlined in green. Scalebar = 100 µm.

Cilia Lengthening

Fenoldopam mesylate (Sigma) was used at 10 µM diluted in dimethyl sulfoxide (DMSO) (Sigma) and culture medium, as previously described (*Upadhyay et al., 2014*). This, or the DMSO vehicle control, was added to cells for 16 hours (*Spasic & Jacobs, 2017*). After treatment, cells were washed with PBS and incubated in fresh medium supplemented with M-CSF and RANKL for an additional 4-8 days before being fixed or lysed.

RNA Interference

Gene silencing was performed by siRNA mediated knockdown and compared to stealth siRNA control (Invitrogen). For primary cilia disruption, cells were transfected with IFT88 siRNA (5′-CCAGAAACAGATGAGGACGACCTTT-3′) or scrambled siRNA control using Lipofectamine RNAiMAX (Invitrogen). Twenty-four hours after seeding, cells were washed with PBS. Stealth RNAi (control) or ift88 siRNA (knockdown) were diluted in Opti-MEM (GIBCO) at 1.33% (13.3 µL of 20 µM siRNA in 1 ml Opti-MEM). Lipofectamine RNAiMAX was diluted in Opti-MEM at 0.2%. These dilutions were incubated at RT for 5 minutes, after which equal volumes of diluted siRNA and Lipofectamine were combined and incubated at RT for 20 minutes. Next, 200 µL of each mixture was combined with 800 µL of reduced-serum media (5% FBS) and added to the cells. This incubated at 37°C for 6 hours, after which cells were washed with PBS and normal media applied.

Oscillatory Fluid Flow

Macrophages were exposed to oscillatory fluid flow as a mechanical stimulus (see Figures 2.6 and 2.7). Cells were seeded onto four-well plates for 24h. Flow was applied for 12h at 0.75 Hz and amplitude 11 mm, with 0.16 Pa peak wall shear stress (calculated according to *Zhou et al., 2010*). Cells continued to grow for 4-8 days in M-CSF and RANKL before being lysed.

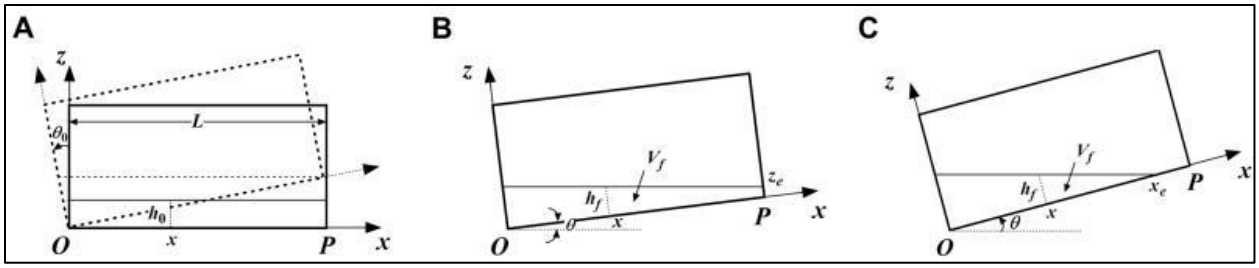

Figure 2.6. Mathematical model of a rocking system. (A) The side view of a culture dish of length *L* and width *b* that contains culture medium of depth of h_0 rocks up and down sinusoidally in the vertical plane (*xz*) along the pivotal point *O*. The critical flip angle (θ_0) is defined when the fluid free surface contacts the outer edge *P* of the dish bottom. Depending the maximal flip angle θ_{max}, there are two cases considered. (B) If $\theta_{max} \leq \theta_0$, the entire dish bottom is covered by the medium and a finite fluid depth z_e occurs at the outer edge of the dish; (C) If $\theta_{max} > \theta_0$, some peripheral region of the dish bottom including points *O* and *P* may be exposed to air during the rocking. The fluid free surface makes a contact with the dish bottom at the location of x_e. For both cases and at an arbitrary location *x*, the fluid height h_f at the vertical cross-section (dashed line) and the fluid volume V_f located on the right side of the cross-section can be estimated from purely geometric considerations, assuming a horizontal free fluid surface (*Zhou et al., 2010*).

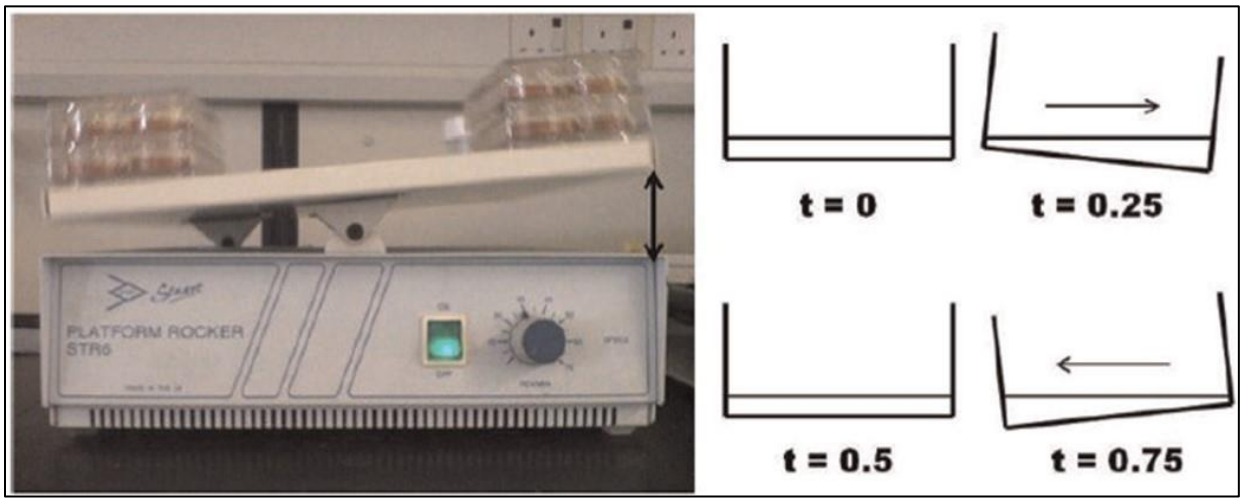

Figure 2.7. Sample rocker photo and schematic. A platform rocker used to subject cells to fluid flow–induced shear stress (left) and a schematic representation of gravitational movement of fluid in a well plate during different time points of one cycle (t) (right) (*Osman et al., 2014*).

Immunocytochemistry (ICC)

For primary cilia imaging and analysis, cells cultured on round glass-bottom dishes (MatTek) were fixed in 10% formalin and treated with anti-acetylated α-tubulin primary antibody, 1:10, from a C3B9 hybridoma cell line (Sigma). Cilia were visualized with Alexa-

Fluor 568 secondary antibody, 1:500 (Life Technologies), and imaged with a 100x oil objective on an Olympus Fluoview FV1000 confocal microscope. Nuclei were stained with NucBlue (Invitrogen). Cilia lengths were analyzed using ImageJ. Cells were also treated with 488 phalloidin (Invitrogen) to visualize the F-actin cytoskeleton and pericentrin (Abcam) to visualize the centrosome and its alignment with respect to the primary cilium.

mRNA Expression

After fenoldopam treatment, cells were washed with PBS and total mRNA was isolated using TriZol (Life Technologies). Total mRNA was converted to cDNA by TaqMan reverse transcriptase (Applied Biosystems). Gene expression was analyzed by quantitative real-time PCR using primers and probes (Life Technologies) for analysis of tartrate-resistant acid phosphatase, ACP5 (Mm00475698_m1); cathepsin k, CTSK (Mm00484039_m1), and GAPDH (4351309). Samples and standards were run in triplicate, and all gene expression was normalized to GAPDH endogenous control, as previously performed (Kwon et al., 2010). Outputs from qPCR studies were analyzed using the Delta-Delta Ct Method (*Livak & Schmittgen, 2001*).

Osteoclast Surface Area Quantification

As a secondary measure to compare rates of osteoclast formation for treated and untreated groups, the surface area of osteoclasts was quantified. Samples were again cultured on glass-bottom dishes and fixed in 10% formalin. Samples were visualized on an Olympus CKX41 microscope, and images were captured using a DP20 digital microscope camera that includes a 2-megapixel CCD. These images were collected and inputted into ImageJ with a ratio of 9.0333 pixels per micrometer. The outer edge of each osteoclast was traced, with the corresponding output being converted to surface area in μm2. The total osteoclast surface area of a given frame

divided by the total surface area of that glass coverslip yields a quantified percentage surface area to compare osteoclast formation across conditions.

Statistical Analysis

Data were analyzed using Student's t-test, Welch's t-test for samples of unequal variances, or Mann-Whitney test for data not following a Normal distribution. Quantitative data are reported graphically as mean ± SEM (*$p<0.05$, **$p<0.01$, ***$p<0.001$, ****$p<0.0001$). Sample size, n, represents biological replicates.

2.4 Results

Primary cilia are present in osteoclast precursors but absent from mature osteoclasts

In order to test our hypothesis that the primary cilium directly affects osteoclast formation, we first verified the presence of primary cilia on macrophages in multiple phases. Using MLO-Y4 cells (*Y. Kato et al., 1997*) as a control (which our lab had previously successfully intracellularly stained) with our monocyte/macrophage cell line, RAW 264.7, we first set a baseline of primary cilia presence by performing a double immunocytochemistry (ICC) using two different antibodies: 1) an anti-acetylated α-tubulin primary antibody isolated from a C3B9 hybridoma cell line, and 2) an anti-Arl13b primary antibody (a small GTPase that is enriched in primary cilia and regulates Sonic hedgehog signaling) (*Caspary et al., 2007*). Given the fact that both of these antibodies stain for primary cilia, we would be able to differentiate cilia from potential imaging artifacts (see Figure 2.8). We also know that structurally, the primary cilium elongates from a cell's centrosome. Thus, we subsequently performed another double ICC, but using instead C3B9 and gamma-tubulin. This would help with cilia identification (as all cilia should overlay with a centrosome), as well as approximating the naturally occurring cilia incidence of our RAW 264.7 cell line, as every cell should have a centrosome, but not every cell may have a primary cilium (see Figure 2.9).

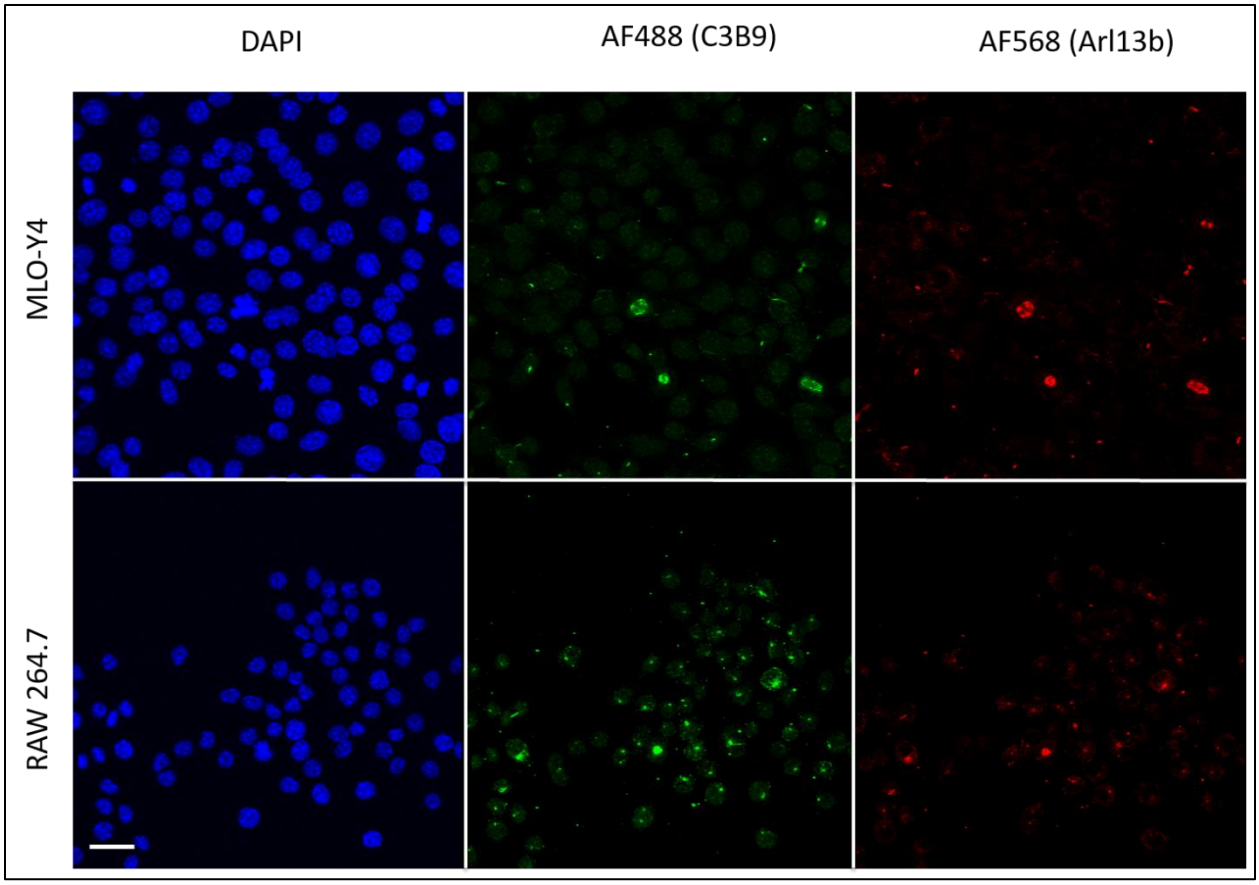

Figure 2.8. RAW 264.7 cells can be stained for primary cilia using multiple antibodies. Maximum projection of confocal image z-stack at 40X. Scalebar = 10 µm.

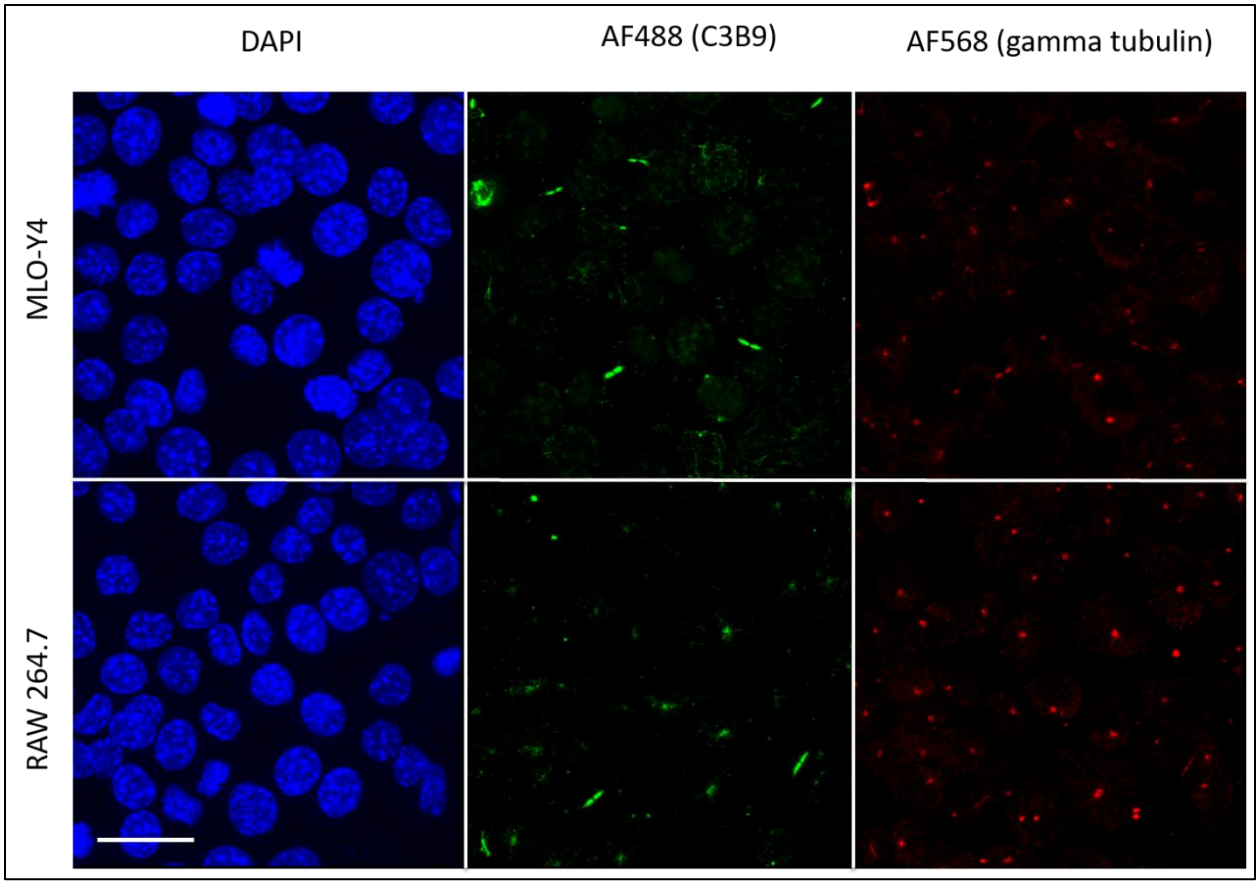

Figure 2.9. RAW 264.7 cells display primary cilia and centrosome overlay. Maximum projection of confocal image z-stack at 100X. Scalebar = 10 µm.

We utilized immunocytochemistry to image both centrosomes (anti-pericentrin) and primary cilia (anti-acetylated alpha-tubulin) on RAW 264.7 cells after incubating in macrophage colony-stimulating factor. Macrophages were found to have a primary cilium incidence of 46.8% ± 6.4% (shown in Figure 2.10). However, cilia were predominantly absent from differentiated osteoclasts, with an incidence of just 3.3%, and exclusively found in the immature osteoclast population, evident by fewer than three nuclei. Distinct multinuclear and cortical actin staining were used to visually distinguish osteoclasts from their precursors.

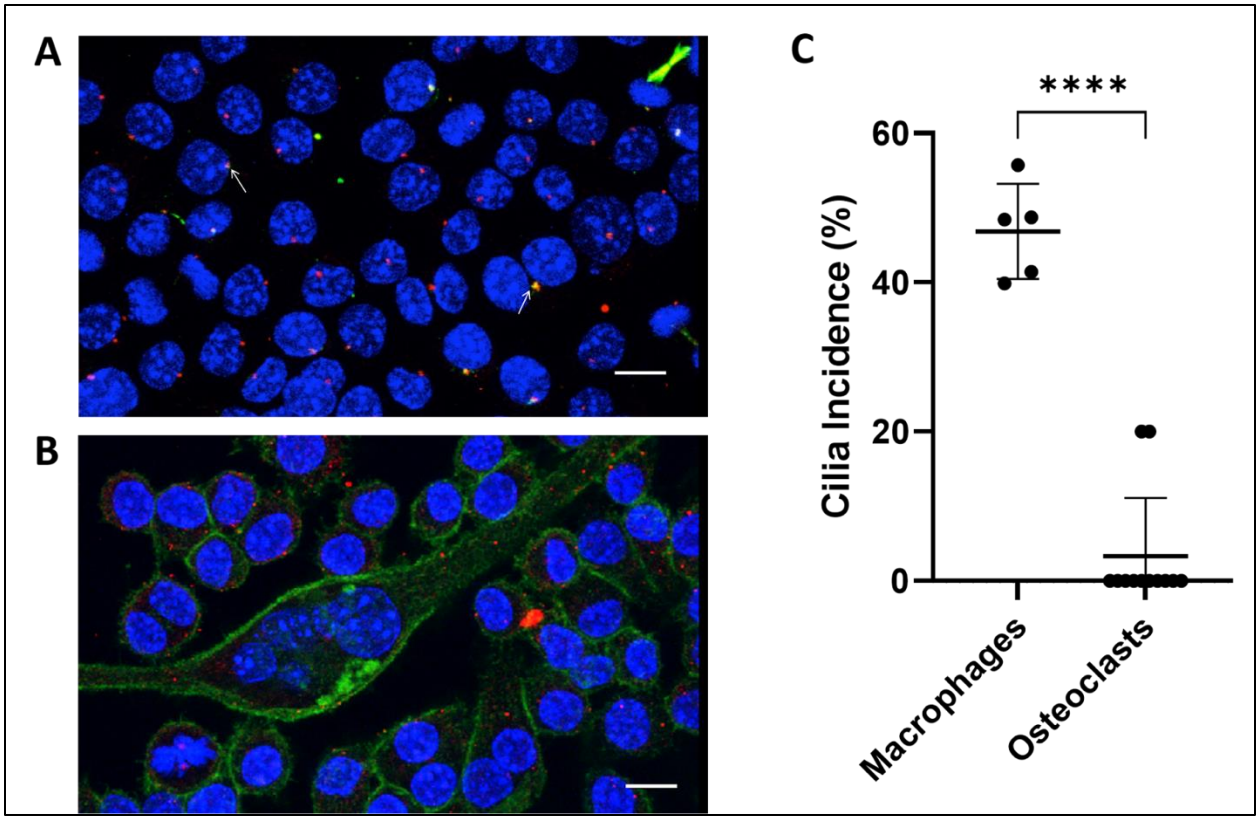

Figure 2.10. Macrophages possess primary cilia, but mature osteoclasts do not. Maximum projection of confocal image z-stack. (A) Primary cilia were found on macrophages. Blue = DAPI (nuclei), green = acetylated alpha-tubulin (primary cilia), red = γ-tubulin (centrosomes). Arrows highlight examples of centrosome/primary cilium overlay. (B) Primary cilia were mostly absent from differentiated osteoclasts, shown via distinct multi-nuclear and cortical actin staining. Blue = DAPI (nuclei), green = phalloidin (actin), red = acetylated alpha-tubulin (primary cilia). Scalebar = 10 μm. C) Macrophages were found to have a primary cilia incidence of 46.8% (n = 5), while differentiated osteoclasts were found to have a cilia incidence of just 3.3% (n = 12).

Fenoldopam effectively increases macrophage primary cilium incidence and length

Although the procedure had been previously carried out on other cell types, we next needed to verify that the macrophage primary cilium could in fact be modulated. Cells were cultured in fenoldopam mesylate – an FDA-approved compound known to extend cilia length – for 16 hours (*Spasic and Jacobs, 2017*). Immunocytochemistry was used to visualize primary cilia and assess changes in both cilia incidence and length. Fenoldopam was shown to induce

significant increases in primary cilia incidence (from 42.9% to 53.5%) and length (from 1.75 µm to 2.26 µm) compared to vehicle control (shown in Figure 2.11).

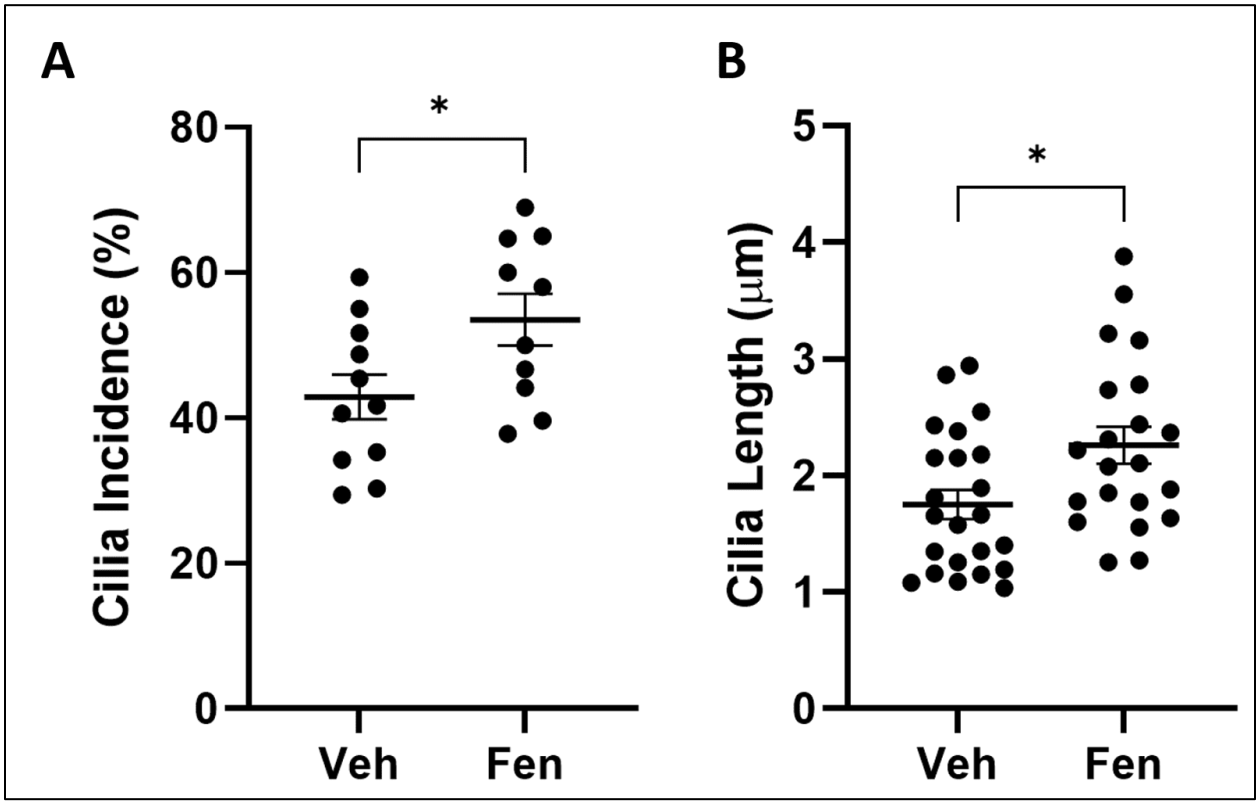

Figure 2.11. Fenoldopam effectively increases macrophage-primary cilia incidence and length. Macrophages were treated with fenoldopam mesylate or DMSO vehicle control. Fenoldopam-treated cells showed a significant increase in both (A) cilia incidence (from 42.9% to 53.5%; n = 11, 10) and (B) cilia length (from 1.75 µm to 2.26 µm; n = 23, 21) compared to control samples.

Macrophage primary cilium lengthening inhibits osteoclastogenesis

After confirming that the primary cilia of osteoclast precursors could in fact be elongated using fenoldopam treatment, we examined the effect of this lengthening on osteoclast formation. Differentiation was quantified at the mRNA level by analyzing ACP5 and CTSK expression and presented as fold changes relative to our housekeeping gene, GAPDH. ACP5 is the gene that codes for tartrate-resistant acid phosphatase (TRAP), which degrades skeletal phosphoproteins; CTSK codes for cathepsin K, which catabolizes elastin and collagen. Macrophages treated with

fenoldopam had an 18.2% decrease in ACP5 expression and a 20.3% decrease in CTSK expression, compared to non-lengthened DMSO controls (shown in Figures 2.12A and 2.12B). These fenoldopam-treated macrophages also exhibited a markedly decreased rate of fusion, evident by the osteoclast surface area coverage decreasing by almost half, from 27.6% surface coverage in the DMSO control group to 14.6% in the fenoldopam-treated samples (shown in Figure 2.12C).

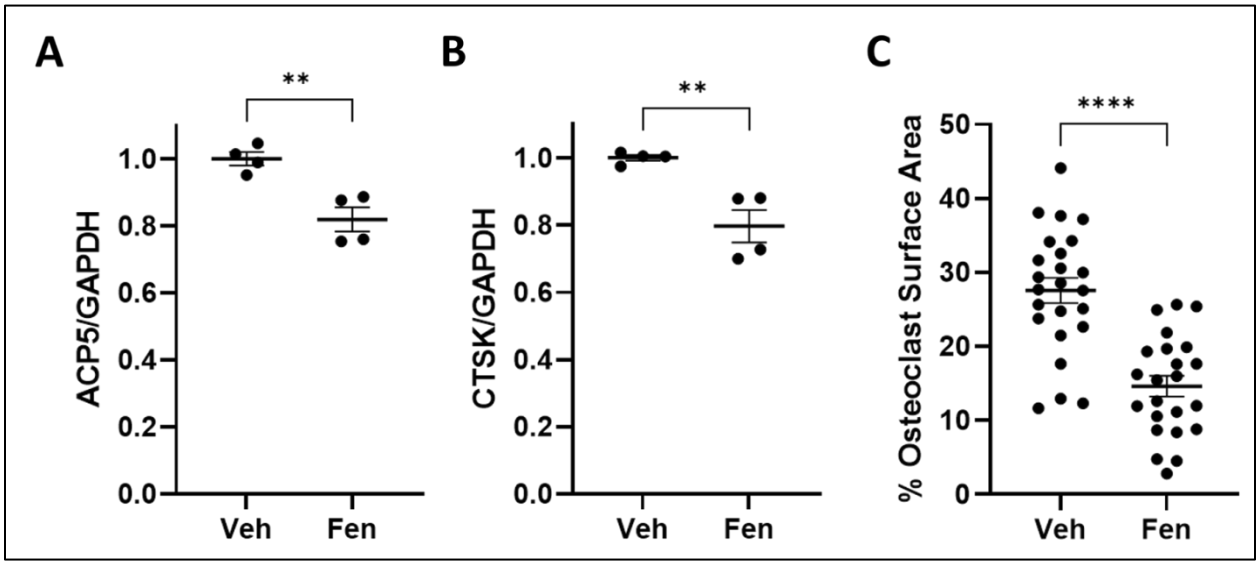

Figure 2.12. Macrophage primary cilium lengthening inhibits osteoclastogenesis. mRNA quantification showed that macrophages treated with fenoldopam prior to osteoclast differentiation treatment resulted in (A) an 18.2% decrease in expression of tartrate-resistant acid phosphatase (ACP5) and (B) a 20.3% decrease in expression of cathepsin K (CTSK), both measures of osteoclast differentiation and function, when compared to the DMSO vehicle control (n = 4). (C) Samples treated with fenoldopam also formed osteoclasts at a lesser rate, indicated by a 13% drop in osteoclast surface area coverage (n = 24, 23).

Cells failed to survive siRNA-mediated knockdown treatments

Naturally, after determining not only that macrophages possessed primary cilia but also that lengthening them led to a decrease in osteoclastogenesis, we explored whether or not the opposite effect was true: would macrophages in the absence of cilia fuse to form osteoclasts at an increased rate. Using a range of concentrations to optimize our transfection procedure using

Lipofectamine, cells failed to survive more than 48 hours post-transfection. As a result, we were unable to verify the efficacy of the treatment, and therefore unable to determine the downstream effect on osteoclast formation.

Fluid flow/mechanical stimulation does not affect osteoclastogenesis

Given that primary cilia are believed to play a role in the ability of other bone cells to direct cell function when mechanically stimulated *(Delaine-Smith et al., 2014; K. L. Lee et al., 2015*), we sought to determine whether or not the same was true of macrophages by subjecting the cells to oscillatory fluid flow. The results were again quantified at the mRNA level by analyzing ACP5 and CTSK expression, presented as normalized fold changes (Figure 2.13). Neither expression levels of the genes tested showed a significant change between the flow and static groups, indicating that the progression of osteoclastogenesis in response to mechanical loading does not rely on the primary cilium as a mechanosensor.

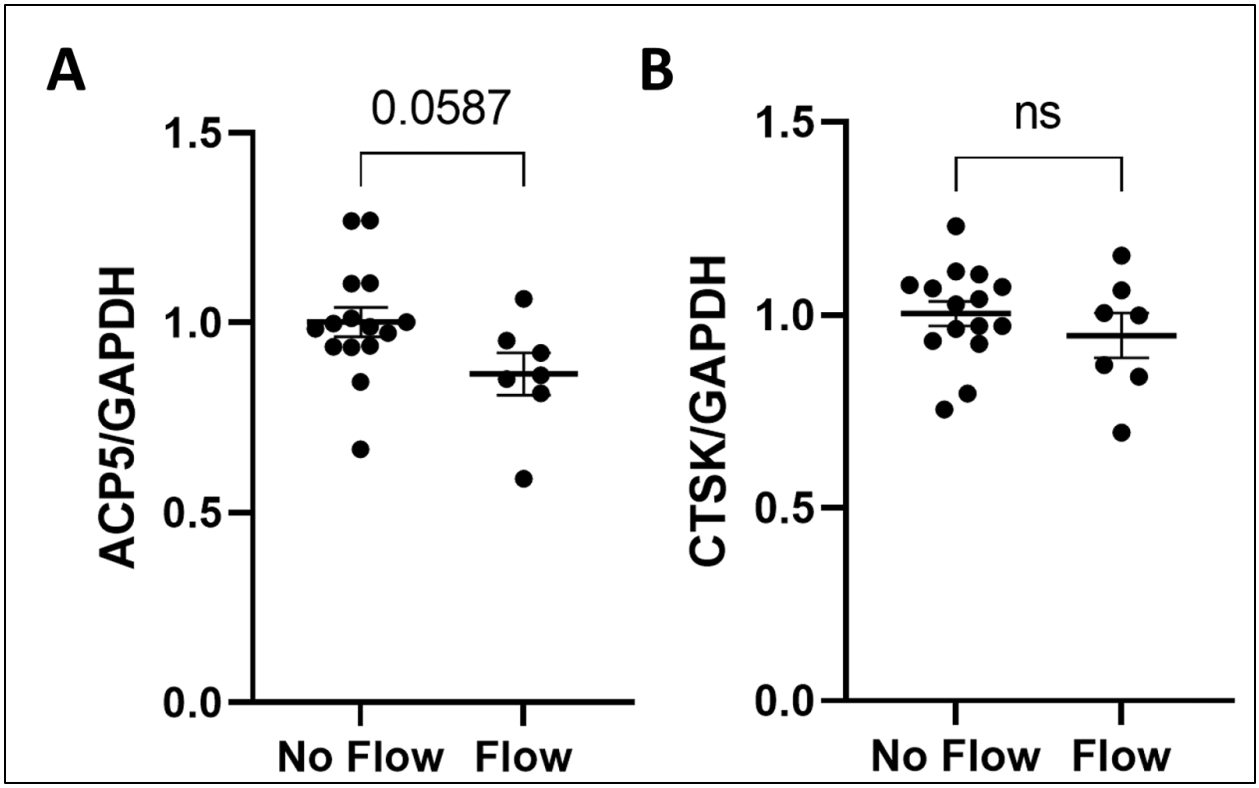

Figure 2.13. Mechanical stimulation of macrophage primary cilia did not result in a significant change in osteoclastogenesis. Macrophages were subjected to oscillatory fluid flow prior to being incubated with M-CSF and RANKL to induce osteoclast differentiation. Mechanically-stimulated cells did not demonstrate a significant change in osteoclastogenesis when compared to the static control samples (n = 15, 7).

2.5 Discussion

Our results demonstrated for the first time that osteoclasts do not form primary cilia. Interestingly, they are present on their macrophage precursors, indicating that loss of primary cilia is a key step in osteoclastogenesis. In fact, we show that by treating with fenoldopam, macrophage primary cilia incidence and length are increased, and osteoclast differentiation is decreased when cultured with M-CSF and RANKL. Since the primary cilium is shown to function both as a biochemical signaling nexus and mechanosensor, we applied fluid flow to mechanically stimulate the primary cilium and found it had no effect on osteoclast differentiation as measured by gene expression levels. This indicates the primary cilium likely doesn't play a role in osteoclast differentiation from a mechanosensing perspective.

We quantified the primary cilia incidence of macrophages at 46.8%, while bone marrow aspirate mononuclear cells have been reported to have a primary cilia incidence around 97–99% (*Singh et al., 2016*). The difference is likely due to the need for cell cycle-dependent disassembly of the primary cilium in proliferating cells in culture (see Figure 2.14) (*Sánchez & Dynlacht, 2016*). We observed that primary cilia are virtually absent as macrophages fuse to form mature osteoclasts, as they were only found sparingly on cells (~3%) at the earliest stage of fusion and none were found on mature osteoclasts. We also did not observe more than one cilium on an immature osteoclast. This finding suggests that the loss of the primary cilium is either a byproduct of fusion or a checkpoint on osteoclast maturation.

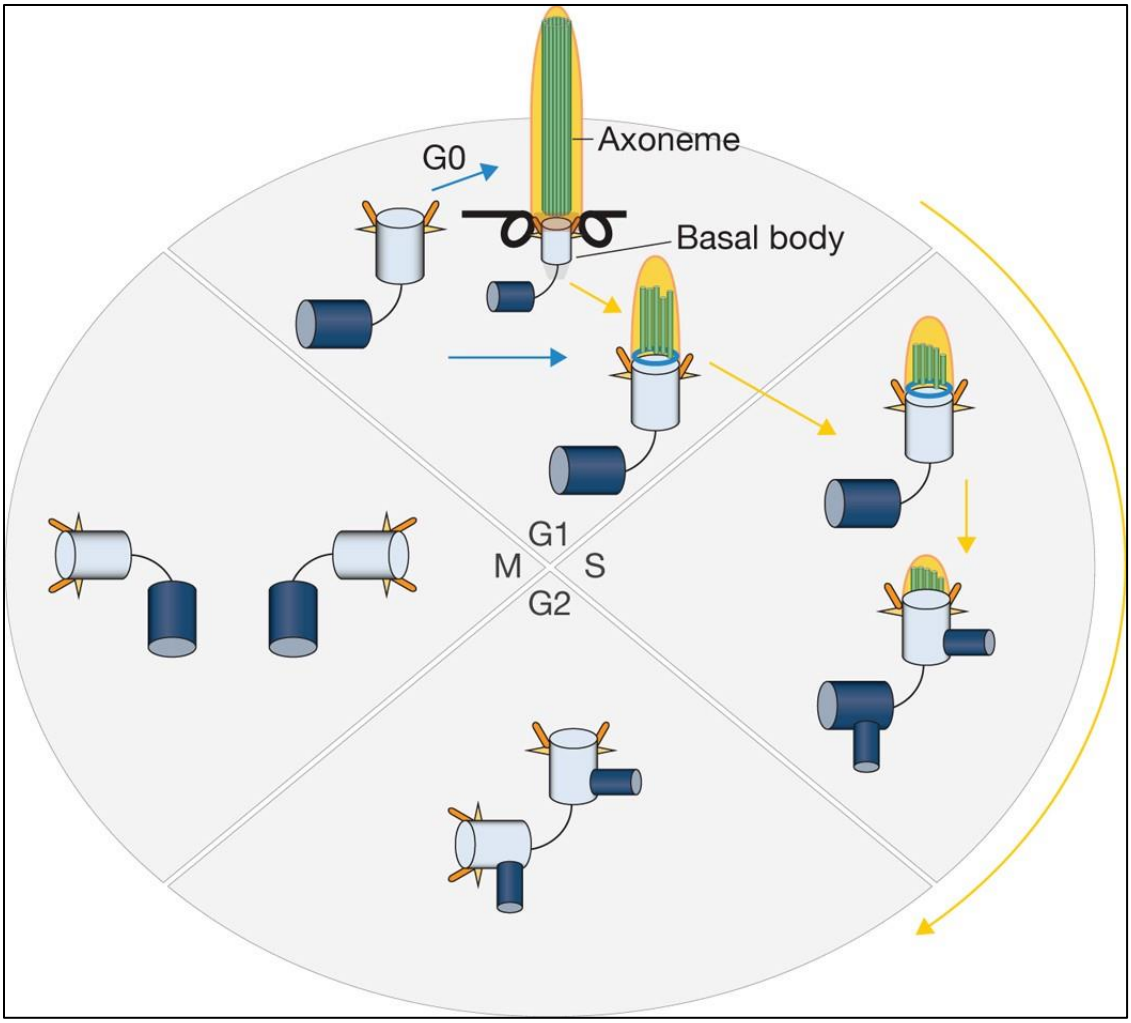

Figure 2.14. Linkage of the centrosome–cilium cycle to the cell cycle. Primary cilia assemble specifically when cells exit the cell cycle and become quiescent or differentiate. Cells are also competent to form cilia in G1. Phases of the cell cycle are indicated, and blue and yellow arrows indicate cilium assembly and disassembly, respectively. Only the mother centriole (light blue) can initiate ciliogenesis. The daughter centrioles are shown in dark blue. During the process of ciliogenesis, an axoneme is assembled. This microtubular structure (indicated with parallel green rods) is disassembled as cells progress towards S phase, concomitant with remodelling of the distal end of the basal body (aqua ring). During S phase, centrosomes commence duplication, at which point cilia have largely disassembled. After mitosis, centrosomes are again competent to assemble primary cilia, either in G0 or in early G1 phase (*Sánchez & Dynlacht, 2016*).

To see if the primary cilium acts as a checkpoint on osteoclast maturation, we treated with an agent, fenoldopam, known to lengthen and increase the incidence of primary cilia (*Corrigan et al., 2019; Spasic & Jacobs, 2017*). The exact mechanism by which this chemical mechanistically lengthens cilia is somewhat multifaceted. Genetic screens of abnormal cilia

length originally identified a family of class A dopamine binding G-protein coupled receptors that are involved in regulation of length of both cilia and flagella (*Avasthi et al., 2012*). Treatment of dopaminergic agonists, such as fenoldopam, seems to modulate cilia function by extending cilia length and therefore cilia sensitivity. DR5 is localized specifically to the primary cilia in epithelial cells, whereas other dopamine receptors are not expressed or are expressed ubiquitously in the cell membrane. This indicates that DR5 is likely responsible for binding dopaminergic agonists to transduce calcium signaling in the primary cilia of other cell types as well (*Abdul-Majeed & Nauli, 2011*).

Applied to macrophages, fenoldopam treatment resulted in a statistically significant increase in both macrophage cilia incidence and length. When cilia-lengthened macrophages were then induced in the osteoclast differentiation medium, we found reduced osteoclastogenesis, evident by ACP5 and CTSK gene expression levels, as well as a decrease by almost half in the osteoclast surface area. To ensure that we bypassed any potential toxic effect of fenoldopam on osteoclasts themselves, we applied treatment to macrophages and washed off the agent prior to differentiation taking place. Therefore, it seems that the primary cilium resorption is not just a byproduct of osteoclast maturation, but an important step in the process. Although, a role for the primary cilium in macrophage fusion cannot be ruled out because this process is not yet fully understood (*Yao et al., 2021*) and is further complicated by the fact that osteoclasts may undergo successive rounds of fusion and fission (see Figure 2.15) *(Jansen et al., 2012; McDonald et al., 2021*).

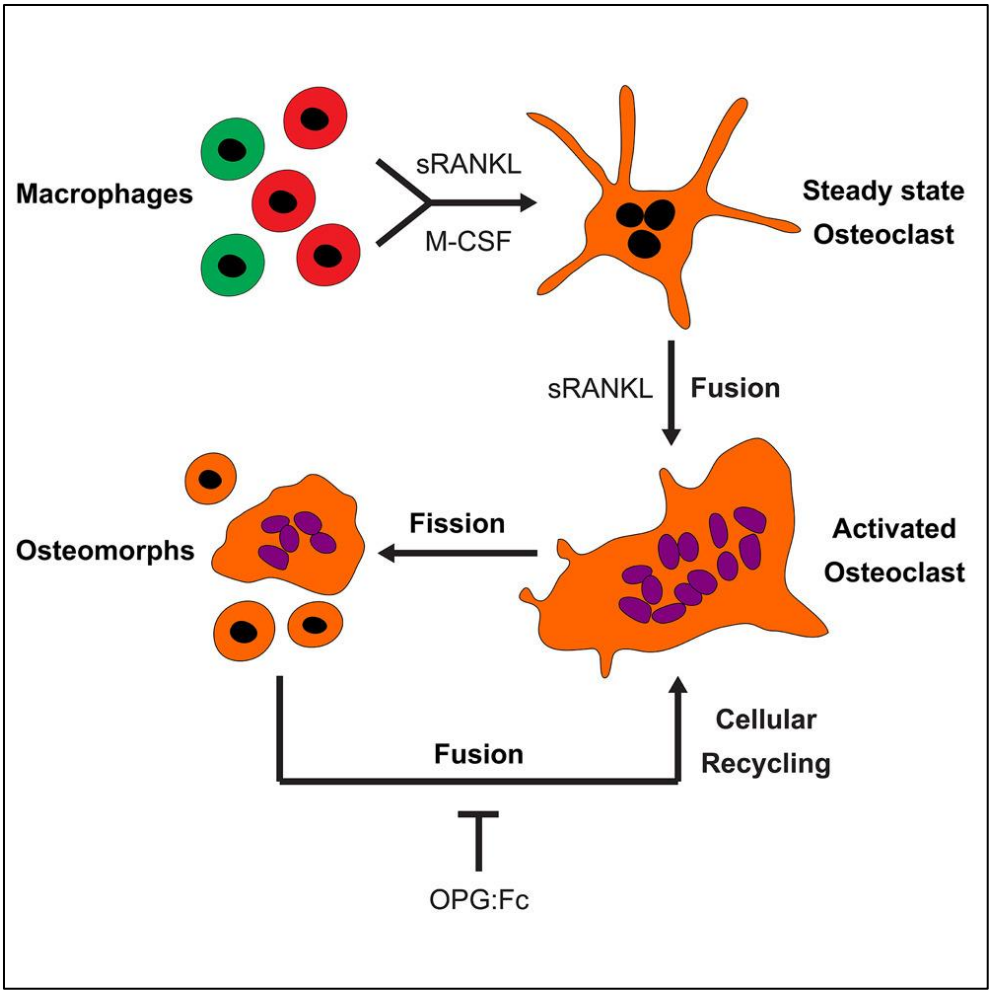

Figure 2.15. Osteoclasts recycle via osteomorphs during RANKL- stimulated bone resorption (*McDonald et al., 2021*).

The primary cilium has been shown to be intimately related to actin and microtubule function in the cytosol, which are both important to osteoclast differentiation. In chondrocytes, inhibited primary cilia formation results in increased F-actin staining intensity and reduced cell stiffness (*Z. Wang et al., 2016*); in an osteocyte-like cell line, an inhibition of primary cilia formation altered microtubule dynamics in response to physical stimuli (*Espinha et al., 2014*). As osteoclasts undergo maturation, there is an observable morphological change from spindly macrophages to rounded pre-osteoclasts (*Takeshita et al., 2000*) and finally large mature osteoclasts with a distinct actin cortical ring. Additionally, osteoclast differentiation is also

highly dependent on Rho-GTPases (see Figure 2.16) (*He et al., 2022*), an actin cytoskeleton regulator, and substrate-stiffness-dependent cytoskeletal reorganization is critical to osteoclast maturation (*Q. Wang et al., 2022*). It is possible the primary cilium plays a role in the coordination of cytoskeletal changes that are dependent on cilia resorption.

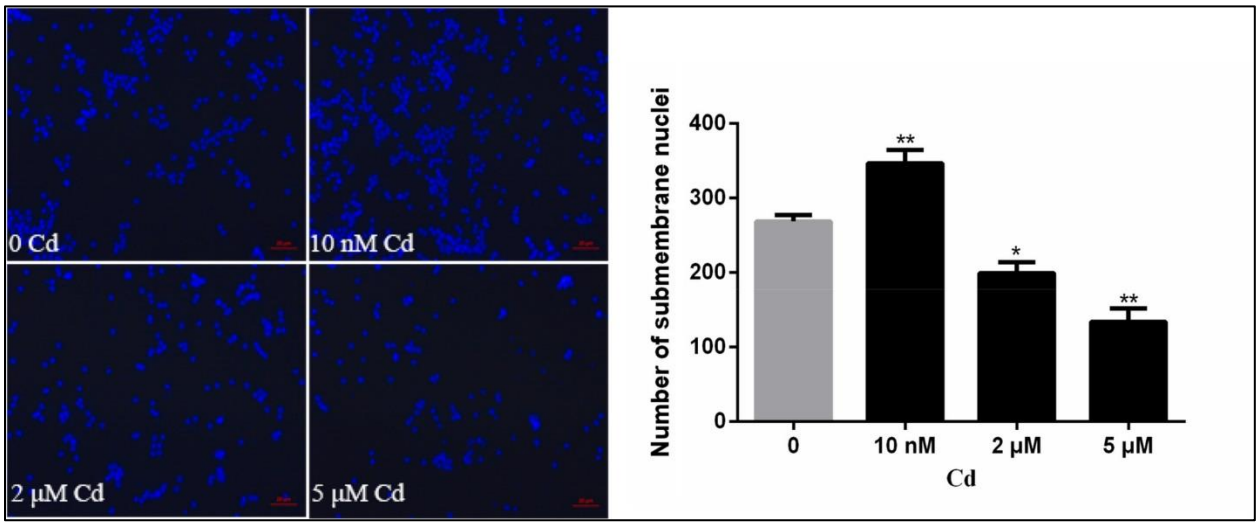

Figure 2.16. Effect of Cd exposure on the migration ability of osteoclast precursor cells. In the presence of M-CSF and RANKL, RAW264.7 cells were induced for 48 h, then treated with different concentrations of Cd (0, 10 nM, 2 μM, and 5 μM) for 24 h. Cells in the upper layer of the membrane were removed, and the cells in the lower layer were stained with DAPI and counted (Scale bar = 20 μm). Data are shown as the mean ± SD (n = 3). *p < .05 indicates a significant difference compared with the control group; **p < .01 indicates a very significant difference compared with the control group (*He et al., 2022*).

Osteoclasts are shown to respond to substrate strain (i.e., substrate deformation), but reports on whether strain promotes or inhibits osteoclast formation are contradictory and seem to depend on strain levels and duration of loading (*Kurata et al., 2001; Q. Wang et al., 2022; Xu et al., 2012*). Since the primary cilium is shown to be a potent mechanosensor (*Delaine-Smith et al., 2014; K. L. Lee et al., 2015; Malone et al., 2007*), we sought to determine if it played a mechanosensing role in osteoclast formation. Since primary cilia extend from the apical surface of most cells into the extracellular fluid space, we applied fluid flow to mechanically stimulate the cells. We showed no effect of mechanical stimulation on osteoclast maturation, indicating

that fluid flow stimulation may not play a role in osteoclast mechanobiology; this is of particular note when compared to substrate deformation — the most commonly applied form of mechanical stimulation in osteoclast studies — a mechanism unlikely to directly stimulate the primary cilium. We applied a modest level of shear stress (0.16 Pa), which we deemed appropriate as it is within the range of bone marrow shear stress (0.02–0.26 Pa) found computationally in trabecular bone volumes (*Birmingham et al., 2013*), it has been shown to be adequate to stimulate other cells in culture (*Spasic et al., 2022*), and the primary cilium is shown to deflect at fluid shear as low as 0.03 Pa (*Malone et al., 2007*).

Although we have demonstrated the capability to lengthen macrophage primary cilia and inhibit osteoclast formation using fenoldopam, the protocol was adapted from previous studies experimenting with osteocyte primary cilia. While the primary cilium itself seems to be structurally preserved across cell types, the specific way in which fenoldopam lengthens primary cilia is not yet fully understood. Used as a vasodilator in acute emergency settings, fenoldopam is a dopamine D1-like receptor agonist and is shown to stimulate adenylyl cyclase activity (*M. B. Murphy et al., 2001; Spasic & Jacobs, 2017*). In fact, adenylyl cyclase activity and increased cAMP levels have been shown to also decrease osteoclastogenesis (see Figure 2.17) (*Yoon et al., 2011*). In our study, the application of fenoldopam is removed prior to incubation with differentiation media for a course of 4-8 days, likely minimizing any potential effects of initially elevated cAMP, Though, given the role of G-protein coupled receptors, adenylyl cyclases, and cAMP in osteoclast formation (*Ramaswamy et al., 2018; Yoon et al., 2011*), this warrants future exploration. Other cilia-modifying approaches are available. For instance, tubastatin is an HDAC6-specific deacetylase inhibitor that causes an increase in primary-cilia microtubule acetylation, which both stabilizes the primary cilium and increases its stiffness (*Xiang et al.,*

2017). Additionally, lithium chloride, an antidepressant agent, is shown to increase primary cilia length in a range of contexts (*Mehran et al., 2016; Miyoshi et al., 2009; Thompson et al., 2016*). We chose to explore the use of fenoldopam, as it has shown promise as a bone anabolic agent (*Corrigan et al., 2019; Spasic & Jacobs, 2017; Spasic et al., 2022*), yet its role on osteoclasts was not known.

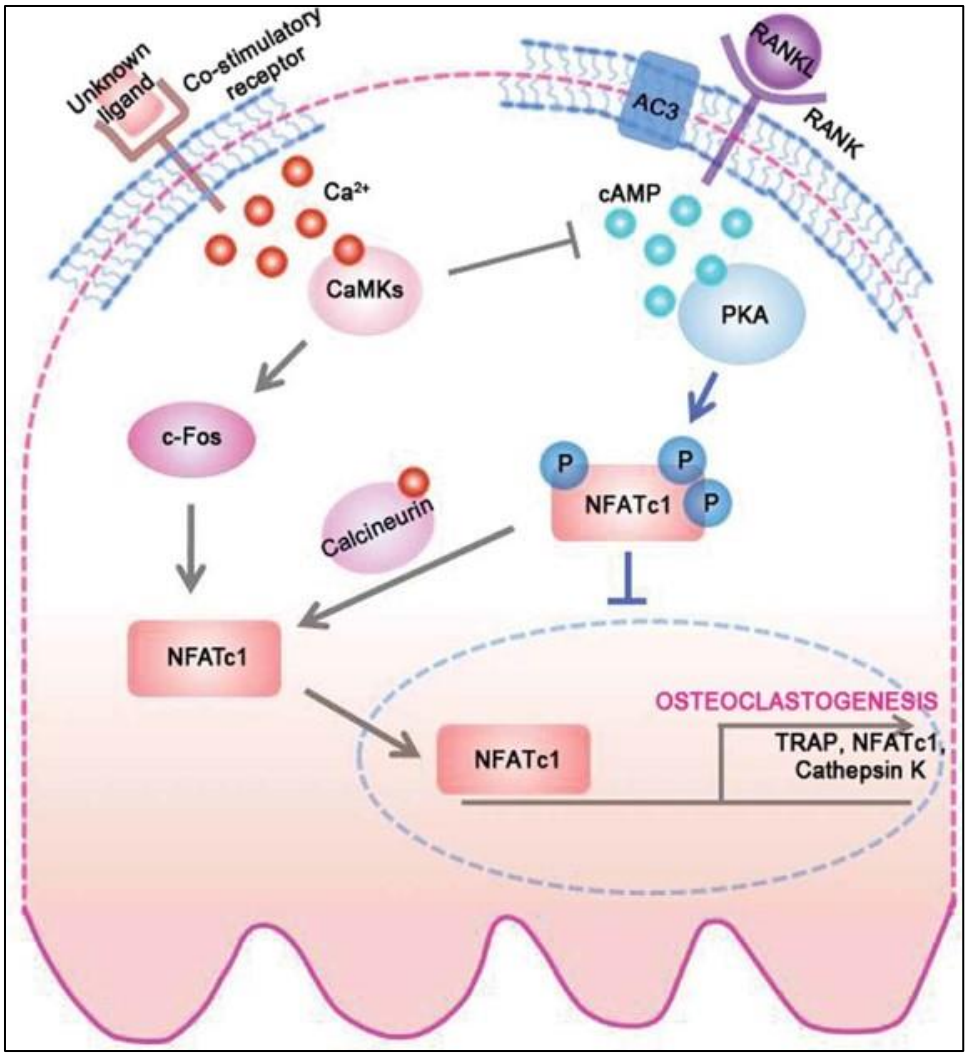

Figure 2.17. The role of AC3- and CaMK-dependent cAMP modulation in osteoclast differentiation. AC3 induction by RANKL results in the accumulation of intracellular cAMP, which culminates in the PKA-mediated phosphorylation and subsequent inactivation of NFATc1. On the other hand, CaMK activities evoked by RANKL curtail intracellular cAMP elevation, limiting the inhibition of osteoclastogenesis by the AC3-cAMP-PKA pathway. Ultimately, the AC3 and CaMK pathways constitute a delicate signaling network for the regulation of osteoclast differentiation (*Yoon et al., 2011*).

While our results certainly suggest that fenoldopam treatment may provide an anti-resorption effect, which would be synergistic with fenoldopam's reported anabolic potential (*Spasic et al., 2022*), its long-term effect on whole-bone has not yet been examined. Together, our data indicate that primary cilium disassembly is an important step in osteoclast formation, and targeting this checkpoint pharmacologically could be a potent avenue for drug development. Given the important function of the primary cilium in the osteogenic role of mesenchymal lineage cells, cilia-targeted treatment strategies could have a two-pronged benefit of promoting bone formation and inhibiting bone resorption. Currently, no such treatment strategy for low bone mass exists and the combination of antiresorptive and anabolic therapies remains in the research phase (*Chan et al., 2016; Tu et al., 2018*). This work is a critical first step in understanding the role of the primary cilium in osteoclast biology and, importantly, provides further support for the potential of ciliotherapies in treating bone disease.

Chapter 3: Characterizing the relationship between actin and microtubule reorganization in T-cell activation

3.1 Abstract

T lymphocytes are vital to the body's adaptive immune response, and their specificity in attachment to APCs contributes to their activation mechanism. Biologically, it has been well-studied that the cytoskeleton is heavily involved in the T-cell activation steps that follow TCR triggering, initiating a downstream signaling cascade in which both actin filaments behave dynamically to initiate the formation of the immunological synapse. It is also increasingly acknowledged that T lymphocytes are both mechanosensitive and mechanoresponsive, as varying mechanical properties of APCs and/or surfaces have been shown to result in varying degrees of activation. Furthermore, the role of the cytoskeleton in this process is well-recognized.

Recent studies, including the aforementioned primary cilia studies, have provided motivation for microtubules (and microtubule-based structures) to also play a part in mechanotransduction in many cell types. While T lymphocytes do not possess this specific organelle, increasing evidence has mounted supporting the hypothesis that MTs contribute heavily to the T-cell activation process. Of note, the microtubule-organizing center (MTOC), or centrosome, localizes to the T cell/APC interface upon TCR triggering. Complementary studies also suggest that microtubules are capable of inhibiting actin dynamics; as such, we sought to better understand the interaction between these two cytoskeletal filaments. Our hypothesis was that microtubule inhibition of actin dynamics is selective for specific types of actin structures and is locally defined. We discovered that WAVE2, but not WASp (both actin-polymerization-related proteins), localize to the same area as microtubules in activated T cells. Furthermore, microtubule depolymerization prior to CD3/CD28 stimulation resulted in a lack of cell adhesion,

which suggests that microtubules likely play a tangential role in the initial formation of the immune synapse.

Combined with findings from previous studies, there is increasing evidence that microtubules of T cells may in fact be a cellular target of interest as further development of immunotherapy approaches continue. As the possible applications of genetically modified T cells expand, the findings of this chapter will have great significance, as the current treatment options for cancer and other immune-related diseases have shortcomings that the medical and scientific communities are still working to resolve.

3.2 Introduction

The molecular interactions underlying cascades of regulation within the adaptive immune response take place in a nanoscale gap between T cells and antigen presenting cells called the immunological synapse (*Dustin, 2014*). Under normally functioning circumstances, this junction provides the basis for a complex and tactical defense against pathogens and infected host cells. However, abnormalities related to the synapse lead to a system breakdown in which the body cannot effectively protect itself. Given the structural design, one defining characteristic of the IS has long been its spatial organization with respect to intercellular signaling. One previous study used planar costimulation arrays containing antibodies against CD3 and CD28 to better mimic the targeted structure of the immune synapse when T cells activate (*Shen et al., 2008*). They combined multiple rounds of microcontact printing on a single surface and noted an increase in IL-2 secretion (one marker of T-cell activation) when anti-CD28 was presented on the cell periphery (see Figure 3.1). This indicated the importance of structure when experimenting with T cell activation properties, but it did not resolve exactly what intracellular mechanisms were involved in this process.

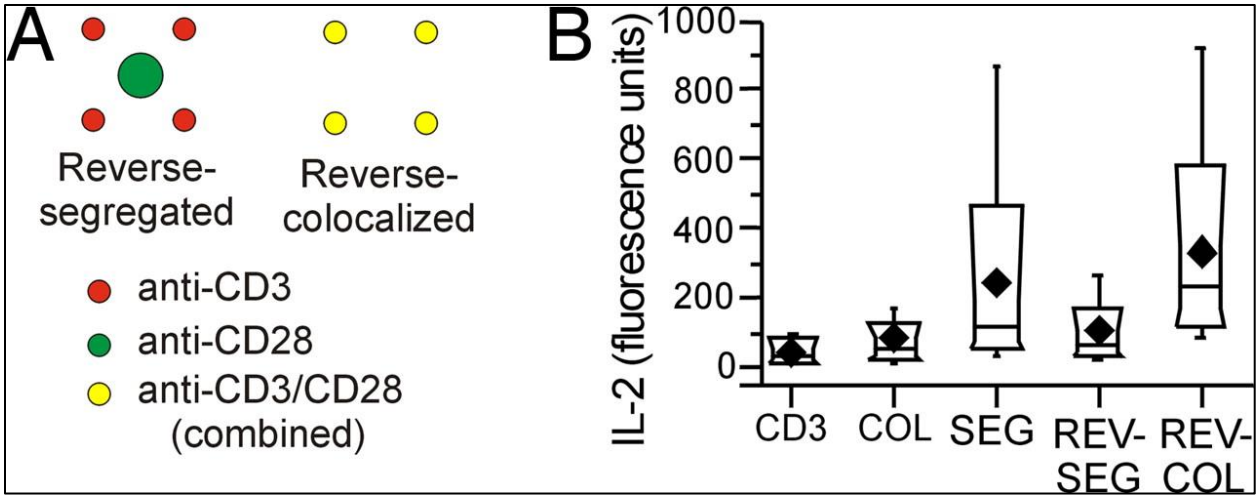

Figure 3.1. IL-2 secretion correlates primarily with CD28 geometry. (A) Additional geometries of anti-CD3 and anti-CD28 ligands. (B) Six-hour IL-2 secretion on these patterns. Data from each pattern are different from all other conditions (Kruskal–Wallis analysis, $\alpha = 0.05$) (*Shen et al., 2008*).

An increasing number of studies conducted began realizing that readouts from *ex vivo* cultures across many cell types depended on the mechanical properties of the culture substrate. As a result, the question of the impact of substrate stiffness on the activation and expansion of T cells was worth exploring. Two studies from 2012 sought to answer this question; interestingly, different experimental features yielded varying results. One study used a mixture of human helper and cytotoxic T cells on PDMS with a higher stiffness range and concluded that softer substrates stimulated greater IL-2 production and proliferation of T cells compared with stiffer substrates (*O'Connor et al., 2012*). The other study used murine CD4+ T cells on PA gels with a lower stiffness range, noting that stronger activation correlated with higher elastic moduli (*Judokusumo et al., 2012*). Despite reaching different conclusions, it was clear from these papers that T cells respond differently to different mechanical properties.

The next logical question to ask was what cellular machinery was regulating this mechanosensing ability of lymphocytes. One study found that T cells are capable of sensing the rigidity of an underlying substrate via TCR/CD3 and CD28. It is this system that helps regulate

the cellular forces needed to test the mechanical properties of the extracellular environment (see Figure 3.2) (*Bashour et al., 2014*). It then become clear, using traction force microscopy, that not only do these lymphocytes sense their mechanical environment, but they also exert forces on APCs during activation, and their ability to do so depends largely on actin dynamics (see Figure 3.3) (*Hui et al., 2015*).

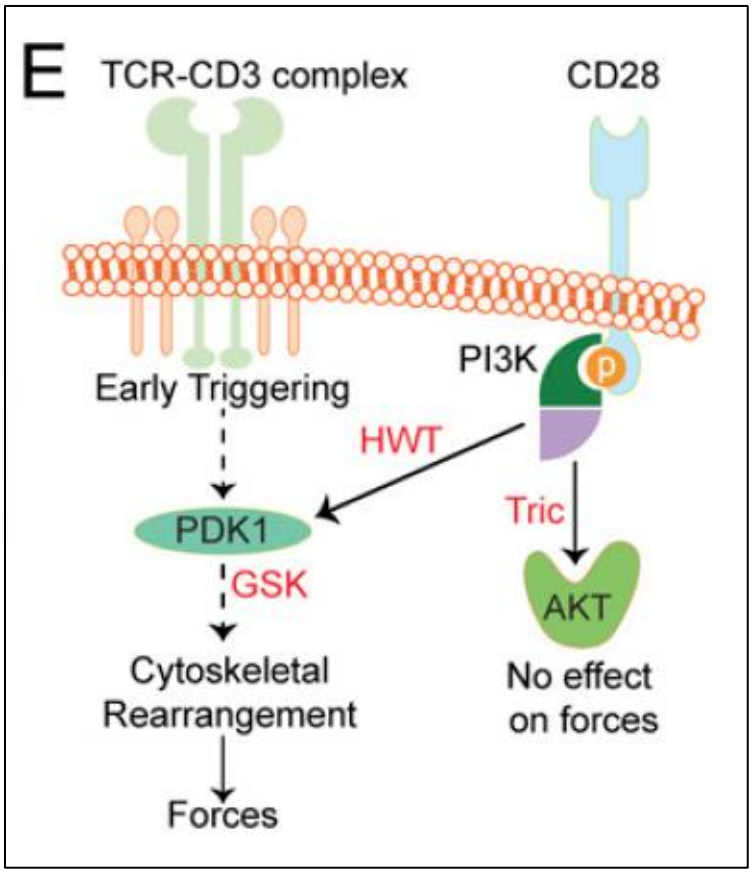

Figure 3.2. Schematic of force augmentation by CD28 signaling. Inhibitors are indicated in red (*Bashour et al., 2014*).

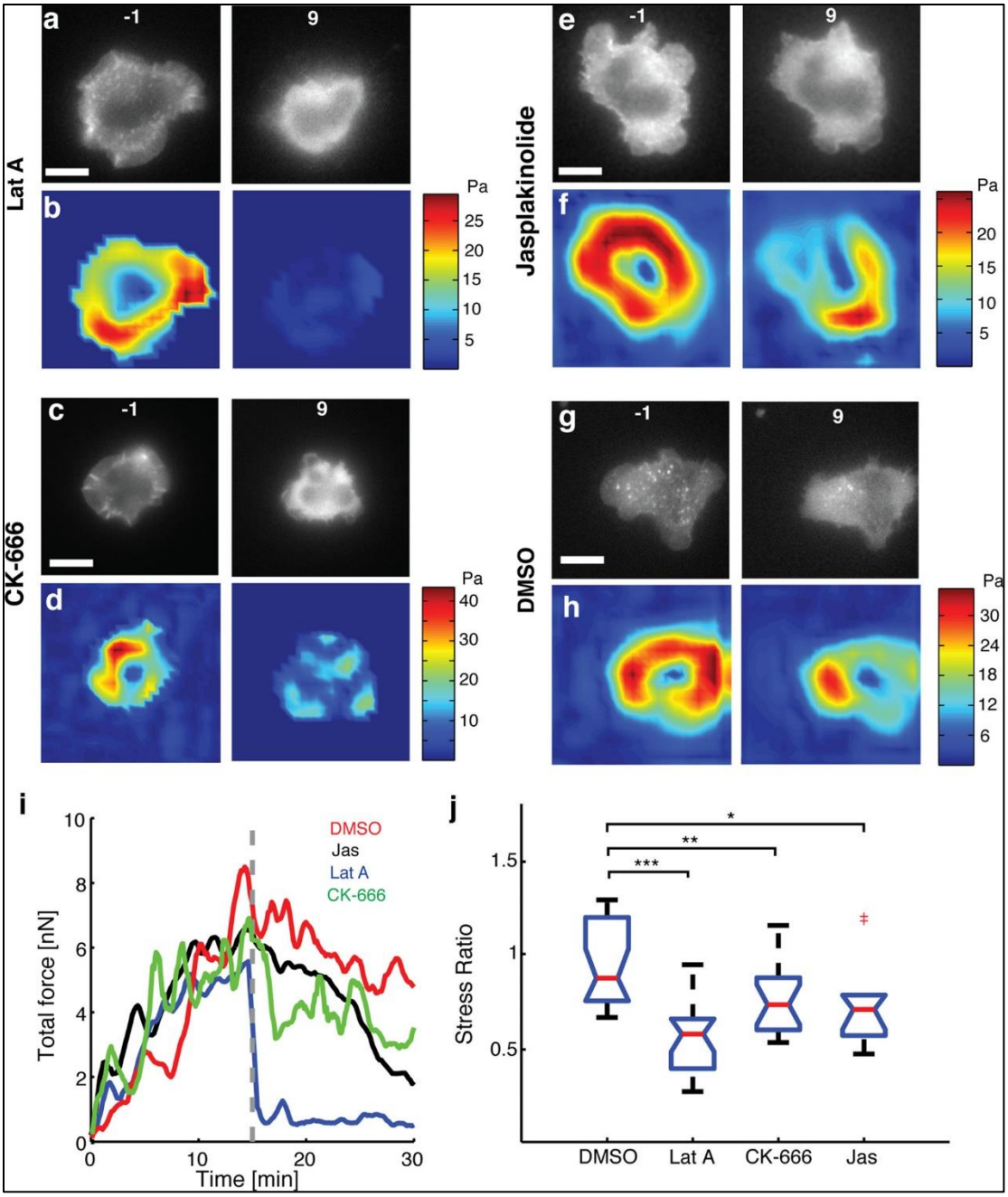

Figure 3.3. Loss of F-actin dynamics reduces cellular force generation. Fluorescence images of EGFP-actin expressing Jurkat T-cells on an elastic substrate 1 min before (left) and 9 min after (right) application of (a) 1 μM latrunculin-A, (c) 100 μM CK666, (e) 1 μM jasplakinolide, and (g) 0.1% DMSO. Color maps of traction stresses of the same cells before (left) and after (right) addition of (b) 1 μM latrunculin-A, (d) 100 μM CK666, (f) 1 μM jasplakinolide, and (h) 0.1% DMSO. (i) Total traction force as a function of time for a representative cell in each of the conditions described. The dashed line represents the time point at which the drug was added. (j) Comparison of the after-to-before ratios of traction stresses for application of Lat-A (N = 20 cells), CK666 (N = 17 cells), and Jasp (N = 10 cells) with control (DMSO carrier, N = 20 cells) (*Hui et al., 2015*).

With implication that actin is featured in T-cell mechanotransduction, scientists began exploring other specific components of the T-cell cytoskeleton with respect to activation and function. It was previously discovered that, upon TCR stimulation a burst of actin polymerization is triggered, leading to an enhancement of the cell-APC contact area as the T cell spreads over the surface of the APC and forms the IS (see Figure 3.4) (*Bunnell et al., 2001; Grakoui et al., 1999; Hui et al., 2012*). In addition, upon contact with the target cell, the microtubule organizing center (MTOC) of the cytotoxic lymphocyte (CTL) polarizes towards the APC, where the immune synapse will begin forming. Lytic granules move along microtubules towards the polarized MTOC. Actin is then cleared away from the synapse, and granules are delivered directly to the plasma membrane (see Figure 3.5) (*Geiger et al., 1982; Stinchcombe et al., 2006*).

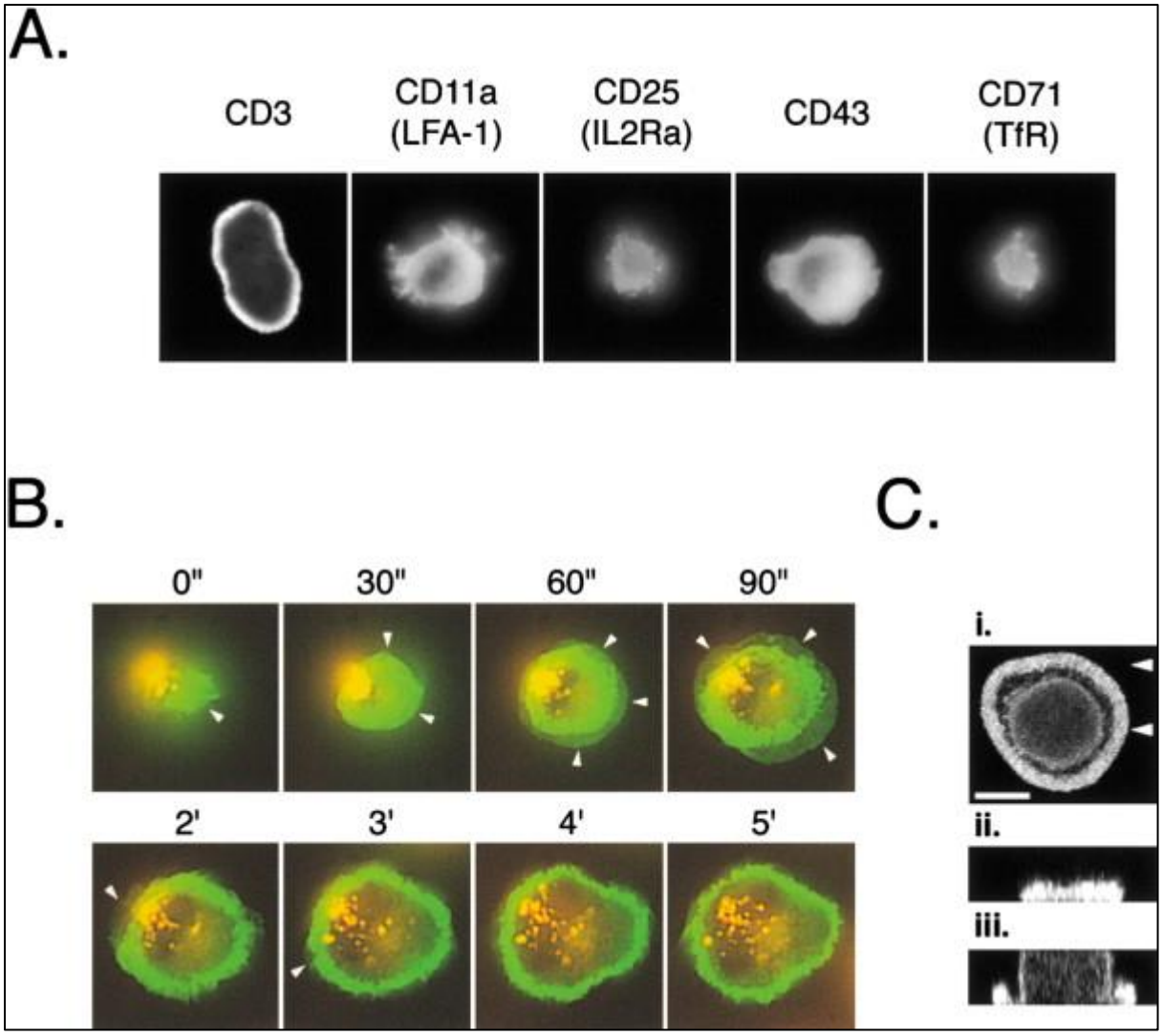

Figure 3.4. Dynamic Remodeling of the Actin Cytoskeleton during TCR-Induced Spreading. (A) Jurkat cells expressing EGFP-actin were plated on coverslips coated with the indicated antibodies. EGFP-actin was imaged at the coverslip every 30 s using the CCD-equipped microscope. The images presented here were acquired 5 min after the initial contact with the coverslip. (B) Jurkat cells expressing EGFP-actin were labeled with DiI, plated on coverslips coated with the TCR-specific antibody UCHT1, and imaged every 7.5 s using the CCD-equipped microscope. Time was measured from the initial contact with the coverslip. EGFP-actin is shown in green. The membrane stain DiI appears yellow orange (see Experimental Procedures) and is not relevant to this discussion. White arrows mark large, sheet-like lamellipodia. (C) EGFP-actin-expressing Jurkat cells were plated on coverslips coated with UCHT1 for 5 min and fixed. Confocal images of EGFP-actin spanning 10 μm of height were collected at 0.5 μm intervals. The images presented were reconstructed as follows: (i) projection of the z-stack onto a horizontal plane; (ii–iii) vertical slices corresponding the arrows in (i); (ii) cross-section through the actin-rich border; (iii) cross-section through the cell body (*Bunnell et al., 2001*).

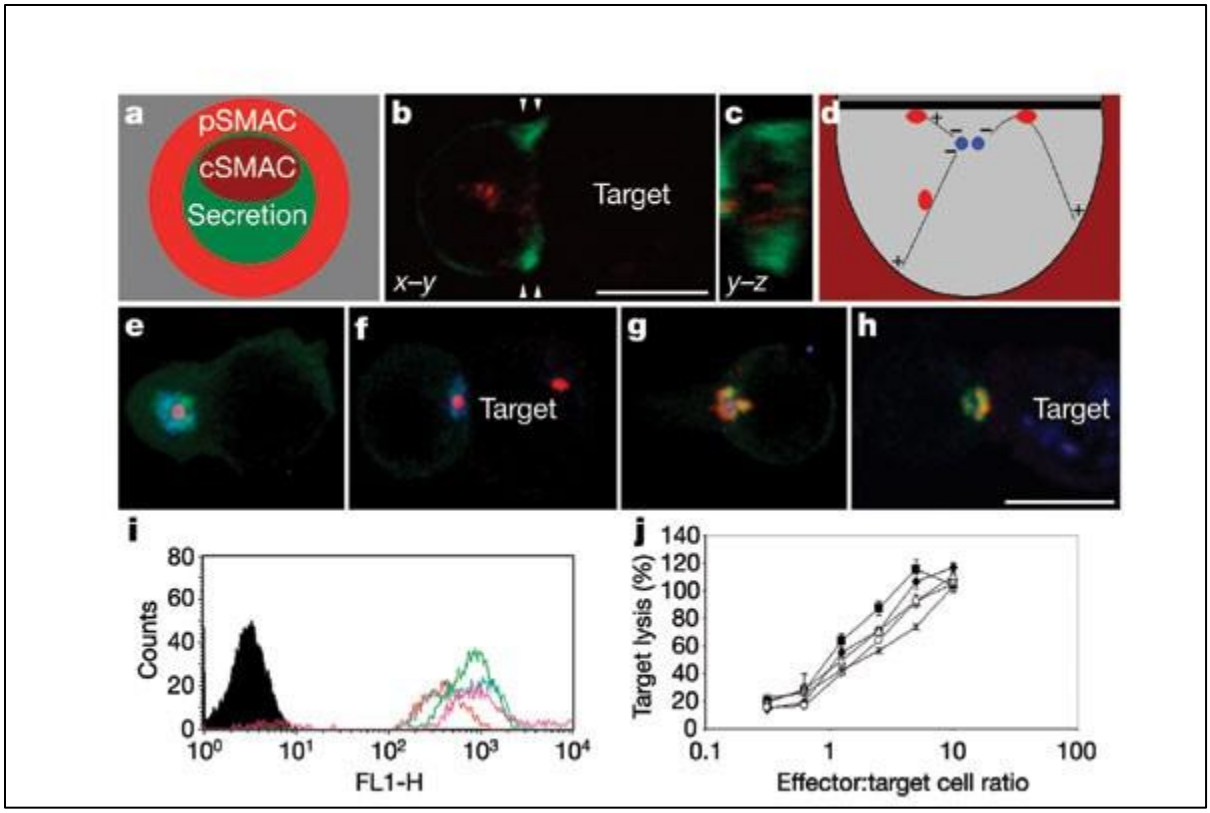

Figure 3.5. Minus-end microtubule transport motors are sufficient for transport of lytic granules to the secretory site during target cell killing. a, En face view of the organization of the CTL immunological synapse. b, c, Single x–y confocal section (b) and en face (y–z) reconstruction (c) of a human CTL, expressing actin–GFP (green) and with CD63-labelled granules (red), conjugated to a target cell. d, Organization of microtubules (thin black lines) with lytic granules (red), relative to the immunological synapse (thick black line) and centrioles (blue). e–h, Projected serial confocal sections through human CTLs, expressing GFP–RILP (green), shown alone (e, g) or conjugated to targets (f, h), and labelled with markers of the centrosome (g-tubulin is red in e, f, but blue in g, h) and granule markers (cathepsin D, blue in e, f; perforin, red in g, h). i, Fluorescence-activated cell sorting (FACS) profile showing GFP expression (FL1-H) of mock-infected (filled histogram) human CTLs and four CTL clones expressing GFP–RILP (unfilled histograms). j, Killing assay using mock-infected CTLs (diamonds), GFP-(squares) or GFP–RILP-(triangles, circles, crosses) expressing CTL clones. Error bars show standard deviation from the mean. Scale bars for b, c and e–h, 10 mm (*Stinchcombe et al., 2006*).

Additional studies began deciphering a potential interplay between actin and microtubules. Accompanying immunological synapse formation, T cells undergo a rapid polarization of the MT cytoskeleton (1–2 min after initial contact) which facilitates directional secretion of cytokines and cytolytic factors toward the APC (*Gomez et al., 2007; Yi et al., 2013*).

This finding provided motivation that the contact zone between T cells and APCs is a site at which the MT and actin cytoskeletons could potentially interact to regulate signaling. An additional study found that traction forces generated by T cells are actually regulated by dynamic microtubules at the interface, and these MTs suppress actin retrograde flow at the T-cell–substrate interface (see Figure 3.6) (*Hui & Upadhyaya, 2017*). Given these motivating bases, we posed the question of which protein(s) associated with the plasma membrane or actin might facilitate the translocation of actin and/or microtubules during T-cell activation. In addition, it would also be worth exploring to what extent this relationship is altered under varying substrate stiffness values as well as micropatterns presenting different orientations of activating antibodies.

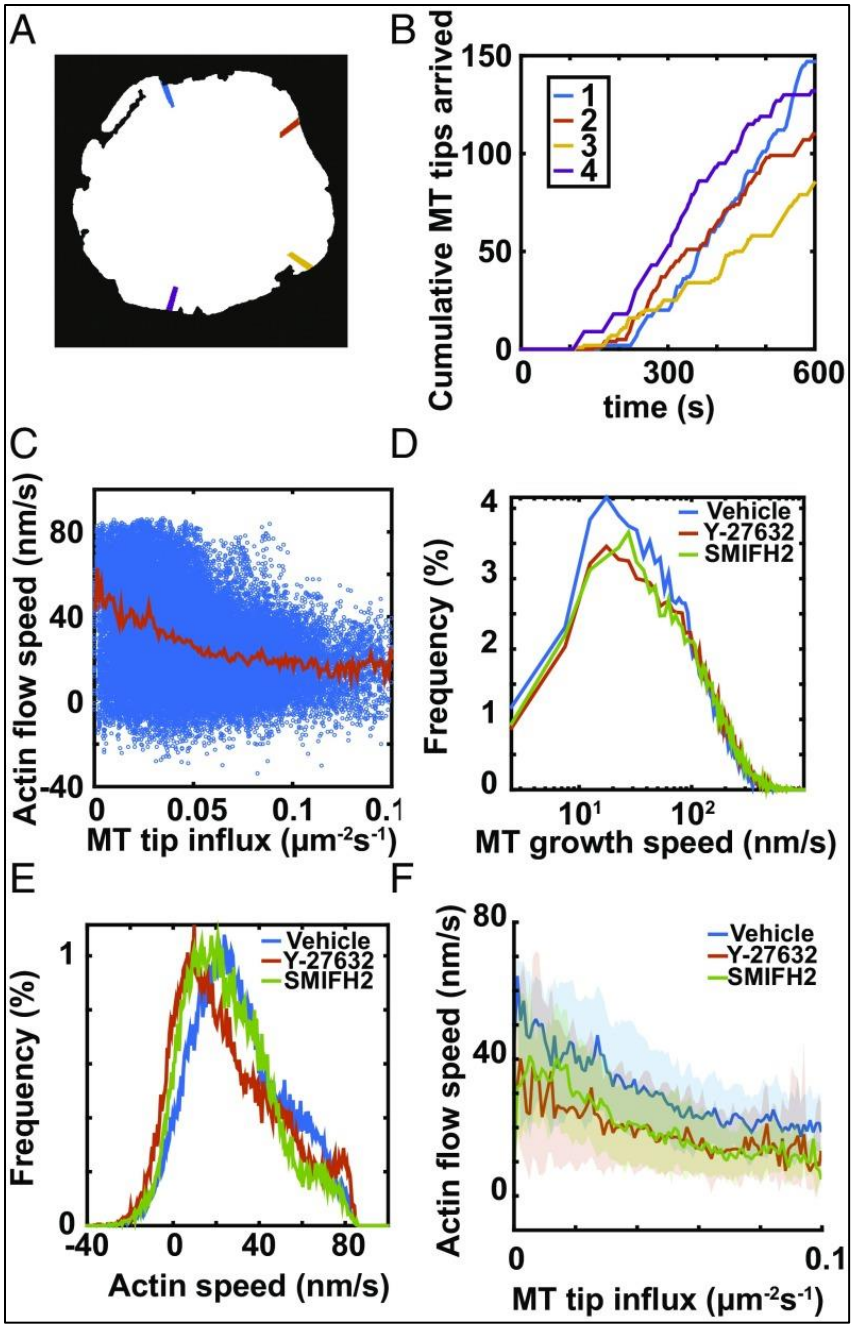

Figure 3.6. MT influx suppresses local actin retrograde flow. (A and B) Cell contact and four regions of different polar angles in which the numbers of MTs entering each region were counted as a function of time. (C) Actin flow speed against MT influx in different polar angles. The pdfs of MT growth speed (D), actin flow speed (E), and the actin flow–MT influx relation for T cells spreading in the presence of vehicle and inhibitors (F) are shown. Data were taken at between 9 and 10 min of activation (*Hui & Upadhyaya, 2017*).

3.3 Materials and Methods

Preparing Glass Coverslips

We first dilute 7x detergent (MP Biomedicals) to 1x in DI water in a 1000-mL beaker. The glass coverslips (22x22mm, size #0; Electron Microscopy Sciences) are set in ceramic holders, which hang from the edge of the beaker via plastic attachments. The beaker is then set on a plate with a magnetic stirrer inside, set to 220°C and 280 rpm. After the solution turns clear (takes approximately 1 hour), leave the beaker on for an additional 30 min. While the beaker is still on the plate, remove one of the ceramic holders using tweezers, and rinse off by submerging repeatedly (10x) in and out of a 250-mL beaker of fresh DI water. Dry the coverslips with compressed nitrogen gas, carefully holding the top of the glass coverslips. Repeat this for the other three ceramic holders. Place ceramic holders into 150-mL beakers (each beaker can hold two ceramic holders), cover this beaker with foil, and bake in an oven at 450°C overnight, or a minimum of 6 hours.

Designing Wafers and Stamps

We start the printing process using a 4-inch diameter master wafer, constructed on a silicon-based disc. It is then treated using an SU-8 negative photoresist process (*Chen & Lee, 2021*). The first step is to perform a dehydration bake with a vacuum. Next, we perform a two-step spin cycle: step 1 settings are 500 rpm, 100 acceleration, 5 seconds, and step 2 settings are 5000 rpm, 500 acceleration, 30 seconds; this yields a 4-µm-thick resist. This bakes at 95°C for 3 minutes. It is then exposed for 12 seconds using SUSS Mask Aligner on CH1 (365 nm, exposure set point 9.5 mW/cm^2) and baked at 65°C for 1 minute, after which the image of the pattern should appear. SU-8 developer is then used for 1 minute before being rinsed with SU-8 developer and isopropanol. The final step is a 30-minute hard bake at 200°C.

For the studies outlined in this chapter, the macro-structure produces sixteen squares (1 cm each side, 0.5 cm spacing), with each square containing a sequence of patterned holes, which may vary. These holes are each 1 µm in depth, but the other design features are variable. For murine cell applications, they are 2 µm in diameter spaced 10 µm apart; this becomes 15 µm for human T cells, which are larger. Another set, used to create a segregated pattern, uses dots that are 1 µm in diameter spaced 5 µm apart (see Figure 3.7).

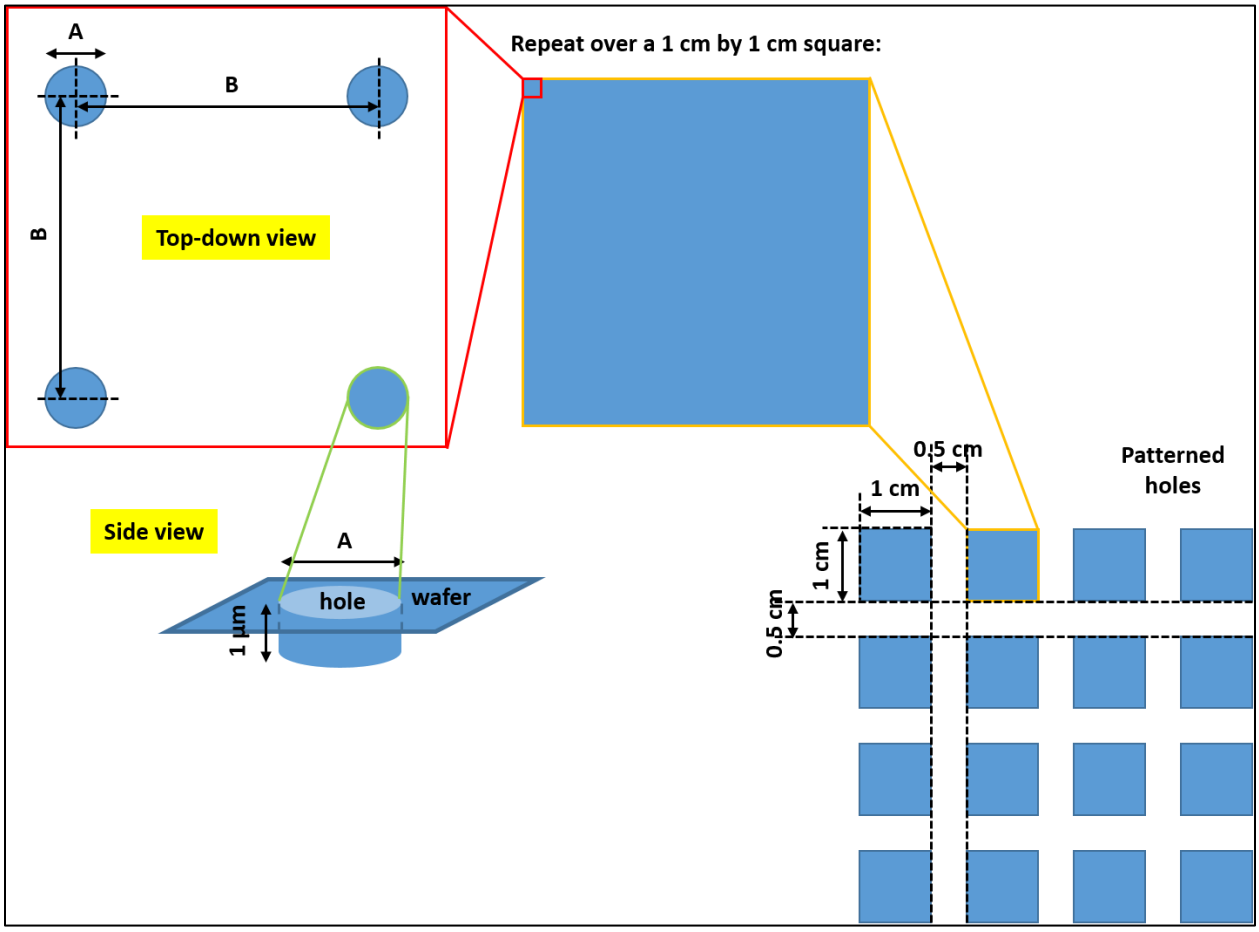

Figure 3.7. Schematic of wafer design used for microcontact printing.

After the master wafer has been fabricated, we clean the master wafer by rinsing with isopropanol and drying it with compressed nitrogen gas. We then place the wafer into a foil-lined 150x20mm petri dish (Fisher Scientific). Separately, we place an open 50-mL centrifuge tube

(Falcon) into a tube holder and tare this on a scale. We then pour 3.5 g of pre-polymer, 7-8% vinylmethylsiloxane-dimethyl-siloxane copolymer (VDT-731-100GM, Gelest). Next, we add 18 µL of our catalyst, platinum-divinyltetramethyldisiloxane complex; 2% Pt in xylene (SIP6831.2, Gelest) and 10 µL of our modulator, 2,4,6,8-Tetramethyl-2,4,6,8-tetravinylcyclotetrasiloxane (396281-10ML, Sigma). Tubes containing catalyst and modulator should be filled with compressed nitrogen gas before closing. These three chemicals are vortexed for 30 seconds to mix. Lastly, we add 1 mL of the second copolymer, 25-30% methylhydrosiloxane-dimethylsiloxane copolymer (HMS-30-100GM, Gelest), to the tube and vortex an additional 15 seconds. The tube is spun down at 3000 rpm for 90 seconds. We then pour a dollop (~2 cm in diameter) of this "hard"-PDMS mixture onto the middle of the wafer, and use a piece of folded Parafilm (Bemis) to evenly spread the PDMS. This dish is covered and incubated at 60°C for 30 minutes. Afterwards, we mark the location of imperfections so that we know which stamps to later omit.

We then prepare a "soft"-PDMS mixture using a 10:1 ratio from a SYLGARD 184 Silicone Elastomer Kit (Dow). We place a disposable plastic conical container on a balance and tare it, before weighing out 60 g of base polymer. We then add an additional 6 g of curing agent and thoroughly mix by hand with a stirring rod for ~2 minutes. This mixture is transferred to a 50-mL tube and spun at 3000 rpm for 3 minutes. It is then poured evenly over the cured hard-PDMS-covered wafer and degas in a vacuum chamber for 30 minutes. This bakes at 60°C overnight, or a minimum of 4 hours.

Microcontact Printing

After the overnight incubation, we peel off the PDMS, now with stamps, from the master wafer. We then wash the wafer with isopropanol and dry with compressed nitrogen gas; this

master wafer can be stored and reused. We then cut a full 1-cm square from the PDMS (see Figure 1) with a decontaminated razor blade, being careful not to touch the top of the pattern. These squares are further cut into four half-inch squares. Each stamp is then washed in 100% ethanol, followed by 100% DI water, and dried with compressed nitrogen gas. We line a petri dish with Parafilm and set these cleaned stamps in pairs, with the patterned sides facing inward toward each other but not touching. Next, we create a solution of fluorescently labeled anti-CD3 and anti-CD28 (Invitrogen) in a 1:3 mass ratio, at a total concentration of 25 µg/mL. We pipette 50 µL of this solution in the space between each pair and incubate this in the dark for 60 minutes.

The stamp is then washed in PBS, followed by DI water, and dried with compressed nitrogen gas. We then place the stamp (pattern side-down) onto a clean glass coverslip and press the top until the fluorescent color appears (see Figure 3.8). A small washer is placed on top of the stamp, and it incubates for 5 minutes (this process is repeated for each stamp being used in the sample). Concurrently, we cut PDMS rings (inner diameter 6 mm) to use as wells. These rings are washed in PBS, followed by DI water, and dried with compressed nitrogen gas. After stamping, these wells are placed onto the coverslips (one each) and incubated overnight with 2 µg/mL of ICAM (R&D Systems).

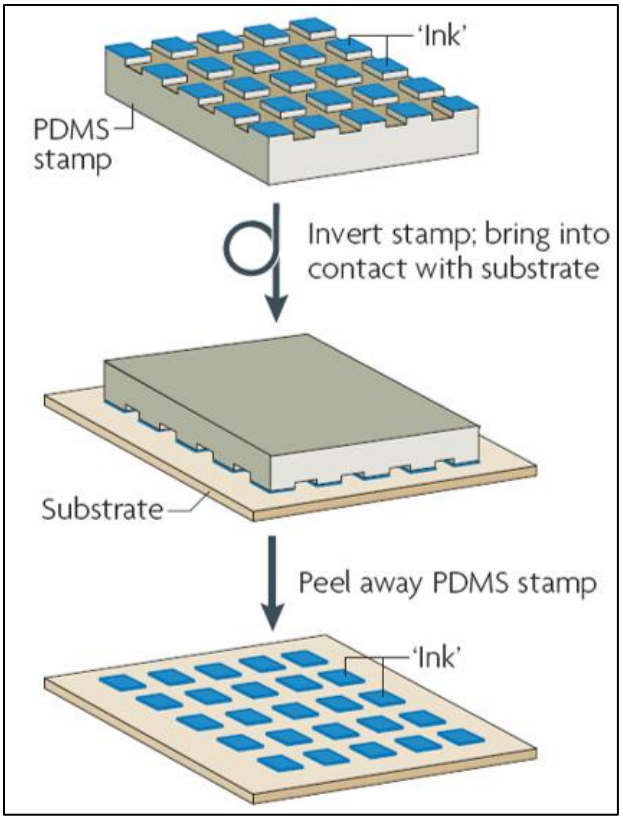

Figure 3.8. Schematic of stamping procedure onto glass coverslips (*J. H. Lee et al., 2015; Weibel et al., 2007*).

CD4+ T Cell Isolation

Six-week-old male C57BL mice (Taconic) are sacrificed under CO_2 gas. We dissect the spleen extract all cells using a 40 µm cell strainer (Falcon) and plunger (BD Biosciences). These cells are suspended in a 50-mL tube of RPMI 1640 media supplemented with 10% fetal bovine serum, 10 mM HEPES, 2 mM L-glutamine, 50 µM β-mercaptoethanol, 50 U/mL penicillin, and 50 µg/mL streptomycin. We determine the concentration of the cell suspension via cell counting using a hemocytometer, and the volume containing 50 million cells is transferred to a new Falcon tube and centrifuged (300 rcf, 8 minutes). The media is aspirated, and the cell pellet is resuspended in 200 µL of cold buffer (mixture of PBS, 2 mM EDTA, and 0.5% bovine serum albumin). We then add 50 µL of Biotin-Antibody Cocktail (Miltenyi) and incubate at 4°C for 5

minutes. We then add 150 µL of cold buffer and 100 µL of Anti-Biotin Microbeads (Miltenyi) and incubate at 4°C for 10 minutes. We then place an LS Column (Miltenyi) into a MACS separator and wash with 3 mL cold buffer into a waste container. We then replace this with a collecting container and transfer all 500 µL of our cell/Biotin/Microbead mixture to the column, followed by 3 mL of cold buffer. We then count the cells to determine the concentration, spin down the desired volume/number of cells, and resuspend in warmed (37°C) complete media to desired final concentration.

Cell Seeding and Immunocytochemistry

Cells are seeded onto coated-glass coverslips at 820,000 cells/cm^2 in 50 µL complete media and incubate at 37°C and 5% CO_2 for 60 minutes. We then fix each sample at RT by adding 50 µL of 4% paraformaldehyde (Electron Microscopy Sciences) to each well for 15 minutes and washing 3x in PBS for 5 minutes each time. We then treat each sample with 0.1% Triton X-100 (Sigma) for 10 minutes and wash in PBS 3x for 5 minutes each time. We then apply a blocking solution of 10% goat serum at RT for 1 hour; this step is not followed by a wash. This is removed and immediately incubated overnight at 4°C with any number of primary antibodies: anti-β-tubulin (mouse monoclonal, BD Biosciences), anti-pericentrin (rabbit polyclonal, Abcam), anti-WAVE2 (rabbit polyclonal, Invitrogen), and anti-WASp (rabbit polyclonal, Abcam). The next day, this primary antibody is washed off, and samples incubate in a fluorescently labeled secondary antibody at RT for one hour. The final step is to wash and image.

IL-2 Secretion Assay and Mechanosensing

In brief, cells are resuspended in cold media and 10 µL of Cytokine Catch Reagent (Miltenyi) per 1M cells is added before incubating on ice for 5 minutes. Then, warm media is

added to dilute the cells suspension before seeding cells onto substrates of varying stiffness. Inhibitor molecules are added 10 minutes after seeding, and samples incubate for an additional 4 hours at 37°C. Cells are then spun down and resuspended in cold buffer with IL-2 detection antibody before incubating on ice for 10 minutes. Additional cold buffer is added before cells are spun down again and resuspended in a 4% fixative solution before incubating at room temperature for 15 minutes. This is then quenched with cold buffer and spun down; cells are resuspended in FACS buffer and stored at 4°C before being used for flow cytometry.

Statistical Analysis

Where applicable, data were analyzed using Pearson's Correlation, where sample size, n, represents biological replicates.

3.4 Results

T cells effectively align to localized areas of activation

Immunocytochemistry (ICC) revealed that T cells correctly locate sites of activating stimuli, evidenced using fluorescently-labeled anti-CD3/anti-CD28. This observation was further solidified by labeling cells with anti-β-tubulin, which binds to both microtubules and centrosomes. Fixed samples that were stained with this antibody revealed an MTOC centralized at the activation location, mimicking the immunological synapse (see Figure 3.9). Furthermore, individual microtubule fibers can also be seen emitting from the centrosome, in addition to populating the exterior of the cell.

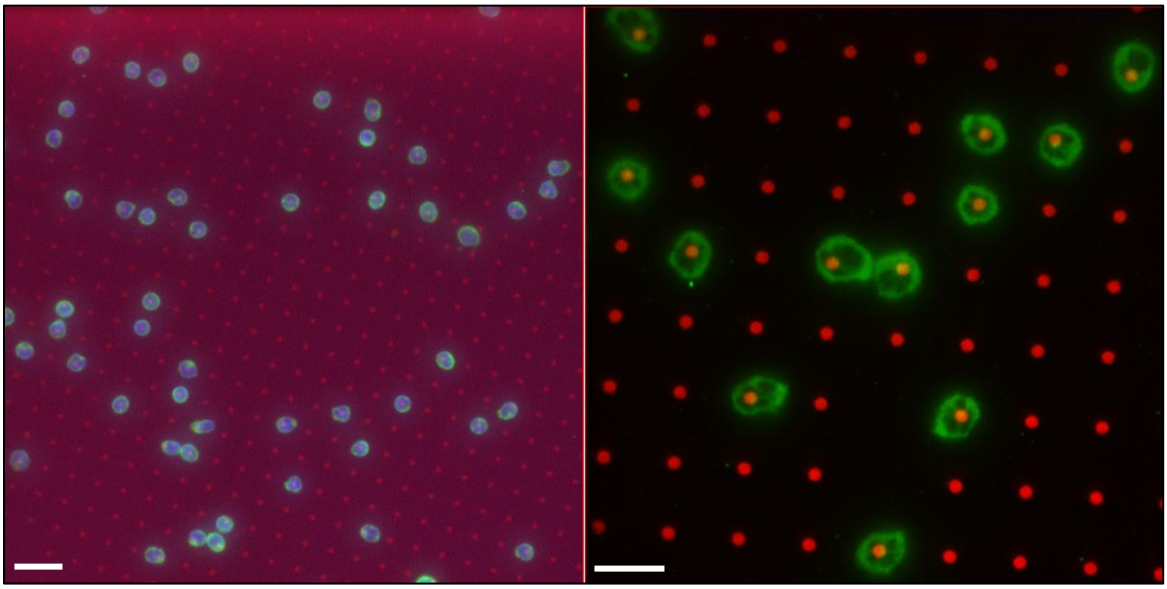

Figure 3.9. MTOC alignment of murine CD4+ cells to local areas of activation. Micropattern (red) made from 2-10 µm wafer and transferred to glass coverslips via PDMS molds were incubated in both anti-CD3 and anti-CD28. The left panel image was captured at 40x; scalebar = 20 µm. The right panel image was captured at 100x; scalebar = 10 µm. Microtubules (green) can be visualized both inside the cell and on the cell periphery.

WAVE2, not WASp, translocates to areas of high-MT concentration near the cell membrane

After confirming the alignment and MTOC features, a double ICC allowed us to view both microtubules and our actin-polymerization-related proteins of interest simultaneously with respect to individual cells. We observed qualitatively not only was the arrangement of the highest intensity regions of WAVE2 evident, but this visually correlated to that of the peripheral microtubules (see Figure 3.10). To quantify this relationship, we traced the outermost areas of fluorescence for individual cells for both wavelengths captured and applied a Pearson correlation to discrete pixels to show the comparison. The average correlation was 0.8771±0.0665, indicating a very strong relationship between the shared localization of microtubules and WAVE2 (see Figure 3.11). Of note, this observation of distinct arrangement was not found when staining for WASp. The resulting images showed inconsistent fluorescence patterns, and none aligned near the periphery of the cell (see Figure 3.12).

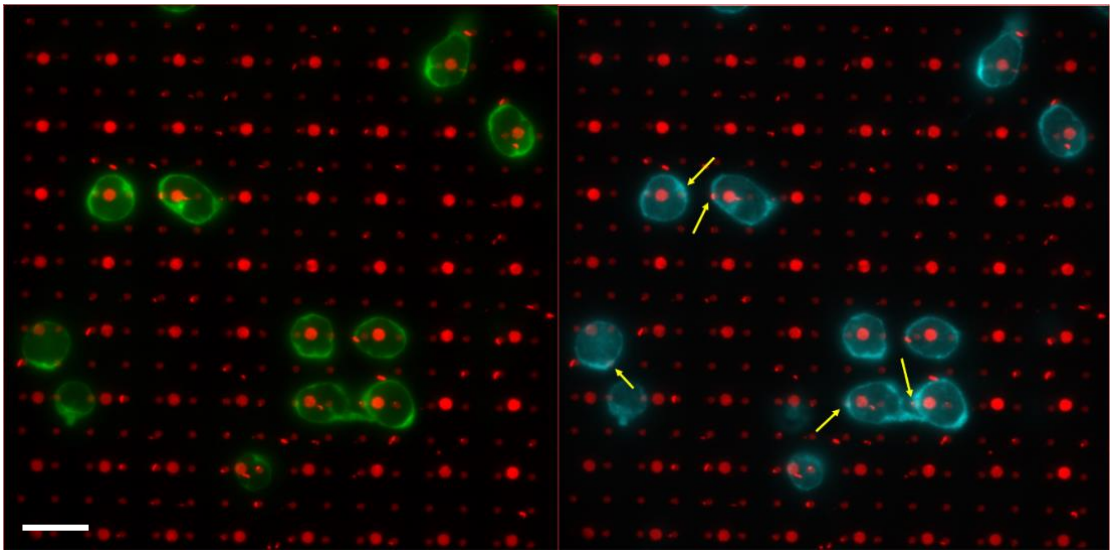

Figure 3.10. Images of spatial proximity of WAVE2 with respect to peripheral microtubules. The pattern used is comprised of segregated activating antibodies; the large red dots (2 µm in diameter, 10 µm spaces between each dot) are incubated with anti-CD3, and the small red dots (1 µm in diameter, 5 µm spaces between each dot) are incubated in anti-CD28. The left panel image shows microtubules (green), while the right panel image shows WAVE2 (blue). The yellow arrows of this panel indicate regions of cells where high intensity of both proteins appears evident. Scalebar = 10 µm.

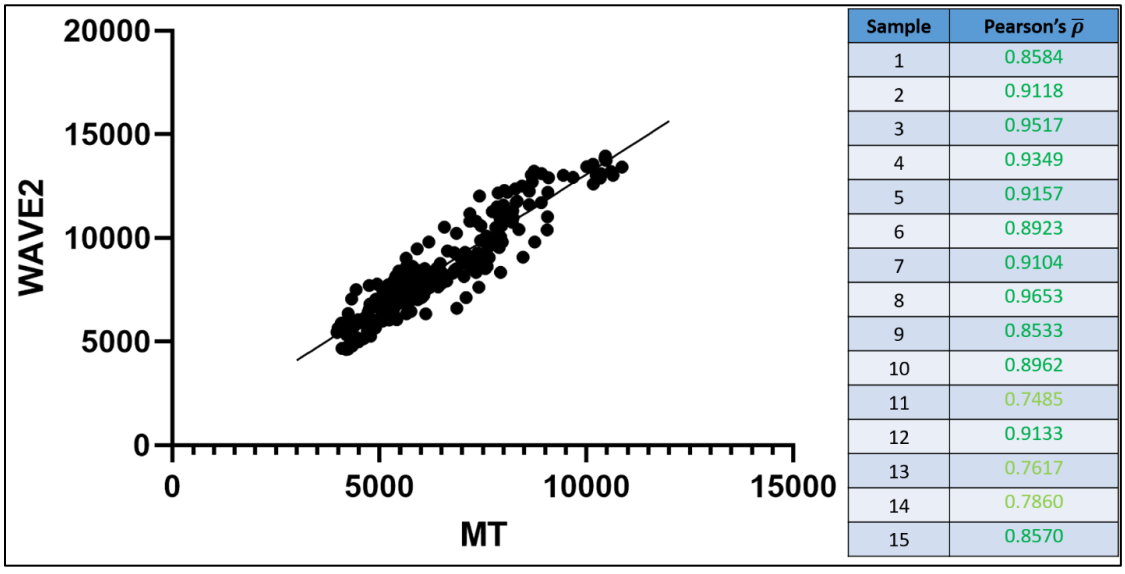

Sample	Pearson's $\bar{\rho}$
1	0.8584
2	0.9118
3	0.9517
4	0.9349
5	0.9157
6	0.8923
7	0.9104
8	0.9653
9	0.8533
10	0.8962
11	0.7485
12	0.9133
13	0.7617
14	0.7860
15	0.8570

Figure 3.11. Scatter plot and correlation showing quantitative relationship between microtubules and WAVE2 concentration. The graph shows the correlation of pixel intensity values (x- and y-axes, arbitrary values) of just one individual cell along its exterior with respect to microtubules and WAVE2 (334 segments). Correlation values of 15 samples (other plots not shown) are listed in the table on the right (correlation values above 0.8, indicating a strong relationship, appear in dark green text); average Pearson's correlation was 0.8771±0.0665.

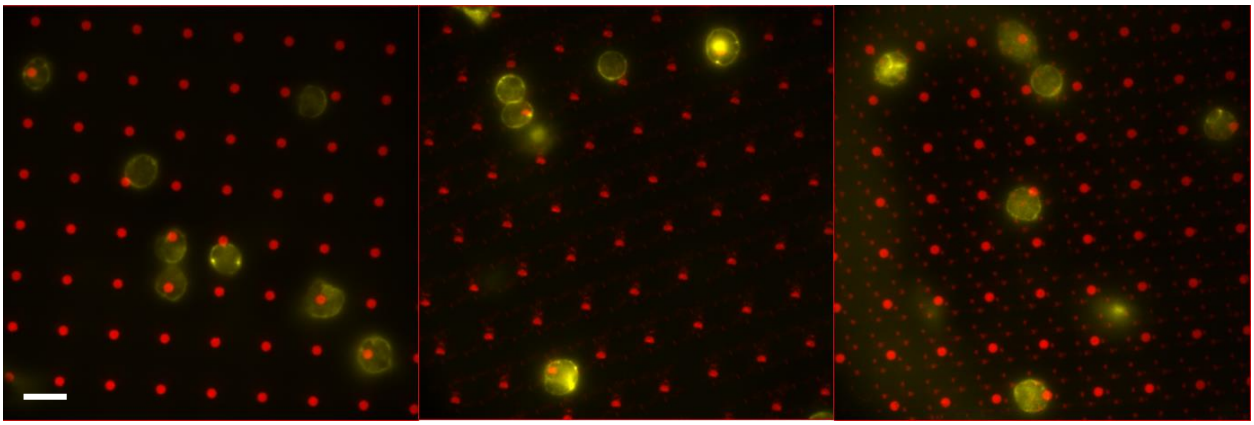

Figure 3.12. Images of spatial organization of WASp. Using both colocalized (first two panels) and segregated (third panel) patterns, we see that the highest intensity locations of WASp staining are inconsistent and rarely present on the cell periphery. Scalebar = 10 μm.

Microtubule inhibition via nocodazole did not alter WAVE2 spatial localization

Given the correlation findings between microtubules and WAVE2, and driven by the observation that MTs play a role in actin dynamics, we hypothesized that inhibiting microtubule polymerization would impact the observed organization of WAVE2. When treated with nocodazole (NZ), the intracellular MT structure was indeed disrupted; however, the relative spatial localization of WAVE2 was unaffected (see Figure 3.13). Of note, from a procedural standpoint, the above results were obtained when NZ was applied 10 minutes after cells were seeded onto activating surfaces. We also conducted iterations in which nocodazole was added to cell suspension for 10 minutes before being seeded. In this study, the cells failed to adhere to the surface, resulting in too low a resulting cell count to complete the analysis.

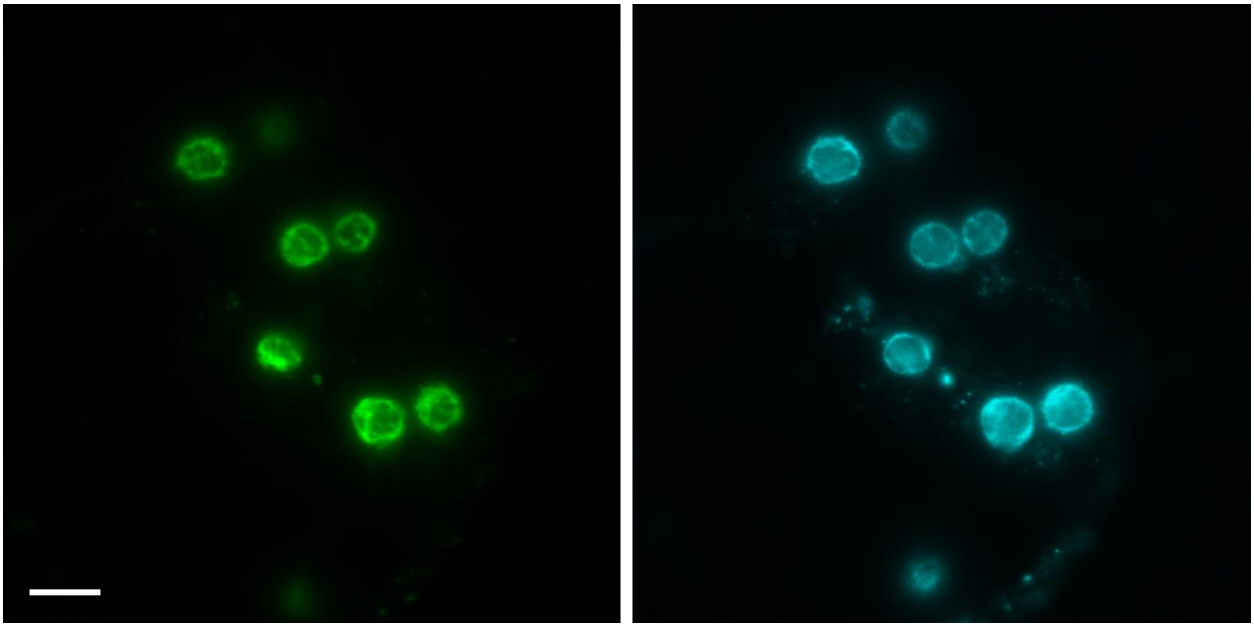

Figure 3.13. Organization of WAVE2 is unchanged despite microtubule inhibition. The left panel image shows microtubules (green), while the right panel image shows WAVE2 (blue). The organization of the intracellular microtubules are clearly disrupted (MTOC and filaments emitting from center are not visible); however, the relative areas of high and low intensity from WAVE2 staining are the same. Scalebar = 10 μm.

Microtubule inhibition reduces T-cell mechanosensing capabilities

In order to explore any potential impact of microtubules on the ability of T cells to sense their mechanical environment, we seeded healthy human CD4+ cells onto PDMS of varying stiffness values under MT-inhibitory conditions. While Taxol had no noticeable effect, the number of cells secreting IL-2 and the total amount of IL-2 secreted seems significantly lower in cells treated with nocodazole (see Figure 3.14). In addition, the difference between stiffness samples of the NZ group seems very similar, implying that the dynamicity of microtubules may be a necessary characteristic of T cells' mechanosensing abilities.

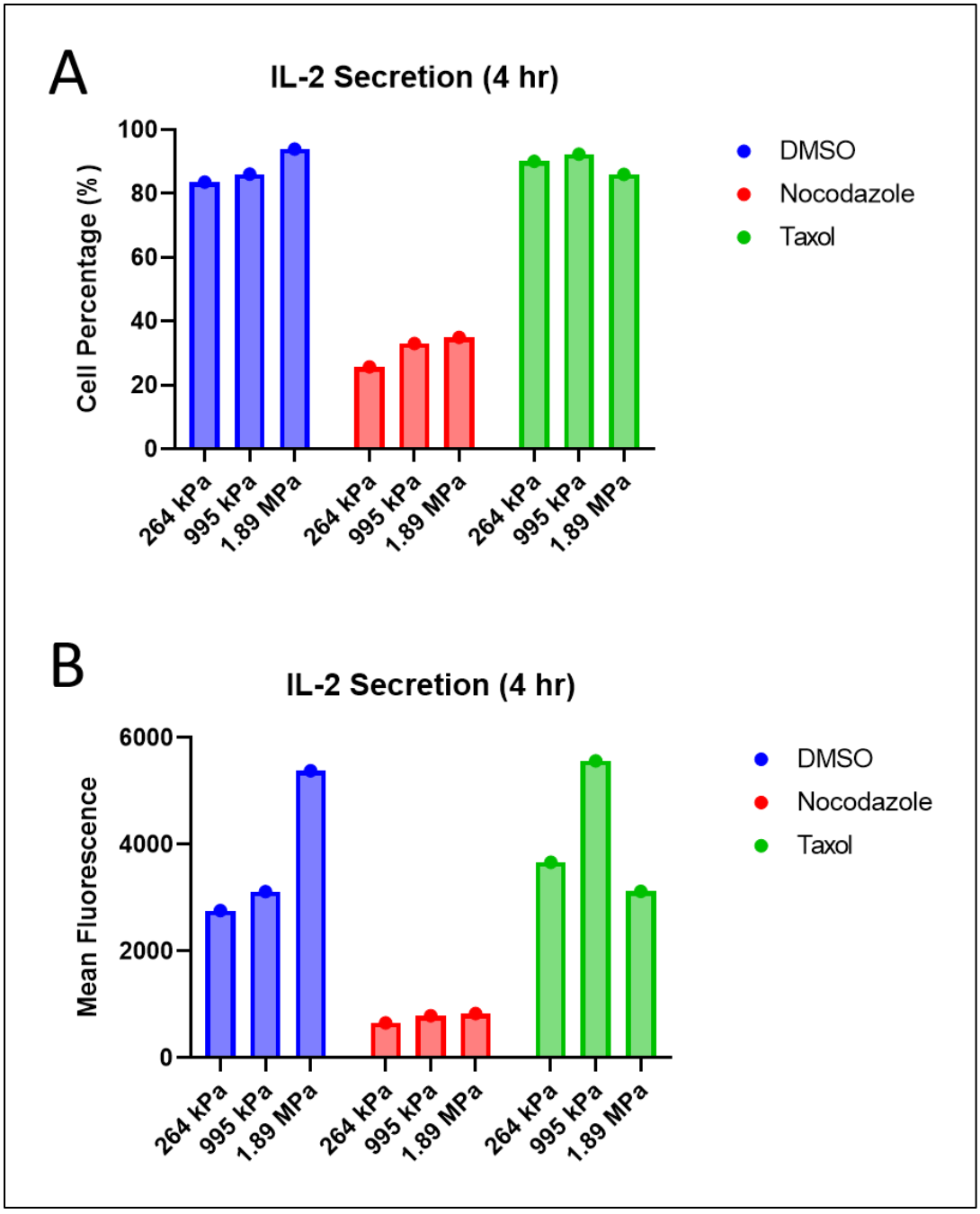

Figure 3.14. IL-2 secretion assay (4 hours) using microtubule inhibitors. A) Percentage of cells secreting IL-2 by inhibitor group under varying substrate stiffness values. B) Mean fluorescence per group, showing total amount out of IL-2 secreted under different conditions as an indicator of comparative activation levels. At the time of this writing, data collected were only from a single biological trial (n = 1), so no statistical analysis could be conducted yet.

3.5 Discussion

Similar to immunoglobulins, TCR α and β chains each consist of a variable (V) amino-terminal region and a constant (C) region, as there exists intentional shuffling during T-cell development in the genes that code for the V region of the TCR. This allows a high degree of specificity during TCR triggering, creating diversity with which the immune system is strengthened, as the human body is estimated to maintain as many as ten billion T-cell clonotypes at any given time (*Janeway et al., 2001; Lythe et al., 2016*). While there does exist some overlap in epitopes, the number of cells capable of recognition of a given antigen is still quite low. As a result, there are experimental methods by which the rarity of a given clonotype may be bypassed. Specifically, it is known that treatment of T cells with monoclonal anti-CD3 and anti-CD28 antibodies provides a costimulatory signal that engages the TCR, which can be used to initiate antigen-induced activation (*Trickett & Kwan, 2003*). This is the rationale for using a micropatterned surface presenting these antibodies: it allows local sites of activation to be visualized for all T cells. To this end, previous researchers constructed planar costimulation arrays containing antibodies against both CD3 and CD28, surrounded by ICAM-1, by using microcontact printing on a single surface (see Figure 3.15). They found that the ability to arbitrarily and independently control the locations of these antibodies offered the opportunity to examine patterns not precisely attainable in cell-cell interfaces, while also observing the direct impact of each receptor as an activating agent (*Shen et al., 2008*). Our results showed that our naïve murine CD4+ T cells consistently localized to our activating patterns, both colocalized and with CD3/CD28 segregated to different locations.

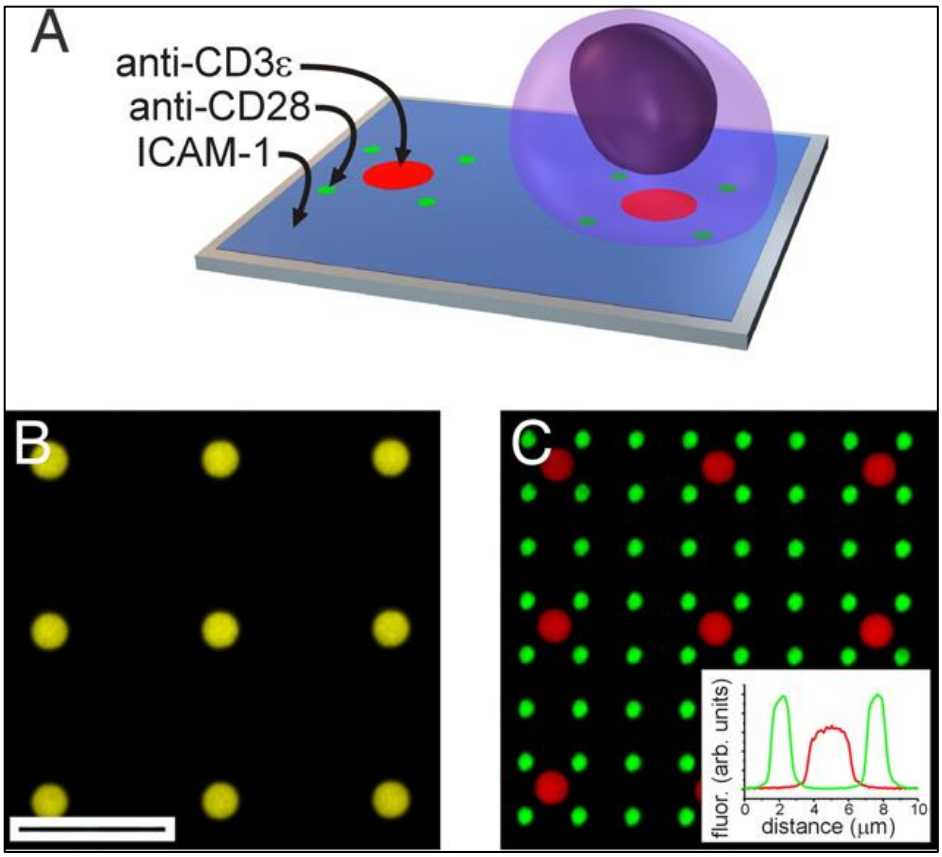

Figure 3.15. T cell interaction with micropatterned, costimulatory arrays. A) CD4+ cells were presented with surfaces that capture the microscale organization of ligands associated with T cell costimulation. Colocalized patterns were created by mixing anti-CD3 and anti-CD28 antibodies (yellow) in a single step B), while segregated patterns were defined by sequential patterning of anti-CD3 (red) and anti-CD28 (green) on a single surface (C). (Inset) Fluorescence profile across a segregated site. ICAM-1 was coated onto the remainder of these surfaces but is omitted here for clarity. Scale bar = 10 μm (*Shen et al., 2008*).

Subsequent studies sought to explore how the mechanical properties of a culture surface, such as substrate stiffness, could influence the *ex vivo* activation and expansion of T cells. While one study concluded that softer substrates stimulated greater IL-2 production and proliferation, another observed stronger activation was observed with increasing substrate elastic modulus (*Judokusumo et al., 2012; O'Connor et al., 2012*). It is worth noting, however, that the study designs were quite inconsistent, each using different species, T-cell subtypes, stiffness ranges, and substrates (see Figure 3.16). A recently published study sought to reconcile this discrepancy

by examining the response of human T cells to polyacrylamide (PA) gels with Young's moduli ranging from 5 to 110 kPa, finding that T-cell proliferation and IL-2 secretion levels exhibited a biphasic functional response to substrate stiffness (see Figure 3.17) (*Yuan et al., 2021*).

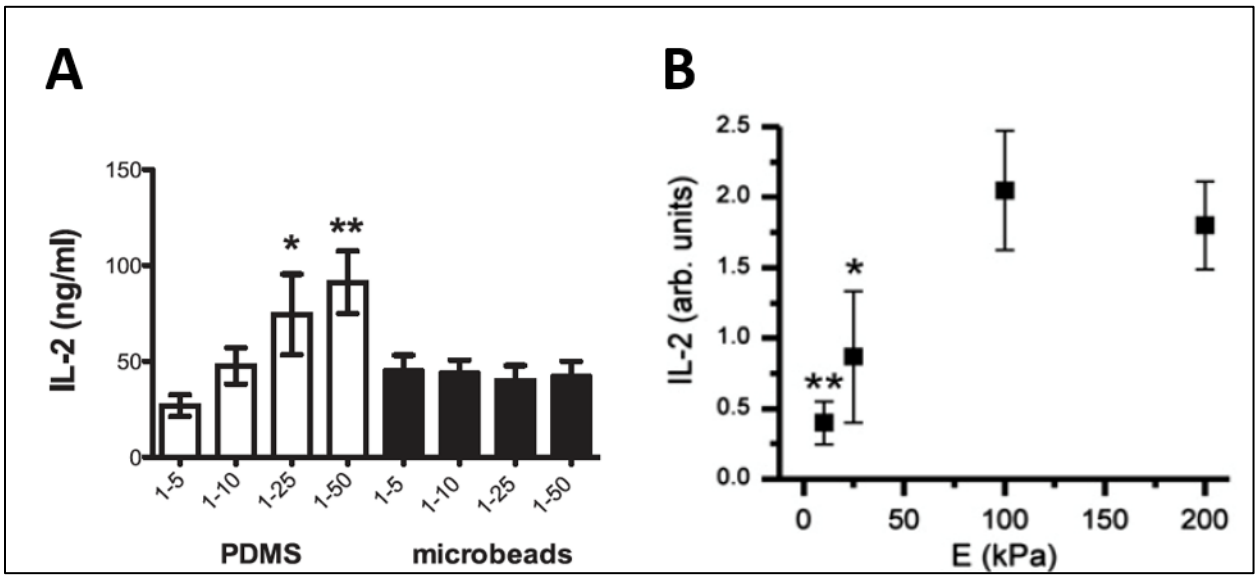

Figure 3.16. IL-2 secretion results under varying substrate stiffness values. A) Results from using human cells, a mixture of CD4+ and CD8+ lymphocytes, a stiffness range from 0.1-2MPa, and PDMS; x-axis values show PDMS formulation ratios of cross-linker to base polymer (more relative base polymer → softer substrate) (*O'Connor et al., 2012*). B) Results from using murine CD4+ lymphocytes, a peak stiffness of 200 kPa, and polyacrylamide (PA) gels (*Judokusumo et al., 2012*).

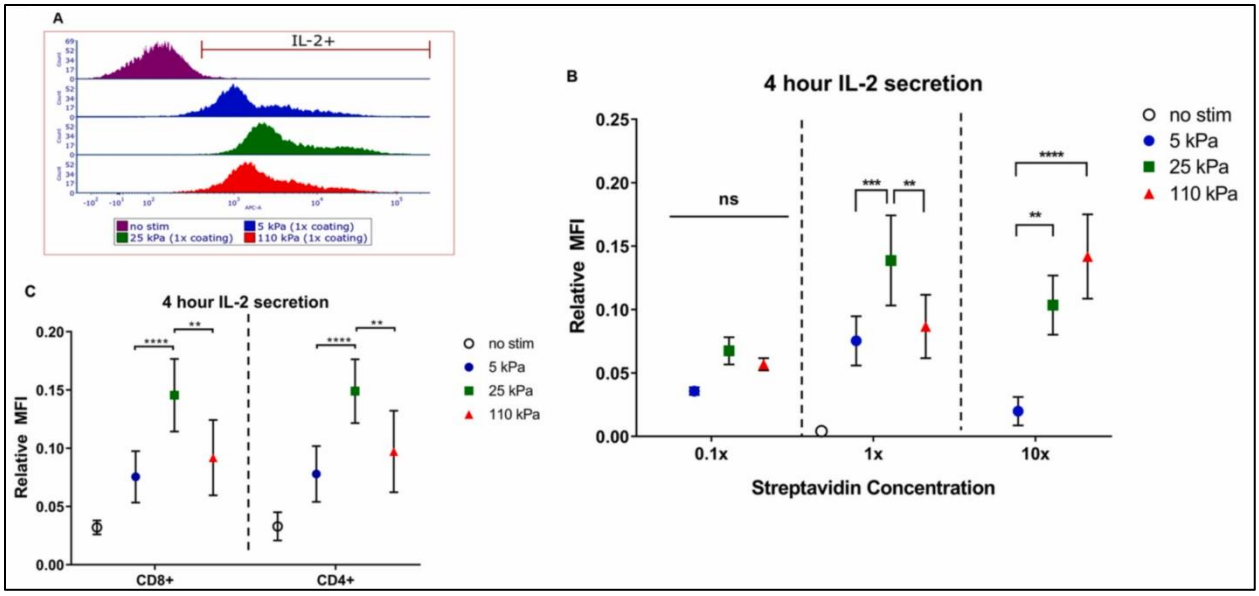

Figure 3.17. Short term IL-2 secretion modulated by substrate stiffness and ligand density. (A) IL-2 secretion of T cells characterized by flow cytometry. (B) IL-2 secretion of T cells activated for 4 h on hydrogels with standardized coating (n = 12 across 5 independent experiments), 0.1x coating (n = 3 across 2 independent experiments), and 10x coating. Data are mean ± s.d., n = 6 across 2 independent experiments. *p < 0.05, **p < 0.01, ***p < 0.001, ****p < 0.0001, 2-way ANOVA, Tukey multiple comparison test. (C) IL-2 secretion of CD4+ and CD8+ T cell subsets. Data are mean ± s.d., n = 12 across 5 independent experiments. *p < 0.05, **p < 0.01, ***p < 0.001, ****p < 0.0001, 2-way ANOVA, Tukey multiple comparison test.

It has been shown via traction force microscopy that forces exerted by T cells during activation are largely due to actin dynamics, indicating that T cells, and specifically TCRs, are mechanosensitive, and the cytoskeleton directly contributes to the observed interfacial forces (*Hui et al., 2015*). However, there still lingers a question as to the regulatory pathways that control these cytoskeletal forces. Clearly essential to T-cell activation and mechanosensing, it is critical to understand what modulates actin flow. The aforementioned group next explored how the polarized MT cytoskeleton interacts with the actin cytoskeleton and influences force generation at the immune synapse. They found that microtubules at the TCR/APC junction are dynamic and suppress Rho-associated contractility and actin flow, effectively regulating force generation during activation in an actin-inhibitory capacity (*Hui & Upadhyaya, 2017*).

A recent review paper looks closely at evidence that mechanical and biochemical signals at the IS are integrated by actin dynamics (see Figure 3.18) (*Roy & Burkhardt, 2018*). One cited study used fluorescent tension sensors to show that actin polymerization, but not myosin contractility, is required for force production through the TCR, presenting an alternative mechanism from the Hui & Upadhyaya paper's hypothesis (*Liu et al., 2016*). Furthermore, inhibition of the Arp2/3 complex actually resulted in an increase in force production, for which Cdc42 was required. They also discussed the relevance of WAVE2, which is activated downstream of Rac1, known to localize to the peripheral actin ring during T-cell activation, and partly responsible for the formation of the branched actin network (*Nolz et al., 2006*).

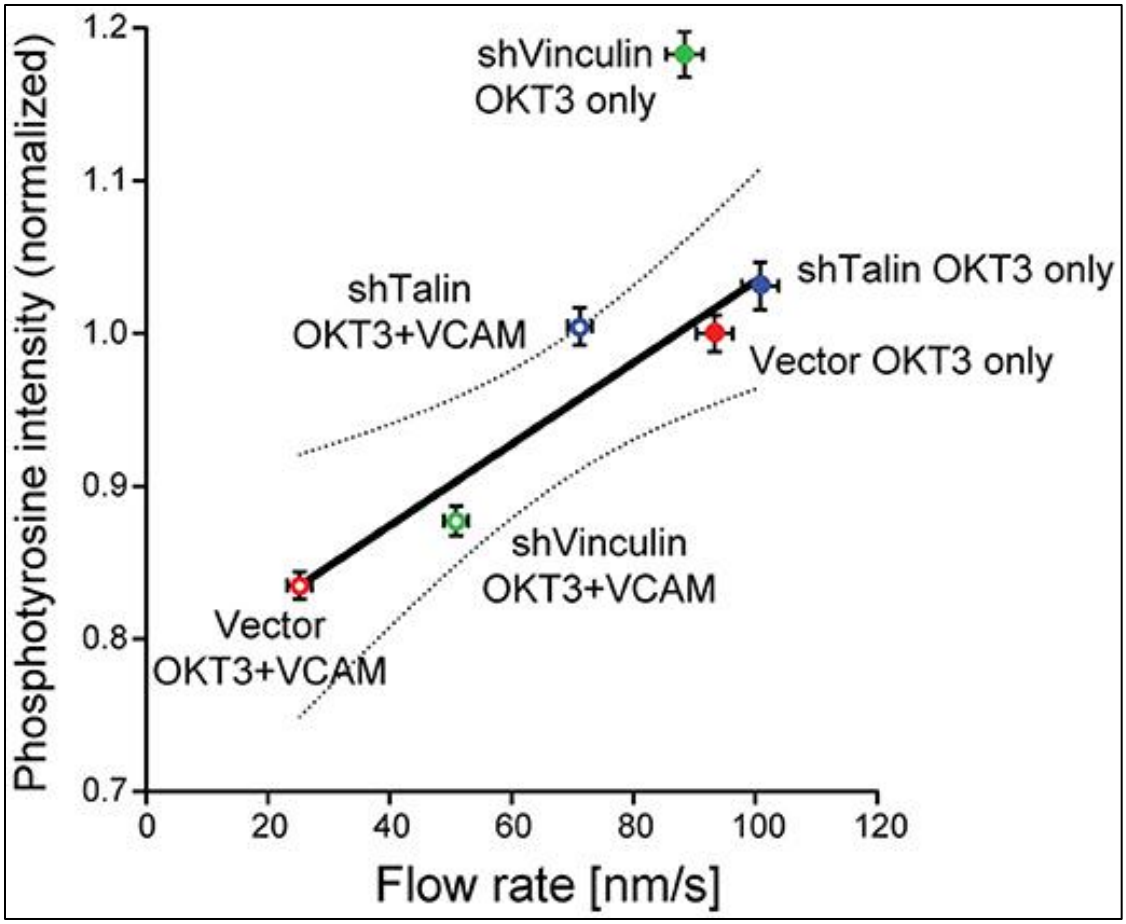

Figure 3.18. Correlation between actin flow rates and tyrosine phosphorylation during T cell activation. Results from two types of experiments were combined to assess how actin flow rates affect TCR signaling. Jurkat T cells stably expressing GFP-actin were transduced with recombinant lentiviruses expressing shRNAs specific for vinculin or talin, or with an empty control vector. Actin flow rates within the lamellipodial region were determined by kymographic analysis. In parallel studies, cells were allowed to spread on stimulatory coverslips for 5 min, fixed, permeabilized, and labeled for phosphotyrosine. Average phosphotyrosine signal per cell was then plotted as a function of actin flow rates. In vector-transduced control cells, VCAM-1 engagement slows the actin flow rate and decreases phosphotyrosine signaling. Knocking down the clutch molecules talin or vinculin relieved the slowing effect of integrin engagement, suggesting that mechanical drag is at least partly responsible for the slowing of the actin network (*Roy & Burkhardt, 2018*).

One study on the induction of cancer-cell migration found that Rac1 induces the formation of lamellipodia via WAVE2 (*Takahashi, 2012*). Moreover, WAVE2 was also found to broadly interact with many proteins that regulate microtubule growth, actin assembly, and membrane-protein targeting. While these findings were motivated as having potentially

important implications for the development of therapeutic agents against cancer cell migration and invasion, there was a question as to whether this biological relationship held true specifically in T cells.

WAVE2 and WASp were identified as two proteins of interest for two reasons. First, they're known to play vital roles in the actin polymerization process through unique activation mechanisms. Secondly, they are known to be involved in T-cell activation (see Figure 3.19). Specifically, WASp is linked to immunological synapse stability and the formation of protrusive structures during antigen scanning, while WAVE2 seems to promote cell spreading and adhesion during IS formation.

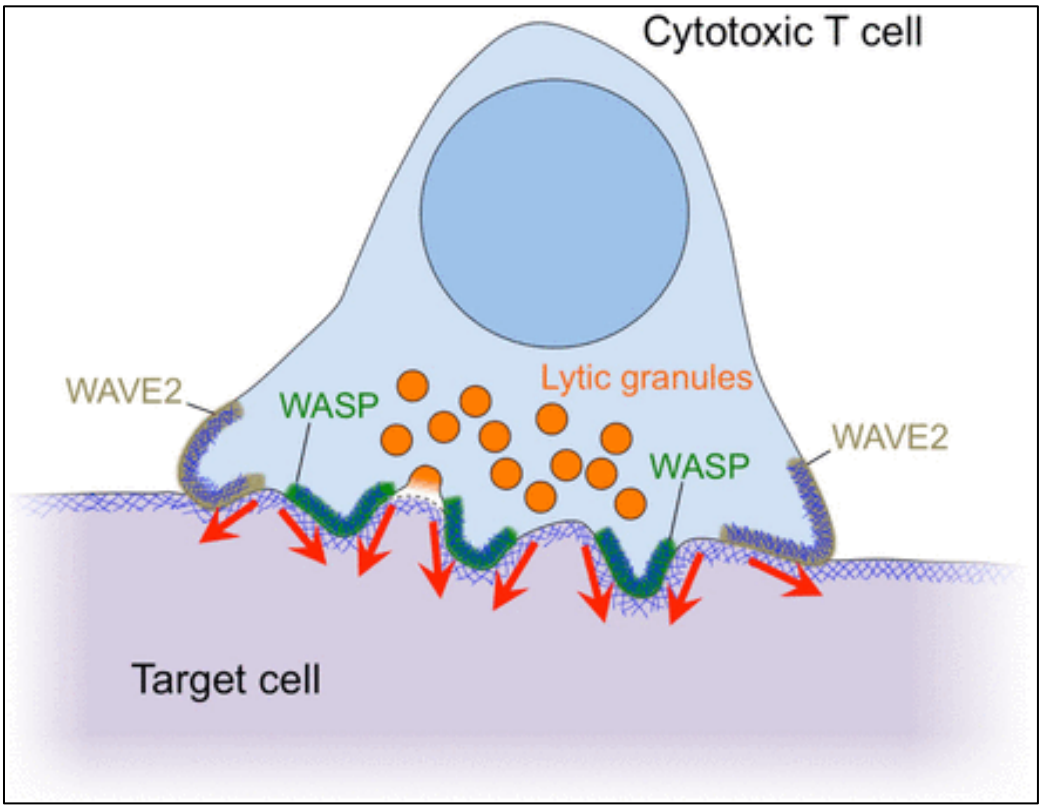

Figure 3.19. Cytolytic mechanopotentiation by WASP-dependent synaptic protrusions. A schematic diagram of the cytolytic IS showing peripheral WAVE2-dependent protrusions and central WASP-dependent protrusions. Red arrows denote force exertion (*Tamzalit et al., 2019*).

Our results demonstrated a spatial correlation between peripheral microtubule localization and that of WAVE2. This supports our hypothesis, given the unique role of WAVE2 in immune synapse formation, operating on the exterior of the T cell. Moreover, WASp is most active on the T-cell inner plane, which supports its lack of correlation with MTs from our studies. The overarching long-term goal is to provide clearer insight into how RhoA, Cdc42, and Rac1 (as well as their associated cytoskeletal system branches) are regulated with regard to microtubules. Current literature has yet to adequately connect regulation of microtubules and actin dynamics with the T-cell receptor triggering system of CD3, CD28, and LFA-1, but doing so should elucidate additional immunotherapeutic targets.

In order to test our hypothesis of microtubules influencing the observed correlation with WAVE2 presence, we wanted to analyze the resulting impact from microtubule inhibition. Experimentally, this is often conducted using either of two chemicals, nocodazole or Taxol, each of which possesses a different mechanism of action (see Figure 3.20). Nocodazole binds to αβ-tubulin dimers, effectively preventing assembly and promoting depolymerization; meanwhile, Taxol binds specifically to the β-tubulin subunit, stabilizing tubulin dimers and preventing depolymerization. The fact that we observed no change in WAVE2 spatial organization after inducing microtubule depolymerization indicates that the relationship between those two proteins may not be as directive as hypothesized. Of note, we used a segregated activation pattern to learn more about any potential localization with respect to stimulator molecules. However, we did not see any noticeable accumulation of WAVE2 or WASp specifically toward smaller anti-CD28 dots, so the association is unlikely to be linked to the surface proteins alone.

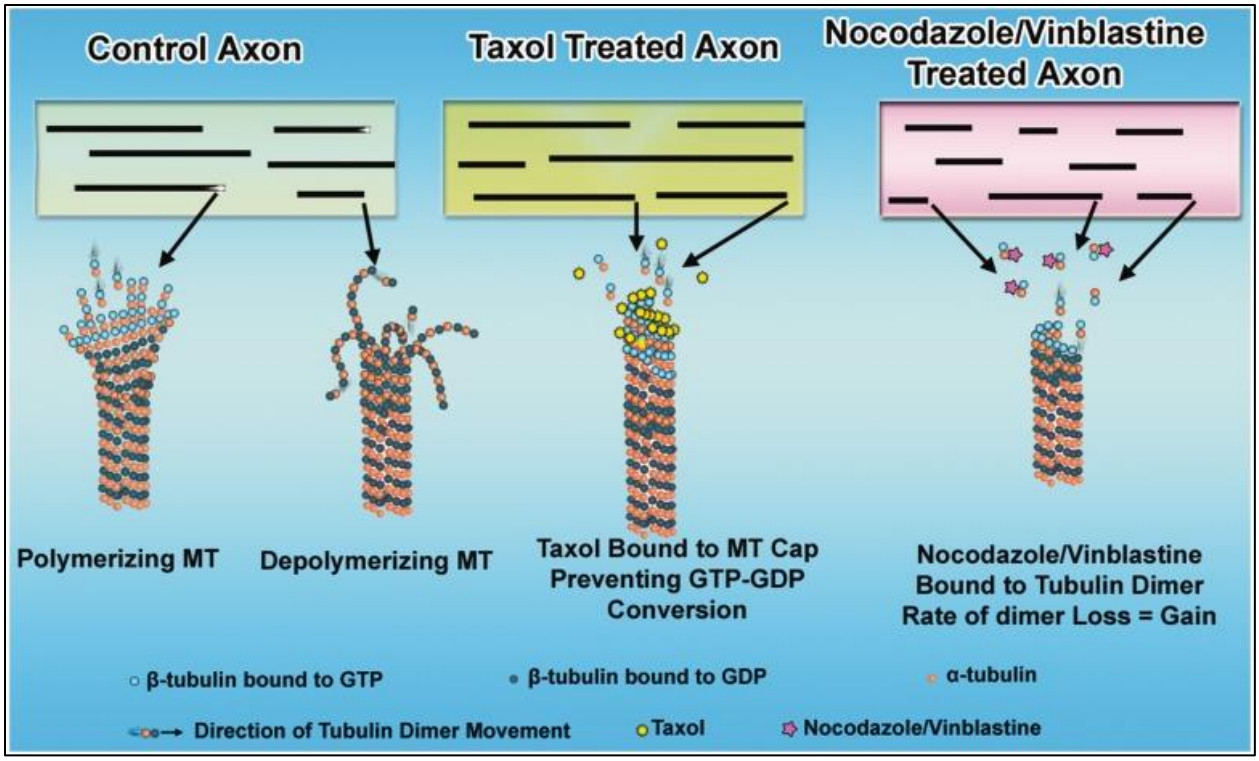

Figure 3.20. Effects of microtubule-active drugs on microtubule dynamics. Shown are a control axon and axons during the first moments of exposure to microtubule-active drugs. In the control axon, the microtubules (MT) display dynamic instability at their plus ends. In taxol-treated axons, the microtubules are stabilized (no longer lose subunits) and no longer show dynamic instability at their plus ends. Hence, they continue to assemble. In axons treated with low concentrations of microtubule depolymerizing drugs, the microtubules become 'kinetically stabilized,' which means they lose and gain subunits at the same rate, resulting in no length change (*Baas & Ahmad, 2013*).

Lastly, we sought to better understand the role of microtubules on T cells' mechanosensing abilities. Compared to DMSO controls, treatment with nocodazole resulted in fewer cells secreting IL-2, as well as a lesser total amount of IL-2 secretion. In addition, there seems to have been no substantial change in IL-2 secretion as substrate stiffness varies. This implies that the dynamic behavior of microtubules may play a vital role in T-cell activation and the T cell's ability to sense and respond to its mechanical environment. We also see an intriguing spike of IL-2 secretion on our medium-stiff substrate, 995 kPa, compared to the softer and harder gels. The current hypothesis draws from the findings of Yuan et al., whereby there exists a

physiological ideal with respect to the mechanical environment most likely to activate T cells. Anything softer or harder may result in suboptimal activation, so the spike observed in Figure 3.14 when Taxol was applied may be reflective of this discovery on a cytoskeletal level.

Chapter 4: Synthesis and Prospective Studies

4.1 Summary of Findings

The degree to which molecular scale structure and function can impact macro-scale structure and function has been more or more elucidated over the last several decades. Within the human body, our increased understanding of cell function has helped improve medical and technological advances immensely. Biomedical engineers are in constant pursuit of ways to improve the state of and extend the span of human life. The works described here focus on two distinct ways in which a better understanding of microtubules and microtubule-based structures can aid in these efforts.

Chapter 1 lays a foundation of background and system-level understanding. From a clinical standpoint, osteoporosis and cancer are each cited as debilitating illnesses for which effective modes of prevention are not guaranteed, and current treatment efforts are accompanied by a slew of side effects. Thus, we present an approach by which scientists may use the body's own intrinsic features as a way to better combat disease.

Chapter 2 dives specifically into our understanding of the primary cilium as it relates to bone remodeling. While much has been learned about primary cilia in osteocytes and osteoblasts, very little has been published about osteoclasts, the cell responsible for bone resorption, let alone the degree to which molecular features may regulate cellular function. We discovered that macrophages, the hematopoietic cellular precursors to osteoclasts, do in fact possess primary cilia, but mature osteoclasts themselves do not. Given this absence, we then wondered if the cilium may actually play a role in osteoclastogenesis. To explore this possibility, we treated macrophages with fenoldopam mesylate, a drug known to effectively increase cilia incidence and length in other cell types. We found that fenoldopam-treated cells had a decrease in genetic

expression of osteoclast markers as well as formed osteoclasts at a decreased rate. This leads us to believe that primary cilia may offer a dual beneficial approach to both promote bone formation and simultaneously downregulate osteoclast activity. A better understanding of the osteoclast formation process (e.g., the molecular changes undergone by macrophages during fusion), and to what extent primary cilia disassembly or resorption may be necessary, has the potential to reveal new targets for more effect bone degenerative diseases.

Following the theme of the impact of microtubules, Chapter 3 shifts to the immune system, where cancer treatment research has been heading in the direction of immunotherapy efforts and using the body's natural machinery as a basis for enhanced approaches. The leading concept behind adoptive T cell therapy is that a patient's very own T cells may be extracted, genetically modified, expanded, and transfused back into the patient. As such, the way in which specific molecular components of T cells are targeted will reveal the most likely candidates for new treatment options. Given our understanding of the cytoskeleton's role in T-cell activation, as well as the capability of microtubules to inhibit actin flow, we wanted to further explore the specifics of this interaction. We discovered that WAVE2, a necessary actin-associated protein, colocalized to the same peripheral regions of the cell as microtubules. While our inhibition studies ruled out the likelihood of a regulatory mechanism (MTs directing WAVE2), the MT colocalization observed with WAVE2 but not WASp does indicate a potential protein-specific connection of how the observed crosstalk between cytoskeletal filaments may be regulated, even if the precise extent of their interaction has yet to be resolved. Furthermore, the abrogated activation and mechanosensing responses in nocodazole-treated samples suggests that microtubules play a vital role in these processes. Comprehensive elucidation of the role of

microtubules in T-cell activation would result in a better understanding of molecular targets for enhanced immunotherapy efforts.

4.2 Future Directions

From a cell biology standpoint, one of the main unifying themes of the chapters in this dissertation is that microtubules themselves have an increasingly recognized role in mechanosensing, and the results of the studies described here seek to make progress in revealing the range of influential roles that these cytoskeletal filaments may possess. The physiological overlap between the skeletal and immune systems, as the name indicates, lies in the field of osteoimmunology. Specifically, some of the cellular observations in Chapter 2 (focused on osteoclastogenesis) are directly tied to those of Chapter 3 (T-cell activation). One truly interesting observation is that both osteoclasts and T lymphocytes lack primary cilia. It is possible that this is related to a differentiation effect, whereby as differentiation away from, in this case, hematopoietic stem cells increases, primary cilia are observed in decreasing incidence. And in terms of cellular design, both of these cells are indeed quite specialized.

Assembly of both the primary cilium and immunological synapse requires centrosome translocation to the plasma membrane. In ciliated cells, this is carried out for purposes of anchoring and forming the basal body from which the primary cilium extends. In T cells, the MTOC migrates to the immune synapse, directing microtubule translocation and providing targeted granule secretion in cytotoxic lymphocytes (*Stinchcombe et al., 2015*). Despite lacking a primary cilium, T cells do possess a number of intraflagellar (IFT) proteins. These IFT proteins are necessary to maintain the structure and function of the primary cilium in other eukaryotic cells, but enable TCR recycling to the IS in T cells (*Finetti et al., 2011*). Given this observation, it would be worth exploring whether or not fenoldopam treatment on T cells affected IFT expression, as the dopaminergic effect observed in primary cilia seems to be structural.

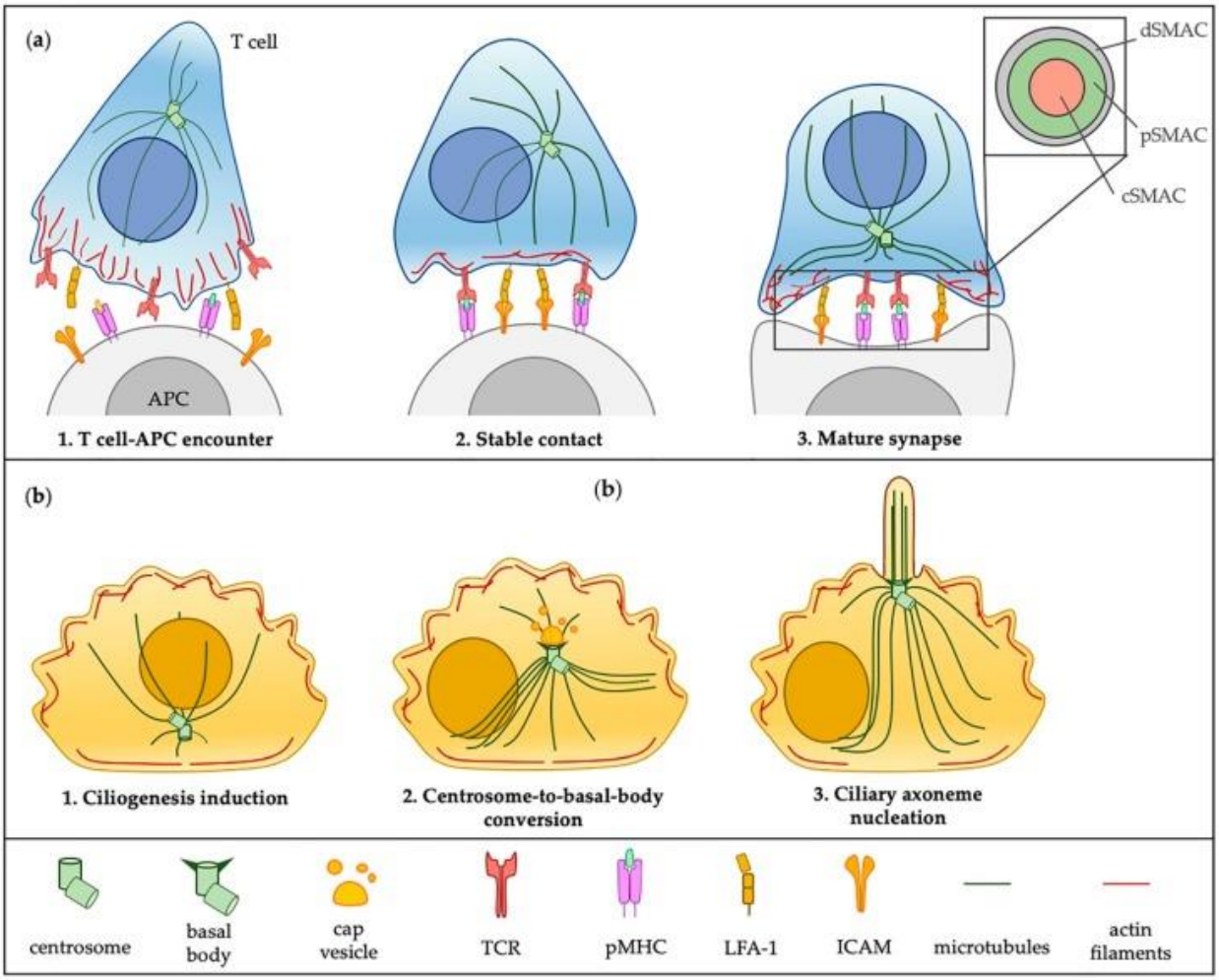

Figure 4.1. Schematic representation of critical steps in immunological synapse (IS) assembly and ciliogenesis. Both IS assembly and ciliogenesis are inducible processes that are initiated in response to external stimuli or triggering events. The encounter of an antigen presenting cell (APC) bearing a cognate peptide-loaded major histocompatibility complex (pMHC) initiates the formation of a stable IS in the T cell (a). At variance, ciliogenesis is activated in vitro by a variety of stressful conditions (e.g., serum and nutrient starvation, ultraviolet light radiation), which generally inhibit cell division (b). In the T cell the centrosome moves toward the synapse as a consequence of early T cell receptor (TCR) signaling events (a) and, at this location, sets the stage for polarized vesicular trafficking. Cilium assembly crucially depends on centrosome-to-basal-body conversion that consists in the polarization and subsequent docking of the mother centriole to the plasma membrane, where it nucleates the ciliary axoneme. At the IS newly polymerized actin filaments contribute to the initial clustering of TCRs in the central supramolecular activation clusters (cSMAC). Following polarization of the centrosome, actin retracts to the distal SMAC (dSMAC) to form a ring, which surrounds the peripheral SMAC (pSMAC) enriched in LFA-1 (a). A redistribution of actin in contractile bundles at the ventral side and a cortical network at the dorsal side helps to break cell symmetry and promotes centrosome migration during ciliogenesis (b). In both structures the docking phase of the centrosome is concomitant with a local clearance of cortical actin (*Cassioli & Baldari, 2019*).

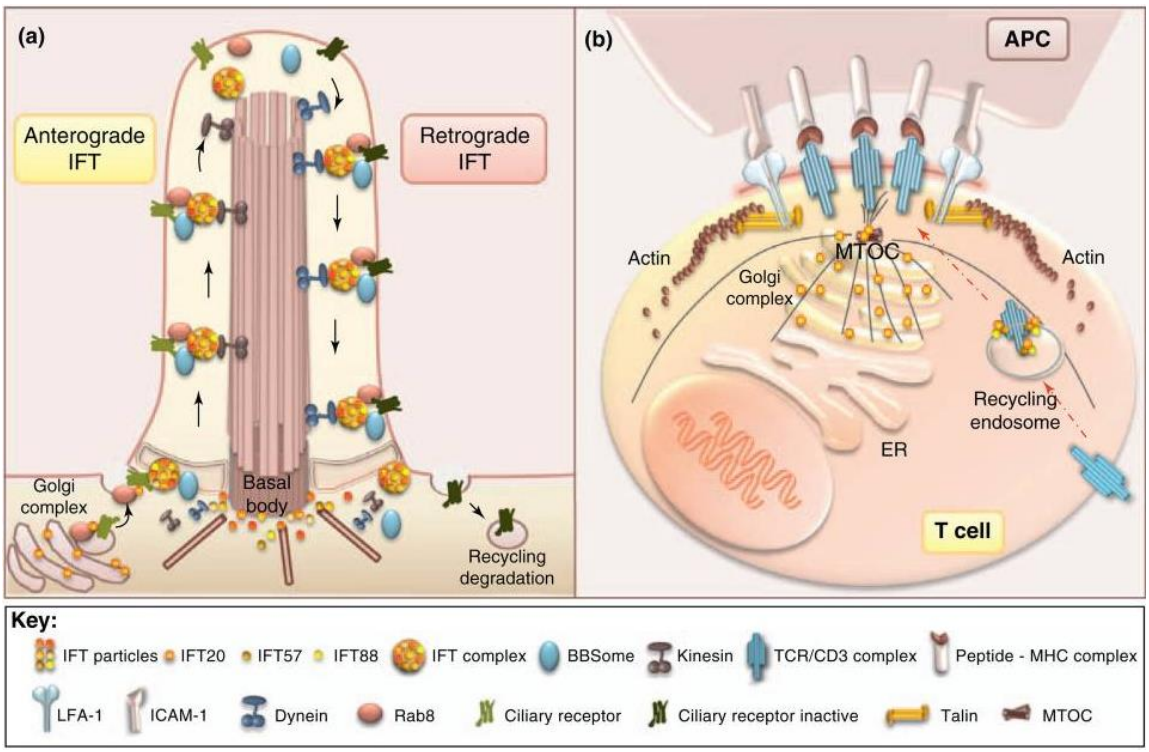

Figure 4.2. IFT in primary cilia and at the immune synapse. (a) Transport of cargo to primary cilia and back to the cell body is ensured by multimeric IFT particles in concert with the BBSome. Molecular motors assist the movement of particles along the axonemal microtubules. (b) When a T cell encounters an antigen-specific APC, the TCR/CD3 complex clusters in the central area of the immune synapse. One of the principal mechanisms of TCR clustering at the immune synapse is through polarized delivery of receptor complexes localized in recycling endosomes. Assembly of a stable immune synapse requires the translocation of the centriole close to the membrane patch at the immune synapse. Following TCR engagement, IFT20 interacts with the TCR and assembles in a complex with IFT57 and IFT88. This IFT complex promotes polarized recycling of the TCR to the immune synapse (*Finetti et al., 2011*).

The comparison of these two components is not simply limited to an architectural framework. Both structures have been well-characterized as operating as chemical and mechanical signaling platforms. At the immune synapse, receptor-ligand interactions and mechanical force sensation of both the naïve T cell and the APC define the basis for the early stages of activation and larger regulation of the adaptive immune response (*Xie et al., 2013*). In a similar signaling vein, the primary cilium of eukaryotic cells, although long thought to be vestigial, is now widely accepted as the cell's antenna, helping facilitate a number of cellular

pathways, such as Hedgehog and Wnt signaling (*Wheway et al., 2018*). In addition, the immunological synapse and the primary cilium are locations of extensive vesicle trafficking. MTOC polarization helps T cells establish directional transport of vesicles and thus acts as a focal point for endocytosis and exocytosis (*Varma et al., 2006*). Similarly, primary cilia assembly relies on vesicular trafficking of proteins to and from the cilium.

In the introduction, we described the process by which RANKL induces the differentiation of macrophages into osteoclasts. Any imbalance in the production of RANKL, its signaling receptor RANK, and/or its decoy receptor osteoprotegerin (OPG) can give rise to debilitating bone diseases, such as osteoporosis. However, RANKL and the upregulation of osteoclast activity is observed in many pathologies and organ systems. In fact, one direct relationship of osteoclasts and the immune system works in a feedback loop. Calcium ion (Ca^{2+}) signaling is vital to T-cell function. Whenever the Ca^{2+} levels in the bloodstream are too low, chief cells of the parathyroid gland release parathyroid hormone (PTH) to help regulate calcium metabolism as part of the endocrine system. One of the major effects of PTH is to activate Wnt signaling in all osteoblastic cells, including osteocytes, which induces osteoclast proliferation and differentiation (*Jilka, 2007; M. Kato et al., 2002*). Receptors for PTH are found in preosteoblasts, osteoblasts, lining cells, and osteocytes; when bound, these cells increase their expression of RANKL and decrease their secretion of OPG (*Silva & Bilezikian, 2015*). This indirectly stimulates osteoclast differentiation and activity, which, in the process of resorbing bone matrix, effectively releases calcium back into the bloodstream.

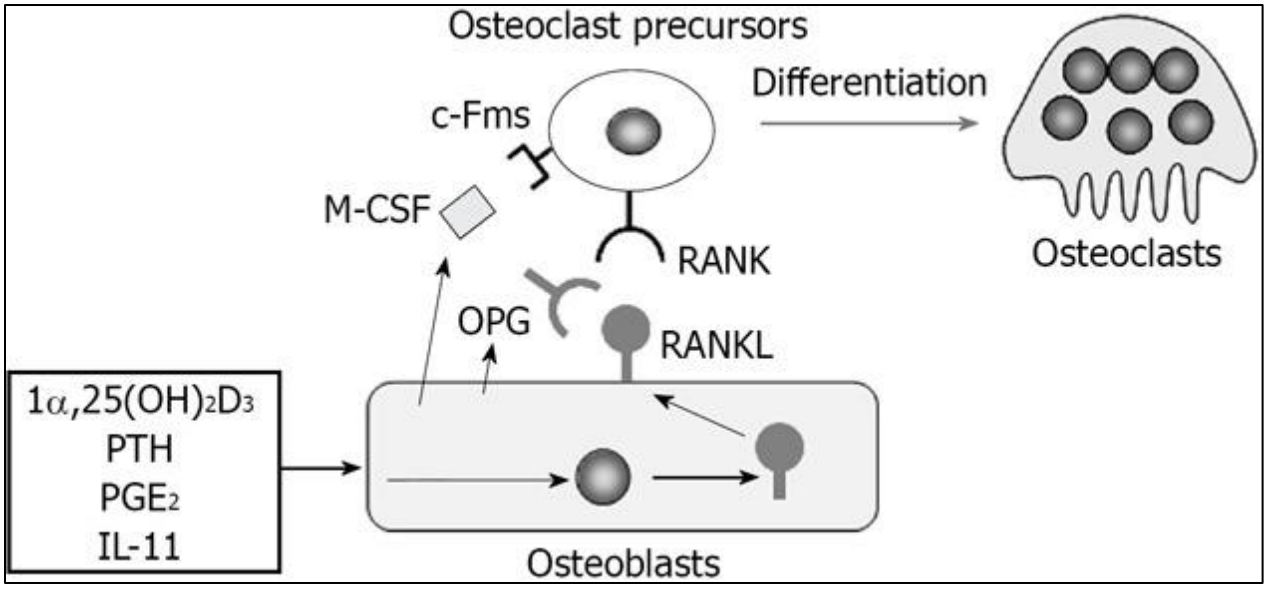

Figure 4.3. Regulation of osteoclast differentiation by osteoblasts through macrophage colony-stimulating factor, receptor activator of nuclear factor-κB ligand, and osteoprotegerin production. Osteoblasts express RANKL as a membrane-associated form in response to bone resorption-stimulating factors. Osteoclast precursors express c-Fms (M-CSF receptor) and RANK (RANKL receptor) and differentiate into osteoclasts in the presence of M-CSF and RANKL. Osteoblasts also produce osteoprotegerin (OPG), which inhibits osteoclastogenesis by blocking the RANKL-RANK interaction (*Yamashita et al., 2012*).

While the relationship between osteoclasts and the immune system broadly is clear, there is also direct crosstalk between osteoclasts and T cells specifically. It is now understood that a number of immune factors, including costimulatory receptors, cytokines (e.g., IFN-γ and TNF), and B and T cells regulate bone cell development, bone turnover, and are involved in the pathogenesis of bone disease (*Pacifici, 2010*). Soluble RANKL is secreted by activated T cells and represents a crucial link between bone metabolism and the immune system. T cells can directly influence osteoclastogenesis and bone remodeling. This observation may also help explain why autoimmune diseases and cancers often result in a systemic and local loss of bone mass (*D'Amico & Roato, 2012*). More directly, it is widely known that bone tissue is generally one of the most common tumor metastasis sites. On arriving in bone tissue, disseminated tumor cells enter a mechanical microenvironment that is substantially different from that of the primary

tumor and is largely regulated by bone cells. Although osteocytes are widely known to orchestrate healthy bone remodeling in response to physical loading, one recent study sought to understand the effects of mechanical loading of osteocytes on cancer cell behavior is still poorly understood. They found that osteocyte paracrine signaling acts to inhibit metastatic tumor growth, with such effects as cancer cell invasion and migration largely reversed by mechanical stimulation of osteocytes (*Verbruggen et al., 2021*).

With respect to clinical applications, bone destruction in rheumatoid arthritis is caused by the enhanced activity of osteoclasts, which results from the activation of T cells and, more specifically, NFATc1, a crucial regulator of immunity. A study in 2019 revealed that the dynamics of the actin cytoskeleton actively adjust to normalize the force experienced by the TCR in an antigen-specific manner, and tuning actin dynamics in response to antigen kinetics may be a mechanism that allows T cells to adjust the timescale and capacity of TCR signaling (*Colin-York et al., 2019*). Given that primary cilia have already been shown to regulate actin cytoskeleton dynamics in other cells, it would be worth exploring how the IFT proteins of T cells might contribute to the mechanosensing and transduction capabilities observed during T-cell activation, as well as the dynamicity of cytoskeletal polymers, as abnormal T-cell activation may mechanistically induce bone destruction when this process is improperly regulated.

References

38.2B: Cell Types in Bones - Biology LibreTexts. (n.d.). Retrieved February 22, 2022, from https://bio.libretexts.org/Bookshelves/Introductory_and_General_Biology/Book%3A_General_Biology_(Boundless)/38%3A_The_Musculoskeletal_System/38.2%3A_Bone/38.2B%3A_Cell_Types_in_Bones

Abdul-Majeed, S., & Nauli, S. M. (2011). Dopamine receptor type 5 in the primary cilia has dual chemo-and mechano-sensory roles. *Hypertension*, *58*(2), 325–331. https://doi.org/10.1161/HYPERTENSIONAHA.111.172080

Ainsworth, C. (2007). Cilia: Tails of the unexpected. *Nature*, *448*(7154), 638–641. https://doi.org/10.1038/448638a

Alberts, B., Johnson, A., Lewis, J., Raff, M., Roberts, K., & Walter, P. (2002). *Molecular Biology of the Cell* (4th ed.). Garland Science. https://www.ncbi.nlm.nih.gov/books/NBK26846/

Alswat, K. A. (2017). Gender Disparities in Osteoporosis. *Journal of Clinical Medicine Research*, *9*(5), 382. https://doi.org/10.14740/JOCMR2970W

Avasthi, P., Marley, A., Lin, H., Gregori-Puigjane, E., Shoichet, B. K., Von Zastrow, M., & Marshall, W. F. (2012). A chemical screen identifies class A G-protein coupled receptors as regulators of cilia. *ACS Chemical Biology*, *7*(5), 911. https://doi.org/10.1021/CB200349V

Baas, P. W., & Ahmad, F. J. (2013). Beyond taxol: microtubule-based treatment of disease and injury of the nervous system. *Brain*, *136*(10), 2937. https://doi.org/10.1093/BRAIN/AWT153

Bashour, K. T., Gondarenko, A., Chen, H., Shen, K., Liu, X., Huse, M., Hone, J. C., & Kam, L. C. (2014). CD28 and CD3 have complementary roles in T-cell traction forces. *Proceedings*

of the National Academy of Sciences of the United States of America, *111*(6), 2241–2246. https://doi.org/10.1073/pnas.1315606111

Beales, P., & Jackson, P. K. (2012). Cilia - the prodigal organelle. *Cilia*, *1*(1), 1. https://doi.org/10.1186/2046-2530-1-1

Bergmann, P., Body, J. J., Boonen, S., Boutsen, Y., Devogelaer, J. P., Goemaere, S., Kaufman, J., Reginster, J. Y., & Rozenberg, S. (2011). Loading and Skeletal Development and Maintenance. *Journal of Osteoporosis*, *2011*, 1–15. https://doi.org/10.4061/2011/786752

Birmingham, E., Grogan, J. A., Niebur, G. L., McNamara, L. M., & McHugh, P. E. (2013). Computational modelling of the mechanics of trabecular bone and marrow using fluid structure interaction techniques. *Annals of Biomedical Engineering*, *41*(4), 814–826. https://doi.org/10.1007/S10439-012-0714-1/FIGURES/8

Black, D. M., Kelly, M. P., Genant, H. K., Palermo, L., Eastell, R., Bucci-Rechtweg, C., Cauley, J., Leung, P. C., Boonen, S., Santora, A., de Papp, A., & Bauer, D. C. (2010). Bisphosphonates and Fractures of the Subtrochanteric or Diaphyseal Femur. *New England Journal of Medicine*, *362*(19), 1761–1771. https://doi.org/10.1056/NEJMoa1001086

Blume, S. W., & Curtis, J. R. (2011). Medical costs of osteoporosis in the elderly Medicare population. *Osteoporosis International*, *22*(6), 1835–1844. https://doi.org/10.1007/s00198-010-1419-7

Bone Signaling & RANKL - Basic Science - Orthobullets. (n.d.). Retrieved April 27, 2022, from https://www.orthobullets.com/basic-science/9010/bone-signaling-and-rankl

Bone Structure | Anatomy and Physiology I. (n.d.). Retrieved February 22, 2022, from https://courses.lumenlearning.com/hccs-ap1/chapter/bone-structure/

Bonifant, C. L., Jackson, H. J., Brentjens, R. J., & Curran, K. J. (2016). Toxicity and

management in CAR T-cell therapy. In *Molecular Therapy - Oncolytics* (Vol. 3, p. 16011). Nature Publishing Group. https://doi.org/10.1038/mto.2016.11

Bunnell, S. C., Kapoor, V., Trible, R. P., Zhang, W., & Samelson, L. E. (2001). Dynamic actin polymerization drives T cell receptor-induced spreading: a role for the signal transduction adaptor LAT. *Immunity*, *14*(3), 315–329. https://doi.org/10.1016/S1074-7613(01)00112-1

Burger, E. H., Klein-Nulend, J., Van der Plas, A., & Nijweide, P. J. (1995). Function of Osteocytes in Bone—Their Role in Mechanotransduction. *The Journal of Nutrition*, *125*(suppl_7), 2020S-2023S. https://doi.org/10.1093/JN/125.SUPPL_7.2020S

Cancer Cells: Types, Formation, and Characteristics. (n.d.). Retrieved March 2, 2022, from https://www.verywellhealth.com/what-are-cancer-cells-2248795

Cancer Disparities — Cancer Stat Facts. (n.d.). Retrieved June 14, 2021, from https://seer.cancer.gov/statfacts/html/disparities.html

Cancer Overview | The University of Kansas Cancer Center. (n.d.). Retrieved March 2, 2022, from https://www.kucancercenter.org/patients-caregivers/cancer-education/cancer-overview

Cancer prevention: 7 tips to reduce your risk - Mayo Clinic. (n.d.). Retrieved March 2, 2022, from https://www.mayoclinic.org/healthy-lifestyle/adult-health/in-depth/cancer-prevention/art-20044816

Cancer Statistics - National Cancer Institute. (n.d.). Retrieved June 10, 2021, from https://www.cancer.gov/about-cancer/understanding/statistics

Cancer treatment - Mayo Clinic. (n.d.). Retrieved March 2, 2022, from https://www.mayoclinic.org/tests-procedures/cancer-treatment/about/pac-20393344

Cancer Treatment Options | Houston Methodist. (n.d.). Retrieved March 2, 2022, from https://www.houstonmethodist.org/cancer/treatment-options/

CAR T Cells: Engineering Immune Cells to Treat Cancer - National Cancer Institute. (n.d.). Retrieved June 10, 2021, from https://www.cancer.gov/about-cancer/treatment/research/car-t-cells

Caspary, T., Larkins, C. E., & Anderson, K. V. (2007). The Graded Response to Sonic Hedgehog Depends on Cilia Architecture. *Developmental Cell*, *12*(5), 767–778. https://doi.org/10.1016/J.DEVCEL.2007.03.004

Cassioli, C., & Baldari, C. T. (2019). A Ciliary View of the Immunological Synapse. *Cells*, *8*(8). https://doi.org/10.3390/CELLS8080789

Centrosome - Structure And Functions Of Centrosome. (n.d.). Retrieved February 17, 2022, from https://byjus.com/biology/centrosome/

Chan, C. K. Y., Mason, A., Cooper, C., & Dennison, E. (2016). Novel Advances in the Treatment of Osteoporosis. *British Medical Bulletin*, *119*(1), 129. https://doi.org/10.1093/BMB/LDW033

Checkpoint inhibitors | Types of immunotherapy | Cancer Research UK. (n.d.). Retrieved March 17, 2022, from https://www.cancerresearchuk.org/about-cancer/cancer-in-general/treatment/immunotherapy/types/checkpoint-inhibitors

Chen, Z., & Lee, J. B. (2021). Biocompatibility of SU-8 and Its Biomedical Device Applications. *Micromachines*, *12*(7). https://doi.org/10.3390/MI12070794

Colin-York, H., Javanmardi, Y., Skamrahl, M., Kumari, S., Chang, V. T., Khuon, S., Taylor, A., Chew, T. L., Betzig, E., Moeendarbary, E., Cerundolo, V., Eggeling, C., & Fritzsche, M. (2019). Cytoskeletal Control of Antigen-Dependent T Cell Activation. *Cell Reports*, *26*(12), 3369-3379.e5. https://doi.org/10.1016/j.celrep.2019.02.074

Cooper, G. M. (2000a). *Intermediate Filaments*. https://www.ncbi.nlm.nih.gov/books/NBK9834/

Cooper, G. M. (2000b). *Microtubules*. https://www.ncbi.nlm.nih.gov/books/NBK9932/

Copelovitch, L., & Kaplan, B. S. (2012). Developmental Abnormalities of the Kidneys. *Avery's Diseases of the Newborn (Ninth Edition)*, 1182–1190. https://doi.org/10.1016/B978-1-4377-0134-0.10083-6

Corrigan, M. A., Ferradaes, T. M., Riffault, M., & Hoey, D. A. (2019). Ciliotherapy Treatments to Enhance Biochemically- and Biophysically-Induced Mesenchymal Stem Cell Osteogenesis: A Comparison Study. *Cellular and Molecular Bioengineering*, *12*(1), 53–67. https://doi.org/10.1007/S12195-018-00561-0/FIGURES/7

Curtis, J. R., Carbone, L., Cheng, H., Hayes, B., Laster, A., Matthews, R., Saag, K. G., Sepanski, R., Tanner, S. B., & Delzell, E. (2008). Longitudinal trends in use of bone mass measurement among older Americans, 1999-2005. *Journal of Bone and Mineral Research*, *23*(7), 1061–1067. https://doi.org/10.1359/jbmr.080232

Curtis, J. R., McClure, L. A., Delzell, E., Howard, V. J., Orwoll, E., Saag, K. G., Safford, M., & Howard, G. (2009). Population-based fracture risk assessment and osteoporosis treatment disparities by race and gender. *Journal of General Internal Medicine*, *24*(8), 956–962. https://doi.org/10.1007/s11606-009-1031-8

D'Amico, L., & Roato, I. (2012). Cross-talk between T cells and osteoclasts in bone resorption. *BoneKEy Reports*, *1*(6), 82. https://doi.org/10.1038/bonekey.2012.82

Definition of CAR T-cell therapy - NCI Dictionary of Cancer Terms - National Cancer Institute. (n.d.). Retrieved June 17, 2021, from https://www.cancer.gov/publications/dictionaries/cancer-terms/def/car-t-cell-therapy

Delaine-Smith, R. M., Sittichokechaiwut, A., & Reilly, G. C. (2014). Primary cilia respond to fluid shear stress and mediate flow-induced calcium deposition in osteoblasts. *The FASEB*

Journal, *28*(1), 430–439. https://doi.org/10.1096/FJ.13-231894

Dempster, D. W., Cosman, F., Parisien, M., Shen, V., & Lindsay, R. (1993). Anabolic actions of parathyroid hormone on bone. *Endocrine Reviews*, *14*(6), 690–709. https://doi.org/10.1210/edrv-14-6-690

Deshmukh, S. K., Azim, S., Ahmad, A., Zubair, H., Tyagi, N., Srivastava, S. K., Bhardwaj, A., Singh, S., Rocconi, R. P., & Singh, A. P. (2017). Biological basis of cancer health disparities: resources and challenges for research. *American Journal of Cancer Research*, *7*(1), 1. /pmc/articles/PMC5250676/

Development and Spread of Cancer - Cancer - Merck Manuals Consumer Version. (n.d.). Retrieved March 2, 2022, from https://www.merckmanuals.com/home/cancer/overview-of-cancer/development-and-spread-of-cancer

Drake, M. T., Clarke, B. L., & Khosla, S. (2008). Bisphosphonates: Mechanism of action and role in clinical practice. In *Mayo Clinic Proceedings* (Vol. 83, Issue 9, pp. 1032–1045). Elsevier Ltd. https://doi.org/10.4065/83.9.1032

Dustin, M. L. (2014). The immunological synapse. *Cancer Immunology Research*, *2*(11), 1023. https://doi.org/10.1158/2326-6066.CIR-14-0161

Dwarshuis, N. J., Parratt, K., Santiago-Miranda, A., & Roy, K. (2017). Cells as advanced therapeutics: State-of-the-art, challenges, and opportunities in large scale biomanufacturing of high-quality cells for adoptive immunotherapies. In *Advanced Drug Delivery Reviews* (Vol. 114, pp. 222–239). Elsevier B.V. https://doi.org/10.1016/j.addr.2017.06.005

Espinha, L. C., Hoey, D. A., Fernandes, P. R., Rodrigues, H. C., & Jacobs, C. R. (2014). Oscillatory Fluid Flow Influences Primary Cilia and Microtubule Mechanics. *Cytoskeleton (Hoboken, N.J.)*, *71*(7), 435. https://doi.org/10.1002/CM.21183

Fang, H., Deng, Z., Liu, J., Chen, S., Deng, Z., & Li, W. (2022). The Mechanism of Bone Remodeling After Bone Aging. *Clinical Interventions in Aging*, *17*, 405–415. https://doi.org/10.2147/CIA.S349604

FDA approval brings first gene therapy to the United States | FDA. (n.d.). Retrieved June 17, 2021, from https://www.fda.gov/news-events/press-announcements/fda-approval-brings-first-gene-therapy-united-states

Finetti, F., Paccani, S. R., Rosenbaum, J., & Baldari, C. T. (2011). Intraflagellar transport: A new player at the immune synapse. In *Trends in Immunology* (Vol. 32, Issue 4, pp. 139–145). NIH Public Access. https://doi.org/10.1016/j.it.2011.02.001

Fliegauf, M., Benzing, T., & Omran, H. (2007). When cilia go bad: cilia defects and ciliopathies. *Nature Reviews Molecular Cell Biology 2007 8:11*, *8*(11), 880–893. https://doi.org/10.1038/nrm2278

Geiger, B., Rosen, D., & Berke, G. (1982). Spatial relationships of microtubule-organizing centers and the contact area of cytotoxic t lymphocytes and target cells. *Journal of Cell Biology*, *95*(1), 137–143. https://doi.org/10.1083/jcb.95.1.137

Goley, E. D., & Welch, M. D. (2006). The ARP2/3 complex: an actin nucleator comes of age. *Nature Reviews Molecular Cell Biology 2006 7:10*, *7*(10), 713–726. https://doi.org/10.1038/nrm2026

Gomez, T. S., Kumar, K., Medeiros, R. B., Shimizu, Y., Leibson, P. J., & Billadeau, D. D. D. (2007). Formins regulate the actin-related protein 2/3 complex-independent polarization of the centrosome to the immunological synapse. *Immunity*, *26*(2), 177–190. https://doi.org/10.1016/J.IMMUNI.2007.01.008

Grakoui, A., Bromley, S. K., Sumen, C., Davis, M. M., Shaw, A. S., Allen, P. M., & Dustin, M.

L. (1999). The immunological synapse: a molecular machine controlling T cell activation. *Science (New York, N.Y.)*, *285*(5425), 221–227. https://doi.org/10.1126/SCIENCE.285.5425.221

Hadjidakis, D. J., & Androulakis, I. I. (2006). Bone remodeling. *Annals of the New York Academy of Sciences*, *1092*, 385–396. https://doi.org/10.1196/annals.1365.035

Han, Y., Liu, D., & Li, L. (2020). PD-1/PD-L1 pathway: current researches in cancer. *American Journal of Cancer Research*, *10*(3), 727. /pmc/articles/PMC7136921/

Harmer, D., Falank, C., & Reagan, M. R. (2018). Interleukin-6 Interweaves the Bone Marrow Microenvironment, Bone Loss, and Multiple Myeloma. *Frontiers in Endocrinology*, *9*(JAN). https://doi.org/10.3389/FENDO.2018.00788

Harrison, D. L., Fang, Y., & Huang, J. (2019). T-cell mechanobiology: Force sensation, potentiation, and translation. In *Frontiers in Physics* (Vol. 7, Issue APR, p. 45). Frontiers Media S.A. https://doi.org/10.3389/fphy.2019.00045

He, S., Zhang, K., Cao, Y., Liu, G., Zou, H., Song, R., & Liu, Z. (2022). Effect of cadmium on Rho GTPases signal transduction during osteoclast differentiation. *Environmental Toxicology*. https://doi.org/10.1002/TOX.23510

How does Arp2/3-mediate the nucleation of branched filaments | MBInfo. (n.d.). Retrieved February 17, 2022, from https://www.mechanobio.info/cytoskeleton-dynamics/what-is-the-cytoskeleton/what-are-actin-filaments/how-does-arp23-mediate-the-nucleation-of-branched-filaments/

Hui, K. L., Balagopalan, L., Samelson, L. E., & Upadhyaya, A. (2015). Cytoskeletal forces during signaling activation in Jurkat T-cells. *Molecular Biology of the Cell*, *26*(4), 685–695. https://doi.org/10.1091/mbc.E14-03-0830

Hui, K. L., & Upadhyaya, A. (2017). Dynamic microtubules regulate cellular contractility during T-cell activation. *Proceedings of the National Academy of Sciences of the United States of America*, *114*(21), E4175–E4183. https://doi.org/10.1073/pnas.1614291114

Hui, K. L., Wang, C., Grooman, B., Wayt, J., & Upadhyaya, A. (2012). Membrane dynamics correlate with formation of signaling clusters during cell spreading. *Biophysical Journal*, *102*(7), 1524–1533. https://doi.org/10.1016/J.BPJ.2012.02.015

Immune Checkpoint Inhibitors - National Cancer Institute. (n.d.). Retrieved March 17, 2022, from https://www.cancer.gov/about-cancer/treatment/types/immunotherapy/checkpoint-inhibitors

Janeway, C. A., Travers, P., Walport, M., & Shlomchik, M. J. (2001). *T-cell receptor gene rearrangement*. https://www.ncbi.nlm.nih.gov/books/NBK27145/

Jansen, I. D. C., Vermeer, J. A. F., Bloemen, V., Stap, J., & Everts, V. (2012). Osteoclast Fusion and Fission. *Calcified Tissue International*, *90*(6), 515. https://doi.org/10.1007/S00223-012-9600-Y

Jilka, R. L. (2007). Molecular and cellular mechanisms of the anabolic effect of intermittent PTH. In *Bone* (Vol. 40, Issue 6, pp. 1434–1446). Bone. https://doi.org/10.1016/j.bone.2007.03.017

Judokusumo, E., Tabdanov, E., Kumari, S., Dustin, M. L., & Kam, L. C. (2012). Mechanosensing in T lymphocyte activation. *Biophysical Journal*, *102*(2), L5–L7. https://doi.org/10.1016/j.bpj.2011.12.011

Kanwal, S., Fardini, Y., Pagesy, P., N'Tumba-Byn, T., Pierre-Eugène, C., Masson, E., Hampe, C., & Issad, T. (2013). O-GlcNAcylation-inducing treatments inhibit estrogen receptor α expression and confer resistance to 4-OH-tamoxifen in human breast cancer-derived MCF-7

cells. *PloS One*, *8*(7). https://doi.org/10.1371/JOURNAL.PONE.0069150

Kathem, S. H., Mohieldin, A. M., Abdul-Majeed, S., Ismail, S. H., Altaei, Q. H., Alshimmari, I. K., Alsaidi, M. M., Khammas, H., Nauli, A. M., Joe, B., & Nauli, S. M. (2014). Ciliotherapy: A novel intervention in polycystic kidney disease. *Journal of Geriatric Cardiology*, *11*(1), 63–73. https://doi.org/10.3969/j.issn.1671-5411.2014.01.001

Kato, M., Patel, M. S., Levasseur, R., Lobov, I., Chang, B. H. J., Glass, D. A., Hartmann, C., Li, L., Hwang, T. H., Brayton, C. F., Lang, R. A., Karsenty, G., & Chan, L. (2002). Cbfa1-independent decrease in osteoblast proliferation, osteopenia, and persistent embryonic eye vascularization in mice deficient in Lrp5, a Wnt coreceptor. *Journal of Cell Biology*, *157*(2), 303–314. https://doi.org/10.1083/jcb.200201089

Kato, Y., Windle, J. J., Koop, B. A., Mundy, G. R., & Bonewald, L. F. (1997). Establishment of an osteocyte-like cell line, MLO-Y4. *Journal of Bone and Mineral Research : The Official Journal of the American Society for Bone and Mineral Research*, *12*(12), 2014–2023. https://doi.org/10.1359/JBMR.1997.12.12.2014

Kroll, M. H., & Kroll, M. H. (2000). Parathyroid hormone temporal effects on bone formation and resorption. *Bulletin of Mathematical Biology 2000 62:1*, *62*(1), 163–188. https://doi.org/10.1006/BULM.1999.0146

Kudo, O., Sabokbar, A., Pocock, A., Itonaga, I., Fujikawa, Y., & Athanasou, N. A. (2003). Interleukin-6 and interleukin-11 support human osteoclast formation by a RANKL-independent mechanism. *Bone*, *32*(1), 1–7. https://doi.org/10.1016/S8756-3282(02)00915-8

Kurata, K., Uemura, T., Nemoto, A., Tateishi, T., Murakami, T., Higaki, H., Miura, H., & Iwamoto, Y. (2001). Mechanical Strain Effect on Bone-Resorbing Activity and Messenger RNA Expressions of Marker Enzymes in Isolated Osteoclast Culture. *Journal of Bone and*

Mineral Research, *16*(4), 722–730. https://doi.org/10.1359/JBMR.2001.16.4.722

Kwon, R. Y., Temiyasathit, S., Tummala, P., Quah, C. C., & Jacobs, C. R. (2010). Primary cilium-dependent mechanosensing is mediated by adenylyl cyclase 6 and cyclic AMP in bone cells. *The FASEB Journal*, *24*(8), 2859–2868. https://doi.org/10.1096/fj.09-148007

Lee, H. G., Cho, M. Z., & Choi, J. M. (2020). Bystander CD4+ T cells: crossroads between innate and adaptive immunity. In *Experimental and Molecular Medicine* (Vol. 52, Issue 8, pp. 1255–1263). Springer Nature. https://doi.org/10.1038/s12276-020-00486-7

Lee, J. H., Dustin, M. L., & Kam, L. C. (2015). A microfluidic platform reveals differential response of regulatory T cells to micropatterned costimulation arrays. *Integrative Biology : Quantitative Biosciences from Nano to Macro*, *7*(11), 1442–1453. https://doi.org/10.1039/C5IB00215J

Lee, K. L., Guevarra, M. D., Nguyen, A. M., Chua, M. C., Wang, Y., & Jacobs, C. R. (2015). The primary cilium functions as a mechanical and calcium signaling nexus. *Cilia*, *4*(1). https://doi.org/10.1186/s13630-015-0016-y

Link, T. M. (2012). Osteoporosis imaging: State of the art and advanced imaging. *Radiology*, *263*(1), 3–17. https://doi.org/10.1148/RADIOL.12110462/ASSET/IMAGES/LARGE/110462FIG08B.JPEG

Liu, Y., Blanchfield, L., Pui-Yan Ma, V., Andargachew, R., Galior, K., Liu, Z., Evavold, B., & Salaita, K. (2016). DNA-based nanoparticle tension sensors reveal that T-cell receptors transmit defined pN forces to their antigens for enhanced fidelity. *Proceedings of the National Academy of Sciences of the United States of America*, *113*(20), 5610–5615. https://doi.org/10.1073/pnas.1600163113

Livak, K. J., & Schmittgen, T. D. (2001). Analysis of Relative Gene Expression Data Using Real-Time Quantitative PCR and the 2−ΔΔCT Method. *Methods*, *25*(4), 402–408. https://doi.org/10.1006/METH.2001.1262

Lythe, G., Callard, R. E., Hoare, R. L., & Molina-París, C. (2016). How many TCR clonotypes does a body maintain? *Journal of Theoretical Biology*, *389*, 214–224. https://doi.org/10.1016/j.jtbi.2015.10.016

Malone, A. M. D., Anderson, C. T., Tummala, P., Kwon, R. Y., Johnston, T. R., Stearns, T., & Jacobs, C. R. (2007). Primary cilia mediate mechanosensing in bone cells by a calcium-independent mechanism. *Proceedings of the National Academy of Sciences of the United States of America*, *104*(33), 13325–13330. https://doi.org/10.1073/pnas.0700636104

Mantegazza, A. R., Magalhaes, J. G., Amigorena, S., & Marks, M. S. (2013). Presentation of phagocytosed antigens by MHC class I and II. *Traffic (Copenhagen, Denmark)*, *14*(2), 135. https://doi.org/10.1111/TRA.12026

Martins, F., Sofiya, L., Sykiotis, G. P., Lamine, F., Maillard, M., Fraga, M., Shabafrouz, K., Ribi, C., Cairoli, A., Guex-Crosier, Y., Kuntzer, T., Michielin, O., Peters, S., Coukos, G., Spertini, F., Thompson, J. A., & Obeid, M. (2019). Adverse effects of immune-checkpoint inhibitors: epidemiology, management and surveillance. *Nature Reviews Clinical Oncology 2019 16:9*, *16*(9), 563–580. https://doi.org/10.1038/s41571-019-0218-0

Marx, R. E. (2003). Pamidronate (Aredia) and zoledronate (Zometa) induced avascular necrosis of the jaws: A growing epidemic [1]. *Journal of Oral and Maxillofacial Surgery*, *61*(9), 1115–1117. https://doi.org/10.1016/S0278-2391(03)00720-1

McDonald, M. M., Khoo, W. H., Ng, P. Y., Xiao, Y., Zamerli, J., Thatcher, P., Kyaw, W., Pathmanandavel, K., Grootveld, A. K., Moran, I., Butt, D., Nguyen, A., Warren, S., Biro,

M., Butterfield, N. C., Guilfoyle, S. E., Komla-Ebri, D., Dack, M. R. G., Dewhurst, H. F., … Phan, T. G. (2021). Osteoclasts recycle via osteomorphs during RANKL-stimulated bone resorption. *Cell*, *184*(5), 1330. https://doi.org/10.1016/J.CELL.2021.02.002

Mechanobiology Institute of Singapore. (2013). *Arp2/3 complex mediated actin nucleation*. https://www.youtube.com/watch?v=d_uWtjyNb-Y

Mehran, N. A., Mallow, J. F., Himmel, N. J., & Blount, M. A. (2016). Lithium Modulates Cilia Length in Renal Collecting Duct Cells. *The FASEB Journal*, *30*(4), 1219.

Microtubules, Filaments | Nature Reviews. (n.d.). Retrieved February 17, 2022, from https://www.nature.com/scitable/topicpage/microtubules-and-filaments-14052932/

Microtubules: the basics | Learn Science at Scitable. (n.d.). Retrieved February 17, 2022, from https://www.nature.com/scitable/content/microtubules-the-basics-14673338/

Min, H. K., Ahn, J. H., Ha, K. Y., Kim, Y. H., Kim, S. I., Park, H. Y., Rhyu, K. W., Kim, Y. Y., Oh, I. S., Seo, J. Y., Chang, D. G., & Cho, J. H. (2019). Effects of anti-osteoporosis medications on radiological and clinical results after acute osteoporotic spinal fractures: a retrospective analysis of prospectively designed study. *Osteoporosis International*, *30*(11), 2249–2256. https://doi.org/10.1007/S00198-019-05125-0/TABLES/3

Miyoshi, K., Kasahara, K., Miyazaki, I., & Asanuma, M. (2009). Lithium treatment elongates primary cilia in the mouse brain and in cultured cells. *Biochemical and Biophysical Research Communications*, *388*(4), 757–762. https://doi.org/10.1016/J.BBRC.2009.08.099

Mohamed, A. M. F. S. (2008). An Overview of Bone Cells and their Regulating Factors of Differentiation. *The Malaysian Journal of Medical Sciences : MJMS*, *15*(1), 4. /pmc/articles/PMC3341892/

Møller, L. L. V., Klip, A., & Sylow, L. (2019). Rho GTPases—Emerging Regulators of Glucose

Homeostasis and Metabolic Health. *Cells*, *8*(5), 434. https://doi.org/10.3390/CELLS8050434

Murphy, K. (2012). *Janeway's Immunobiology* (8th ed.). Garland Science.

Murphy, M. B., Murray, C., & Shorten, G. D. (2001). Fenoldopam — A Selective Peripheral Dopamine-Receptor Agonist for the Treatment of Severe Hypertension. *Http://Dx.Doi.Org/10.1056/NEJMra010253*, *345*(21), 1548–1557. https://doi.org/10.1056/NEJMRA010253

Nakchbandi, I. A., Mitnick, M. A., Masiukiewicz, U. S., Hua Sun, B. E. N., & Insogna, K. L. (2001). IL-6 Negatively Regulates IL-11 Production in Vitro and in Vivo. *Endocrinology*, *142*(9), 3850–3856. https://doi.org/10.1210/ENDO.142.9.8368

Nguyen, A. M., & Jacobs, C. R. (2013). Emerging role of primary cilia as mechanosensors in osteocytes. In *Bone* (Vol. 54, Issue 2, pp. 196–204). Bone. https://doi.org/10.1016/j.bone.2012.11.016

Nolz, J. C., Gomez, T. S., Zhu, P., Li, S., Medeiros, R. B., Shimizu, Y., Burkhardt, J. K., Freedman, B. D., & Billadeau, D. D. (2006). The WAVE2 complex regulates actin cytoskeletal reorganization and CRAC-mediated calcium entry during T cell activation. *Current Biology*, *16*(1), 24–34. https://doi.org/10.1016/j.cub.2005.11.036

O'Connor, R. S., Hao, X., Shen, K., Bashour, K., Akimova, T., Hancock, W. W., Kam, L. C., & Milone, M. C. (2012). Substrate Rigidity Regulates Human T Cell Activation and Proliferation. *The Journal of Immunology*, *189*(3), 1330–1339. https://doi.org/10.4049/jimmunol.1102757

Osman, N. I., Roman, S., Bullock, A. J., Chapple, C. R., & Macneil, S. (2014). The effect of ascorbic acid and fluid flow stimulation on the mechanical properties of a tissue engineered

pelvic floor repair material. *Proceedings of the Institution of Mechanical Engineers, Part H: Journal of Engineering in Medicine*, *228*(9), 867–875. https://doi.org/10.1177/0954411914549393

Osteoporosis - Symptoms and causes - Mayo Clinic. (n.d.). Retrieved February 18, 2022, from https://www.mayoclinic.org/diseases-conditions/osteoporosis/symptoms-causes/syc-20351968

Osteoporosis Causes & Symptoms | NIAMS. (n.d.). Retrieved February 18, 2022, from https://www.niams.nih.gov/health-topics/osteoporosis

Osteoporosis Risk Factors: Are You At Risk? (n.d.). Retrieved February 18, 2022, from https://www.webmd.com/osteoporosis/guide/osteoporosis-risk-factors

Overview of Skeleton | Learn Skeleton Anatomy. (n.d.). Retrieved February 18, 2022, from https://www.visiblebody.com/learn/skeleton/overview-of-skeleton

Pacifici, R. (2010). The immune system and bone. In *Archives of Biochemistry and Biophysics* (Vol. 503, Issue 1, pp. 41–53). Arch Biochem Biophys. https://doi.org/10.1016/j.abb.2010.05.027

Parker, N., Schneegur, M., Tu, A.-H. T., Lister, P., & Forster, B. M. (2016). *Microbiology* (1st ed.). XanEdu Publishing Inc. https://openstax.org/books/microbiology/pages/18-2-major-histocompatibility-complexes-and-antigen-presenting-cells

Perica, K., Varela, J. C., Oelke, M., & Schneck, J. (2015). Adoptive T Cell Immunotherapy for Cancer. *Rambam Maimonides Medical Journal*, *6*(1), e0004. https://doi.org/10.5041/RMMJ.10179

Pettitt, D., Arshad, Z., Smith, J., Stanic, T., Holländer, G., & Brindley, D. (2018). CAR-T Cells: A Systematic Review and Mixed Methods Analysis of the Clinical Trial Landscape. In

Molecular Therapy (Vol. 26, Issue 2, pp. 342–353). Cell Press. https://doi.org/10.1016/j.ymthe.2017.10.019

Praetorius, H. A., & Spring, K. R. (2001). Bending the MDCK Cell Primary Cilium Increases Intracellular Calcium. *The Journal of Membrane Biology 2001 184:1*, *184*(1), 71–79. https://doi.org/10.1007/S00232-001-0075-4

Praetorius, H. A., & Spring, K. R. (2003). Removal of the MDCK Cell Primary Cilium Abolishes Flow Sensing. *The Journal of Membrane Biology 2003 191:1*, *191*(1), 69–76. https://doi.org/10.1007/S00232-002-1042-4

QuickStats: Percentage of Adults Aged ≥50 Years with Osteoporosis, by Race and Hispanic Origin — United States, 2017–2018. (2021). *MMWR. Morbidity and Mortality Weekly Report*, *70*(19), 731. https://doi.org/10.15585/MMWR.MM7019A5

Ramaswamy, G., Fong, J., Brewer, N., Kim, H., Zhang, D., Choi, Y., Kaplan, F. S., & Shore, E. M. (2018). Ablation of Gsα signaling in osteoclast progenitor cells adversely affects skeletal bone maintenance. *Bone*, *109*, 86. https://doi.org/10.1016/J.BONE.2017.11.019

Reyes, C., Hitz, M., Prieto-Alhambra, D., & Abrahamsen, B. (2016). Risks and Benefits of Bisphosphonate Therapies. *Journal of Cellular Biochemistry*, *117*(1), 20–28. https://doi.org/10.1002/jcb.25266

Robling, A. G., & Turner, C. H. (2009). Mechanical Signaling for Bone Modeling and Remodeling. *Critical Reviews in Eukaryotic Gene Expression*, *19*(4), 319. https://doi.org/10.1615/CritRevEukarGeneExpr.v19.i4.50

Rodnick-Smith, M., Luan, Q., Liu, S. L., & Nolen, B. J. (2016). Role and structural mechanism of WASP-triggered conformational changes in branched actin filament nucleation by Arp2/3 complex. *Proceedings of the National Academy of Sciences of the United States of*

America, *113*(27), E3834–E3843. https://doi.org/10.1073/PNAS.1517798113/-/DCSUPPLEMENTAL

Roy, N. H., & Burkhardt, J. K. (2018). The actin cytoskeleton: A mechanical intermediate for signal integration at the immunological synapse. *Frontiers in Cell and Developmental Biology*, *6*(SEP), 116. https://doi.org/10.3389/fcell.2018.00116

Sánchez, I., & Dynlacht, B. D. (2016). Cilium assembly and disassembly. *Nature Cell Biology*, *18*(7), 711. https://doi.org/10.1038/NCB3370

Satir, P., & Christensen, S. T. (2008). Structure and function of mammalian cilia. In *Histochemistry and Cell Biology* (Vol. 129, Issue 6, pp. 687–693). Springer. https://doi.org/10.1007/s00418-008-0416-9

Shen, K., Thomas, V. K., Dustin, M. L., & Kam, L. C. (2008). Micropatterning of costimulatory ligands enhances CD4+ T cell function. *Proceedings of the National Academy of Sciences of the United States of America*, *105*(22), 7791–7796. https://doi.org/10.1073/pnas.0710295105

Silva, B. C., & Bilezikian, J. P. (2015). Parathyroid hormone: Anabolic and catabolic actions on the skeleton. In *Current Opinion in Pharmacology* (Vol. 22, pp. 41–50). Elsevier Ltd. https://doi.org/10.1016/j.coph.2015.03.005

Singh, M., Chaudhry, P., & Merchant, A. A. (2016). Primary cilia are present on human blood and bone marrow cells and mediate Hedgehog signaling. *Experimental Hematology*, *44*(12), 1181-1187.e2. https://doi.org/10.1016/j.exphem.2016.08.009

Skeletal System. (n.d.). Retrieved February 18, 2022, from https://my.clevelandclinic.org/health/body/21048-skeletal-system

Spasic, M., Duffy, M. P., & Jacobs, C. R. (2022). Fenoldopam Sensitizes Primary Cilia-

Mediated Mechanosensing to Promote Osteogenic Intercellular Signaling and Whole Bone Adaptation. *Journal of Bone and Mineral Research*. https://doi.org/10.1002/JBMR.4536

Spasic, M., & Jacobs, C. R. (2017). Lengthening primary cilia enhances cellular mechanosensitivity. *European Cells and Materials*, *33*, 158–168. https://doi.org/10.22203/eCM.v033a12

Stinchcombe, J. C., & Griffiths, G. M. (2007). Secretory mechanisms in cell-mediated cytotoxicity. In *Annual Review of Cell and Developmental Biology* (Vol. 23, pp. 495–517). Annual Reviews. https://doi.org/10.1146/annurev.cellbio.23.090506.123521

Stinchcombe, J. C., Majorovits, E., Bossi, G., Fuller, S., & Griffiths, G. M. (2006). Centrosome polarization delivers secretory granules to the immunological synapse. *Nature*, *443*(7110), 462–465. https://doi.org/10.1038/nature05071

Stinchcombe, J. C., Randzavola, L. O., Angus, K. L., Mantell, J. M., Verkade, P., & Griffiths, G. M. (2015). Mother Centriole Distal Appendages Mediate Centrosome Docking at the Immunological Synapse and Reveal Mechanistic Parallels with Ciliogenesis. *Current Biology*, *25*(24), 3239. https://doi.org/10.1016/J.CUB.2015.10.028

Takahashi, K. (2012). WAVE2 protein complex coupled to membrane and microtubules. In *Journal of Oncology*. https://doi.org/10.1155/2012/590531

Takeshita, S., Kaji, K., & Kudo, A. (2000). Identification and Characterization of the New Osteoclast Progenitor with Macrophage Phenotypes Being Able to Differentiate into Mature Osteoclasts. *Journal of Bone and Mineral Research*, *15*(8), 1477–1488. https://doi.org/10.1359/JBMR.2000.15.8.1477

Tamzalit, F., Wang, M. S., Jin, W., Tello-Lafoz, M., Boyko, V., Heddleston, J. M., Black, C. T., Kam, L. C., & Huse, M. (2019). Interfacial actin protrusions mechanically enhance killing

by cytotoxic T cells. *Science Immunology*, *4*(33). https://doi.org/10.1126/sciimmunol.aav5445

Tatsumi, S., Ishii, K., Amizuka, N., Li, M., Kobayashi, T., Kohno, K., Ito, M., Takeshita, S., & Ikeda, K. (2007). Targeted Ablation of Osteocytes Induces Osteoporosis with Defective Mechanotransduction. *Cell Metabolism*, *5*(6), 464–475. https://doi.org/10.1016/J.CMET.2007.05.001

The immune system and cancer | EdCaN. (n.d.). Retrieved March 4, 2022, from https://www.edcan.org.au/edcan-learning-resources/supporting-resources/biology-of-cancer/defining-cancer/immune-system

Thompson, C. L., Wiles, A., Poole, C. A., & Knight, M. M. (2016). Lithium chloride modulates chondrocyte primary cilia and inhibits Hedgehog signaling. *The FASEB Journal*, *30*(2), 716–726. https://doi.org/10.1096/FJ.15-274944

Topalian, S. L., Muul, L. M., Solomon, D., & Rosenberg, S. A. (1987). Expansion of human tumor infiltrating lymphocytes for use in immunotherapy trials. *Journal of Immunological Methods*, *102*(1), 127–141. https://doi.org/10.1016/S0022-1759(87)80018-2

Treating Cancer with Immunotherapy | Types of Immunotherapy. (n.d.). Retrieved March 4, 2022, from https://www.cancer.org/treatment/treatments-and-side-effects/treatment-types/immunotherapy/what-is-immunotherapy.html

Trickett, A., & Kwan, Y. L. (2003). T cell stimulation and expansion using anti-CD3/CD28 beads. *Journal of Immunological Methods*, *275*(1–2), 251–255. https://doi.org/10.1016/S0022-1759(03)00010-3

Tu, K. N., Lie, J. D., Wan, C. K. V., Cameron, M., Austel, A. G., Nguyen, J. K., Van, K., & Hyun, D. (2018). Osteoporosis: A Review of Treatment Options. *Pharmacy and*

Therapeutics, *43*(2), 92. /pmc/articles/PMC5768298/

Tummala, P., Arnsdorf, E. J., & Jacobs, C. R. (2010). The Role of Primary Cilia in Mesenchymal Stem Cell Differentiation: A Pivotal Switch in Guiding Lineage Commitment. *Cellular and Molecular Bioengineering*, *3*(3), 207. https://doi.org/10.1007/S12195-010-0127-X

Types of Cancer Treatment | American Cancer Society. (n.d.). Retrieved March 2, 2022, from https://www.cancer.org/treatment/treatments-and-side-effects/treatment-types.html

U.S. Office of the Surgeon, G. (2004). Bone Health and Osteoporosis. *US Health and Human Services*, 437. https://www.ncbi.nlm.nih.gov/books/NBK45513/

UC Davis Biological Sciences. (2018). The Cytoskeleton. In *Introduction to Biology: Essentials of Life on Earth*. https://bio.libretexts.org/Courses/University_of_California_Davis/BIS_2A%3A_Introductory_Biology_(Easlon)/Readings/14%3A_The_Cytoskeleton

Upadhyay, V. S., Muntean, B. S., Kathem, S. H., Hwang, J. J., AbouAlaiwi, W. A., & Nauli, S. M. (2014). Roles of dopamine receptor on chemosensory and mechanosensory primary cilia in renal epithelial cells. *Frontiers in Physiology*, *5 FEB*. https://doi.org/10.3389/fphys.2014.00072

Väänänen, H. K., Zhao, H., Mulari, M., & Halleen, J. M. (2000). The cell biology of osteoclast function. *Journal of Cell Science*, *113*(3), 377–381. https://doi.org/10.1242/JCS.113.3.377

Varma, R., Campi, G., Yokosuka, T., Saito, T., & Dustin, M. L. (2006). T Cell Receptor-Proximal Signals Are Sustained in Peripheral Microclusters and Terminated in the Central Supramolecular Activation Cluster. *Immunity*, *25*(1), 117. https://doi.org/10.1016/J.IMMUNI.2006.04.010

Verbruggen, S. W., Thompson, C. L., Duffy, M. P., Lunetto, S., Nolan, J., Pearce, O. M. T., Jacobs, C. R., & Knight, M. M. (2021). Mechanical stimulation modulates osteocyte regulation of cancer cell phenotype. *Cancers*, *13*(12), 2906. https://doi.org/10.3390/CANCERS13122906/S1

Wallace, T. A., Martin, D. N., & Ambs, S. (2011). Interactions among genes, tumor biology and the environment in cancer health disparities: examining the evidence on a national and global scale. *Carcinogenesis*, *32*(8), 1107–1121. https://doi.org/10.1093/CARCIN/BGR066

Wang, Q., Xie, J., Zhou, C., & Lai, W. (2022). Substrate stiffness regulates the differentiation profile and functions of osteoclasts via cytoskeletal arrangement. *Cell Proliferation*, *55*(1). https://doi.org/10.1111/CPR.13172

Wang, X., & Rivière, I. (2016). Clinical manufacturing of CAR T cells: Foundation of a promising therapy. In *Molecular Therapy - Oncolytics* (Vol. 3, p. 16015). Nature Publishing Group. https://doi.org/10.1038/mto.2016.15

Wang, Z., Wann, A. K. T., Thompson, C. L., Hassen, A., Wang, W., & Knight, M. M. (2016). IFT88 influences chondrocyte actin organization and biomechanics. *Osteoarthritis and Cartilage*, *24*(3), 544. https://doi.org/10.1016/J.JOCA.2015.10.003

Weibel, D. B., DiLuzio, W. R., & Whitesides, G. M. (2007). Microfabrication meets microbiology. *Nature Reviews. Microbiology*, *5*(3), 209–218. https://doi.org/10.1038/NRMICRO1616

What does it mean to have a genetic predisposition to a disease?: MedlinePlus Genetics. (n.d.). Retrieved March 2, 2022, from https://medlineplus.gov/genetics/understanding/mutationsanddisorders/predisposition/

What Is Cancer? - National Cancer Institute. (n.d.). Retrieved March 2, 2022, from

https://www.cancer.gov/about-cancer/understanding/what-is-cancer#how-cancer-develops

What is Immunotherapy - Cancer Research Institute (CRI). (n.d.). Retrieved March 4, 2022, from https://www.cancerresearch.org/en-us/immunotherapy/what-is-immunotherapy

Wheway, G., Nazlamova, L., & Hancock, J. T. (2018). Signaling through the Primary Cilium. *Frontiers in Cell and Developmental Biology*, *6*(FEB). https://doi.org/10.3389/FCELL.2018.00008

Why Osteoporosis is More Common in Women - Osteoporosis Center - EverydayHealth.com. (n.d.). Retrieved February 18, 2022, from https://www.everydayhealth.com/osteoporosis/osteoporosis-and-gender.aspx

Wright, N. C., Looker, A. C., Saag, K. G., Curtis, J. R., Delzell, E. S., Randall, S., & Dawson-Hughes, B. (2014). The recent prevalence of osteoporosis and low bone mass in the United States based on bone mineral density at the femoral neck or lumbar spine. *Journal of Bone and Mineral Research*, *29*(11), 2520–2526. https://doi.org/10.1002/jbmr.2269

Xiang, W., Guo, F., Cheng, W., Zhang, J., Huang, J., Wang, R., Ma, Z., & Xu, K. (2017). HDAC6 inhibition suppresses chondrosarcoma by restoring the expression of primary cilia. *Oncology Reports*, *38*(1), 229–236. https://doi.org/10.3892/OR.2017.5694/HTML

Xiao, Z. S., & Quarles, L. D. (2010). Role of the polycytin-primary cilia complex in bone development and mechanosensing. *Annals of the New York Academy of Sciences*, *1192*(1), 410–421. https://doi.org/10.1111/j.1749-6632.2009.05239.x

Xie, J., Tato, C. M., & Davis, M. M. (2013). How the immune system talks to itself: the varied role of synapses. *Immunological Reviews*, *251*(1), 65. https://doi.org/10.1111/IMR.12017

Xu, X. Y., Guo, C., Yan, Y. X., Guo, Y., Li, R. X., Song, M., & Zhang, X. Z. (2012). Differential effects of mechanical strain on osteoclastogenesis and osteoclast-related gene

expression in RAW264.7 cells. *Molecular Medicine Reports*, *6*(2), 409–415. https://doi.org/10.3892/MMR.2012.908/HTML

Yamashita, T., Takahashi, N., & Udagawa, N. (2012). New roles of osteoblasts involved in osteoclast differentiation. *World Journal of Orthopedics*, *3*(11), 175–181. https://doi.org/10.5312/wjo.v3.i11.175

Yao, J., Wu, D., Zhang, C., Yan, T., Zhao, Y., Shen, H., Xue, K., Huang, X., Wang, Z., & Qiu, Y. (2021). Macrophage IRX3 promotes diet-induced obesity and metabolic inflammation. *Nature Immunology*, *22*(10), 1268–1279. https://doi.org/10.1038/S41590-021-01023-Y

Yedjou, C. G., Sims, J. N., Miele, L., Noubissi, F., Lowe, L., Fonseca, D. D., Alo, R. A., Payton, M., & Tchounwou, P. B. (2019). Health and Racial Disparity in Breast Cancer. In *Advances in Experimental Medicine and Biology* (Vol. 1152, pp. 31–49). Springer New York LLC. https://doi.org/10.1007/978-3-030-20301-6_3

Yi, J., Wu, X., Chung, A. H., Chen, J. K., Kapoor, T. M., & Hammer, J. A. (2013). Centrosome repositioning in T cells is biphasic and driven by microtubule end-on capture-shrinkage. *Journal of Cell Biology*, *202*(5), 779–792. https://doi.org/10.1083/jcb.201301004

Yoon, S. H., Ryu, J. Y., Lee, Y., Lee, Z. H., & Kim, H. H. (2011). Adenylate cyclase and calmodulin-dependent kinase have opposite effects on osteoclastogenesis by regulating the PKA-NFATc1 pathway. *Journal of Bone and Mineral Research*, *26*(6), 1217–1229. https://doi.org/10.1002/JBMR.310

Yuan, D. J., Shi, L., & Kam, L. C. (2021). Biphasic response of T cell activation to substrate stiffness. *Biomaterials*, *273*. https://doi.org/10.1016/j.biomaterials.2021.120797

Zhou, X., Liu, D., You, L., & Wang, L. (2010). Quantifying Fluid Shear Stress in a Rocking Culture Dish. *Journal of Biomechanics*, *43*(8), 1598.

https://doi.org/10.1016/J.JBIOMECH.2009.12.028